FINAL REPORT

A MECHANISTIC-EMPIRICAL TIE BAR DESIGN APPROACH FOR CONCRETE PAVEMENTS

Presented to:

American Concrete Pavement Association
5420 Old Orchard Rd., Suite A-100
Skokie, IL 60077-1059

Submitted by:
Jagannath Mallela (Principal Investigator)
Dr. Alex Gotlif
Dr. Michael I. Darter, P.E.
Ahmad Ardani, P.E.
Paul Littleton, P.E.

Applied Research Associates, Inc.
100 Trade Centre Dr., Suite 200
Champaign, IL 61820

August 2009

ACKNOWLEDGEMENTS

The authors express their deep gratitude to the American Concrete Pavement Association (ACPA) for sponsoring this work. The Colorado Department of Transportation (CDOT) has also supported this work through their approval of the use of longitudinal joint testing data collected by ARA under a CDOT contract.

We are particularly grateful to Mr. Robert Rodden and Mr. Jerry Voigt of ACPA for their counsel and their timely and constructive comments and support throughout the planning and execution of this research project. Special thanks are also due to the following industry and State Department of Transportation (DOT) personnel for helping coordinate and complete the field testing of longitudinal joints:

- Mr. Larry Scofield, ACPA.
- Mr. Doug Forstie, Paul Patane, Michael Jones, David Miller and other Arizona Department of Transportation (ADOT) staff.
- Mr. John Donahue, Mr. Jeff Lambert and other Missouri DOT staff.
- Mr. Roberto DeDios, Mr. William (Skip) Outcalt, Mr. Edward Trujillo and other CDOT staff.

The project team also acknowledges the contributions of Mr. Suri Sadasivam for his assistance with the technical report.

EXECUTIVE SUMMARY

BACKGROUND

Longitudinal joints are used in concrete pavements to relieve curling and warping stresses in concrete pavement slabs and to control longitudinal cracking. These joints also may serve as construction joints for accommodating paving operations. Tie bars typically are used across the joints to hold the adjacent slabs together. Field experience has shown that the longitudinal joints can widen over time if tie bars are not adequately designed and installed in the longitudinal joints. Widening of longitudinal joints increases the risk of transverse slab cracking and loss of joint load transfer, and if the joint becomes wide enough it may cause safety concerns. Most State highway agencies use standard design details for tie bar size, depth of embedment, and spacing; however, the design and installation practices may vary from one agency to another.

The current method of tie bar design is based on the concepts of subgrade drag theory (SDT). The theory determines the quantity of steel required to drag a concrete slab over an underlying layer without yielding or pulling out the steel bars. The dragging force is calculated based on the slab thickness, its unit weight, the friction between the slab and the underlying layer, and the distance to the closest free edge of the pavement. Based on this concept, the American Association of State Highway and Transportation Officials (AASHTO) 1993 *Guide for Design of Pavement Structures* provides charts for estimating tie bar sizes and spacings. However, this method fails to take into account the effects of temperature drop, drying shrinkage, and loading conditions on tie bar design when determining the required steel content. This report addresses the need for a more rational procedure for tie bar design based on mechanistic-empirical (M-E) concepts.

LITERATURE SURVEY

Chapter 2 presents a review of theoretical and experimental studies on characterization of the interface friction between a concrete slab and the layer immediately below it and the bonding between the embedded rebar and concrete. These two factors affect tie bar design significantly.

On the subject of concrete slab/supporting layer friction, it was found that the classical Leonardo da Vinci and Amontons approaches considered only shear as a source of restraint between the contacting surfaces. However, according to more recent considerations (including that of Coulomb), factors including adhesion and particle interlock also may contribute to the overall slab/support layer restraint. Additionally, some “push-off” test investigations have demonstrated that, in contradiction with Coulomb’s postulation, slab thickness practically does not influence the maximum frictional stress generated at the interface. The most recent experimental investigations to characterize concrete slab/supporting layer friction were conducted in the mid-1980s. These studies have modeled the relationship between the shear stress and the

sliding displacement at the slab and the support layer interface using a bilinear function. This model, although not inclusive of all aspects of the contacting surface characteristics and test conditions that could affect friction, attempts to strike a practical balance from an input characterization standpoint for analytically modeling the effects of friction on concrete slab and rebar stresses. The validation of the model parameters for the main types of base material in use today was performed using the Federal Highway Administration's (FHWA's) HIPERPAV program.

Published literature indicates that the shear transfer models for steel-concrete bonding generally are based on the relationships between bond slip and bond stresses but with different assumptions of bond distribution along the embedded steel surface. Models have been developed on assumptions of either average bond condition or variations in bond condition along the interface. Most of the numerical models developed were based on the results of pull-out tests. The literature review identified the factors that primarily affect bond behavior in a pull-out test, which include the concrete strength, yield strength of steel bar, bar size, and surface condition of bars. In models developed for the analysis of reinforced concrete pavements, both linear and bilinear relationships between bonding and slip have been used.

FIELD INVESTIGATIONS

As a part of this study, researchers collected anecdotal evidence to identify typical longitudinal joint failures (separation or faulting) that are attributable to improper tie bar design or construction and to determine if tying pavement widths greater than currently recommended increases the likelihood of longitudinal cracking. In addition, field testing was performed to study longitudinal joint response parameters such as joint opening and load transfer as functions of cyclical temperature changes. The information gathered revealed that typical joint failures include excessive joint openings, longitudinal joint faulting, and slab slippage. The data support the notion that well designed and constructed tied joints maintain tight joint openings and high load transfer efficiencies over the life of the pavement. Both design and construction causes for the failure of tied joints were discovered during the data collection process. The field investigations were not conclusive with regard to the role of tying too many lanes together on pavement distress. Longitudinal cracking was observed on pavements with varying tied widths starting from as low as 24 ft, establishing it as a form of distress that needs to be addressed in design.

DESCRIPTION OF THE ANALYTICAL MODEL AND THE RESPONSE DATABASE

Developing the proposed M-E design procedure involved two steps. First, the research team created a database of critical tie steel yield stress solutions using the ISLAB2005 finite element program for several combinations of loading, materials, and pavement

inputs. Second, the researchers developed design solutions using the database as a basis for a variety of scenarios.

The ISLAB2005 model used to generate the database was a two-layered system that consisted of a concrete pavement with tied joints and a base layer resting on a Winkler foundation. The input parameters to the model included the model geometry, properties of concrete, base, and foundation, slab-base interface friction definition, tie bar parameters, temperature and shrinkage loading expressed as an equivalent temperature load, and meshing. The dimensions of the slab used in the model were 15 x 12 feet for a standard section and 15 x 14 feet for a widened slab section. Some of the important model assumptions are described below:

- The concrete and base layers were modeled as linear elastic materials.
- The slab-base interface in the model utilized two sets of springs, one in the vertical direction (based on the Totsky model) and one in the horizontal direction (based on the modified Coulomb friction model). The horizontal spring parameters were defined from slab push-off testing data available from the literature.
- The ISLAB2005 model treated the tie bar as a beam element, and its stiffness was adjusted to account for bar-concrete interaction. A well established shear transfer model was used for computing vertical displacements at the adjacent points of the two slabs. A linear spring model was employed that utilizes equivalent spring stiffness in the axial (or pull-out) direction to account for tie bar restraint in that direction. The pull-out stiffness for a given tie bar-concrete material combination (i.e., for a given bar diameter, embedment length, steel grade, and concrete strength) was obtained from the ratio of the limiting value of the pull-out force to the limiting value of free edge slip using the pull-out bond-slip, suggested by the Comité Européen du Béton (CEB).
- Total equivalent free strains due to drying shrinkage and temperature drop in the concrete were used to define the environmentally-induced loading conditions for which tie bar analysis was performed.

Using a range of numerical values for the model parameters, ISLAB2005 computed joint openings and tensile stresses in the steel bars. Joint openings were calculated as the difference between the horizontal nodal displacements of adjacent slab edges at a longitudinal joint. The computed joint opening then was compared to the critical (maximum allowable) joint opening for a given tie bar size and embedment length. If the critical joint opening is exceeded, it would result in excessive yield stress in the tie steel. In this way, steel yield stress and maximum joint opening both were used as design criteria.

TIE BAR DESIGN GUIDANCE

The design tables in this report provide guidance for pavements with two, three, and four tied standard width (12 ft) lanes and a widened (14 ft) lane placed on cement treated bases (CTBs), asphalt treated bases (ATBs), and unbound bases. The M-E design process is provided in a step-by-step procedure and illustrated using examples. The design process includes the following steps:

1. Obtain design inputs.
2. Estimate design thermal loading.
3. Compute drying shrinkage strain.
4. Determine equivalent free strain in concrete.
5. Determine the tie bar design parameters from standard tables.

Appendix B provides supplementary tie bar design tables for unbound bases. Appendices C, D, E and F provide supplementary tie bar design tables for soil cement bases, permeable cement treated bases, CTBs, and lean concrete bases, respectively. Appendix G provides supplementary tie bar design tables for ATBs.

SENSITIVITY ANALYSIS

A sensitivity analysis was conducted to study the effects of design inputs on computed responses—joint opening and tensile stresses in steel—using the proposed M-E tie bar design procedure. A significant finding was that the base modulus is perhaps more important than the concrete slab-base interface friction. In previous modeling of this problem, the base has been considered to have infinite stiffness (rigid base assumption) and, hence, this aspect was never fully appreciated. The joint opening (and tie steel stress) increase with increasing base thickness and base modulus due to the increased resistance of the base to movement caused by the concrete slab. This implies that higher steel contents are needed for stiffer bases to ensure that the steel does not yield. The thickness of the concrete slab does not have a significant effect on either joint opening or tensile stresses in tie bars. Increasing the lane width and number of tied lanes will likely increase the opening of longitudinal joints. The total area of steel per slab has a significant effect on the computed joint opening and steel tensile stresses.

The tie bar designs from the M-E approach were compared with the SDT-based AASHTO 1993 procedure for two locations—Chicago and Las Vegas. The same input parameters were selected for these locations, except that Chicago experiences higher relative humidity than Las Vegas. The comparison of design solutions for these two locations indicated that there was little difference between the two methods for concrete slabs placed on an unbound base. However, for CTBs or ATBs, designs based on the M-E method required significantly more steel than those based on the SDT method when only two or three lanes were tied together. The sensitivity of the climatic differences between the two selected locations was conspicuous in the proposed M-E design

method, whereas the SDT method apparently was insensitive. Furthermore, as the number of lanes tied together increased, the M-E approach required much less steel for unbound bases and about the same amount of steel for treated bases as the SDT-based approach. Finally, the M-E based approach was by and large concrete slab thickness insensitive, whereas the SDT-based approach required higher steel content as the pavement thickness increased.

IMPACT OF MULTIPLE TIED LANES AND SHOULDERS ON SLAB STRESSES

The proposed M-E tie bar design procedure was used to evaluate the effect of multiple tied lanes and shoulders on critical tensile stresses in the slab. Cases with different tie bar configurations and base types were selected for evaluation. The results indicated that the concrete tensile stresses did not increase significantly when three or more lanes were tied. However, a significant increase in stresses was observed when the number of tied lanes increased from two to three. In comparing the selected base types, the tensile stresses in the slabs were lowest on unbound bases and highest on lean concrete bases (LCBs). As the base modulus and friction between the slab and base increased, the tensile stresses in the concrete slabs also increased.

CONCLUSIONS AND RECOMMENDATIONS

The M-E tie bar design procedure developed under this study is a practical procedure that balances the need to ensure joint integrity over the life of the pavement with excessive restraint caused by tying multiple lanes together. The results obtained from the procedure appear to be reasonable from an engineering standpoint. It is recommended that the guidance developed in this study be verified through actual design cases in the field.

A number of other recommendations also were made, stemming from the identified shortcomings in this research. Significant among these are (1) the systematic investigation of the pull-out stiffness characteristics of tie bars of different sizes and lengths embedded into paving concrete, (2) refinement of the excessive restraint check developed in this research through a thorough investigation of in-service pavements that are tied together and expanding analytical approach to include other mechanisms causing longitudinal cracking in pavements, and (3) development of practical tie bar placement tolerances.

TABLE OF CONTENTS

LIST OF FIGURES

LIST OF FIGURES, CONTINUED

LIST OF TABLES

APPENDIX-A

APPENDIX-B (UNBOUND BASE)

LIST OF TABLES, CONTINUED

APPENDIX-C (SOIL CEMENT BASE)

APPENDIX-D (PERMEABLE CEMENT TREATED BASE)

APPENDIX-E (CEMENT TREATED BASE)

APPENDIX-F (LEAN CONCRETE BASE)

LIST OF TABLES, CONTINUED

APPENDIX-G (ASPHALT TREATED BASE)

CHAPTER 1. INTRODUCTION

BACKGROUND

Introduction

Longitudinal joints are needed in concrete pavements to (a) provide a contraction joint to relieve excessive curling and warping stresses in the slab that may otherwise (without the joint) result in longitudinal cracking and (b) provide a construction joint to accommodate paving operations as needed to facilitate multiple lane and shoulder situations.

Field surveys and observations over many years have shown that traffic lanes not connected with deformed rebar or other mechanical ties may not remain together and the longitudinal joint may widen over time, regardless of base type, thickness of slab, climate, or geographic location. Opening of the longitudinal joint between traffic lanes results in two major problems:

1. Loss of load transfer efficiency (LTE) across the longitudinal joint, resulting in higher bending stress in the concrete slab under wheel loading. This increases the likelihood of transverse fatigue cracking. The American Association of State Highway Transportation Officials (AASHTO) Interim Mechanistic-Empirical Pavement Design Guide (MEPDG) includes the long-term LTE as a direct design input (AASHTO, 2008). Figure 1 shows the sensitivity of the long-term LTE of the longitudinal joint on transverse cracking for a given project. As shown, the impact of long-term longitudinal LTE is significant.
2. Loss of LTE across the longitudinal joint also will increase differential deflection across the joint, which creates a greater potential for erosion/faulting and loss of support near the joint and corners.
3. Widening of the longitudinal joint too much can lead to safety concerns with motorcycles and other vehicles and require maintenance activities over time.

The standard detail in concrete paving calls for tie bars to be placed at mid-depth of the concrete slab perpendicular to the traffic direction. Tie bar size and spacing—key design details—vary from one agency to the other. The techniques for installing tie bars at the proper depth with the proper embedment and alignment also can vary. Installation practices range from supporting them on secured metal chairs placed on grade (used for contraction and construction joints), placing them into holes drilled on the face of construction joints and grouting them (used for construction joints), and automatically inserting and vibrating them into place with mechanical inserters (used for both contraction and construction joints).

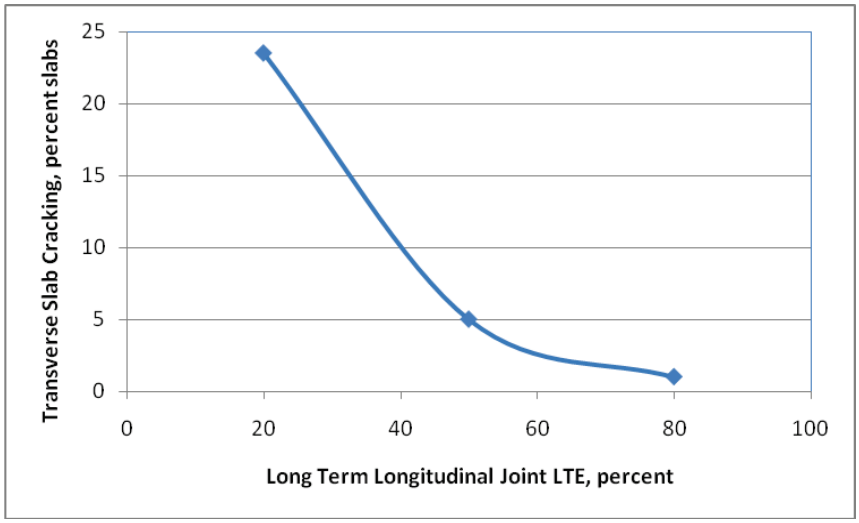

Figure 1. Impact of longitudinal joint long-term LTE on transverse cracking using the MEPDG for a given project in central Illinois.

Current Tie Bar Design Practice

The most commonly cited basis for tie bar design in the United States is the subgrade drag theory, or SDT. This theory, which has its origins in the design of steel reinforcement for slab-on-grade concrete flooring, is explained in several textbooks and industry references (Yoder & Witczak, 1975; Huang, 1993; PCA, 2008). The SDT method of design is based on the concept of providing sufficient steel to allow the "dragging" of the concrete slab across the base course without yielding the steel or pulling out the tie bars. The basic concepts are as follows:

1. The maximum force a tie bar can sustain without yielding, F_{TB} (lb), is expressed as:

$$F_{TB} = a_s * f_s \quad (1a)$$

where

a_s = cross-sectional area of one tie bar, in^2

f_s = the allowable stress in steel f_s, lb/in^2 (usually taken as two-thirds of the yield strength)

2. The force to drag a concrete slab across the base course, F_{drag} (lb), is computed as

$$F_{drag} = L_{slab} D_{fe} H_{PCC} WF \quad (1b)$$

where:

L_{slab} = slab length, in

D_{fe} = distance to the closest free edge, in

H_{PCC} = concrete slab thickness, in

W = unit weight of concrete, lb/in^3 (approximately 0.0868 lb/in^3 for a typical paving concrete mixture).

F = coefficient of friction at the slab-base interface (e.g., a value of 1.5 for unbound bases is recommended by the 1993 AASHTO *Guide for Design of Pavement Structures* or simply the 1993 AASHTO Guide)

3. If *n* is taken as the number of tie bars per slab length, then the equation of equilibrium of the SDT is:

$$nF_{TB} = F_{drag} \tag{2a}$$

4. From equation (2a), the total area of steel per slab can be determined as:

$$na_s = A_s = \frac{L_{slab} D_{fe} H_{PCC} WF}{f_s} \tag{2b}$$

where A_s (in^2) = total area of steel for a given slab length.

5. The required tie bar spacing, J_{TB} (in), can be determined as:

$$J_{TB} = \frac{L_{slab} a_s}{A_s} \tag{2c}$$

Example Application of the SDT Method for Tie Bar Design

Problem statement:
Compute the total area of steel (A_s) required for a 12-in concrete slab with a 15-ft transverse joint spacing over an unbound base for a highway consisting of two 12-ft lanes tied at the centerline joint. Assume Grade 60 steel (steel yield strength, f_y = 60,000 psi). Also compute the tie bar spacing required for #4 deformed bars. Assume the unbound base coefficient of friction to be 1.5.

Solution:
Area of steel calculation (variables previously defined)

$A_s = L_{slab} * D_{fe} * H_{PCC} * W * F / [f_y * 2/3]$

A_s = [180 in * 144 in * 12 in * 0.0868 lb/in^3 * 1.5] / [60,000 psi * (2/3)]

= 1.01 in^2

Tie bar spacing calculation:
The area of a #4 bar is 0.20 in^2. Thus, and using equation (2c), a maximum spacing of 35.6 in should be used to drag the concrete slab over the unbound base course and while keeping the steel stress safely below its yield stress. This could practically translate to providing 6 #4 bars per slab at a 30 in spacing.

If the base course in the above illustration is instead a cement treated base (CTB), then F will assume a value of 1.8 according to the 1993 AASHTO Guide. The maximum spacing of #4 bars, assuming all other variables remain constant, will become 29.6 in (requiring seven #4 bars or perhaps more economically, four #5 bars at 45 in spacing).

Of course, the SDT procedure does not model the pavement loading scenarios in the field. The tie bars across a longitudinal joint in actual pavements are subjected to tensile stress primarily from two sources: a uniform temperature "drop" and the drying shrinkage of the concrete. The temperature "drop" occurs between the set temperature of the concrete and a lower temperature during the winter. This causes a tensile strain in the concrete slab and tensile stress in the tie bars. The drying shrinkage also adds tensile stress in the steel. In reality, there may also be some relaxing of these stresses through early creep of the concrete. However, this aspect is not considered in this research since reliable modeling of this effect is difficult at the present time. Future revisions to this procedure could consider creep relaxation provided more advanced material models or experimental data are available.

The net result of the thermal, shrinkage, and creep forces is the contraction of the concrete slab. This contraction is countered by the slab-base friction which, in turn, generates displacements in the base (ignored in the SDT) and generates restraint stresses in the tie steel.

Based on this discussion, the SDT procedure has at least the following deficiencies:

1. Does not consider the temperature drop from the set temperature or the drying shrinkage of the concrete slab, but rather calculates the steel stress as that required to "drag" the slab over the base course.
2. Does not compute the actual stresses in the steel, instead computing only a maximum value for design based on ultimate stress during sliding.
3. Calls for the "minimum" distance to a free longitudinal joint as a design variable. However, when there are more than two lanes tied together, this definition is no longer sufficient.
4. Is based on a simplistic friction model and assumes a single parameter to define the complex behavior at the slab-base interface.
5. Includes a large safety factor by reducing the steel yield stress (e.g., yield stress is multiplied by 2/3) to obtain an allowable stress in the steel.
6. Does not account for displacement of the base layer (a rigid base is assumed).

In light of some of these observations, agency practice with regard to tie bar selection has been guided largely by experience or consensus opinion. The prevailing tie bar design practice in the mid-1990s was documented in the design catalog developed under National Cooperative Highway Research Program (NCHRP) Project 1-32 (Darter et al., 1998), as excerpted below:

> The predominant diameter of deformed tie bar used today is 0.625-in or #5 bar. Grade 40 or higher steel is used. Only a few States use #4 bars (6 States); however, about 10 States use #6 bars. The spacing of the bars is predominantly 30 in, with a few SHAs [State highway agencies] using shorter (18 to 24 in) and longer (36 to 48 in) spacings. There does not appear to be any research data that show that any of these designs are superior to the others, with the exception that the longitudinal joint between traffic lanes or lanes and shoulders has separated at some locations where #4 bars have been used. The following design is recommended for most lane-to-lane applications:
>
> #5 (0.625 in diameter) minimum deformed reinforcing bars spaced at 30 in.

Several SHAs that observed longitudinal joint problems (e.g., wide joint openings, loss of load transfer, joint shear failure) when using #4 or #5 bars have upgraded to #6 bars. Some countries in Europe are using even bigger bars, but fewer of them (e.g., three #8 bars per slab length of approximately 15 ft).

While *ad hoc* adjustments based on experience are valid, they often are built on the lessons learned from potentially expensive failures. There is a need for a more rational tie bar design procedure that preempts failures by overcoming the limitations of the current design practice. The design procedure should ensure that the primary purpose for which tie bars are inserted at longitudinal joints—to prevent excessive joint openings—is addressed adequately.

An interesting corollary to maintaining the longitudinal joint too tight is the increased potential for longitudinal cracking in highways with many lanes and shoulders tied together. The current industry guidance limits the total width of highway pavements that can be tied together to approximately 48 ft[1]. However, empirical evidence gathered from several pavement sections confirms the inadequacy of current design practices.

RESEARCH OBJECTIVES

This study addresses the following aspects of tie bar and concrete pavement design:

- To maintain the structural benefit of concrete shoulders for given site conditions, what is the required spacing of deformed tie bars, and what is their optimum diameter and embedment length for various longitudinal joints?

[1] For very wide roadways, there is a limit to width of pavement that can be tied together without concern for cracking. Current recommendations limit the tied width of highway pavement to about 48 ft (14.5 m) based on the subgrade drag theory. However, there has been good field performance of certain intersections with up to 70 ft (21 m) of tied pavement.
Source: ACPA's TB019P, "Concrete Intersections - A Guide for Design and Construction" (https://www.netforumondemand.com/eweb/shopping/shopping.aspx?site=acpa_org&prd_key=a90866d0-32e7-400c-ae71-779713241ec4)

- How many traffic lanes and shoulders can be tied together over a wide range of climates and base courses to avoid significant risk of longitudinal cracking? This is perhaps the most frequently asked question concerning tie bars.

REPORT ORGANIZATION

This report provides a description of the effort undertaken to achieve the project's objectives. An overview of pertinent literature is provided in chapter 2. Chapter 3 presents results from data collected on in-service pavements to understand the predominant longitudinal joint failure modes, pavement failure modes resulting from tying too many lanes together, and longitudinal joint behavior when subject to routine environmental loading. The technical development of the M-E tie bar design procedure, including a discussion of underlying structural modeling and its assumptions, the step-by-step procedure to perform tie bar design, and a few tie bar designs using this new procedure are presented in Chapter 4. Chapter 5 presents a sensitivity study of the M-E procedure and a comparison of the designs obtained from the new procedure and the traditional SDT-based design. Chapter 6 addresses the issue of how many lanes/shoulders can be tied together for a given project site and design. Finally, Chapter 7 presents a summary of findings from this research and the salient conclusions and recommendations.

CHAPTER 2. LITERATURE REVIEW

INTRODUCTION

The literature review performed for this study focused mainly on defining two of the most critical inputs related to the analytical modeling of tie bars: friction between the concrete slab and the supporting layer (base, subbase, or subgrade) and steel/concrete bond. A brief review of the current tie bar design guidance was also conducted and presented.

CONCRETE SLAB/BASE FRICTION MODELS

Leonardo Da Vinci and Amontons are credited with the early discoveries of the friction phenomenon between sliding objects. Their theories assumed that the normal weight of a sliding object and the amount of frictional force resisting the sliding is constant (coefficient of friction), as expressed in equation 3.

$$F_H = \mu N \quad (3)$$

where:

F_H = applied horizontal force, lbf
μ = coefficient of friction, or friction factor
N = vertical force transmitted across the contact area, lbf

The implicit assumptions of this theory are that the sliding objects are non-deformable and that there is no adhesion between them. Coulomb built upon their works to introduce the concept of adhesion in the definition of friction. As numerical approaches to problem solving began to emerge in the later part of the 20th century, more complex considerations of interface friction were possible and the interest in this area has steadily grown in several fields including that of pavements. However, the practical challenge of supplying input data required to model interfacial friction behavior in accordance with these theoretical considerations still remains unresolved.

Ioannides and Salsilli-Murua (1988) presented an overview of the interlayer pavement friction characterization for concrete pavements. Lee (2000) also studied the characterization and characteristics of friction between a concrete slab and its supporting layer from a historical perspective in an attempt to develop a practical model for the determination of friction between a concrete slab and a base. Some of their observations and conclusions based on an analysis of the published body of work are presented in the following paragraphs.

The earliest study on friction development along the underside of a concrete slab was the sliding tests of Goldbeck (1924). Goldbeck studied the frictional characteristics of a

concrete slab sliding on unbound base or subbase materials such as a broken stone, gravel, and sand in both near optimum moisture and saturated states. Several other researchers dedicated much effort to the study of the slab/unbound support layer interface frictional characteristics until the 1960s. The frictional characteristics of concrete slabs resting on stabilized bases, including asphalt treated bases and CTBs, were studied in the 1980s, primarily by Wesevich et al. (1987). Different test conditions such as rates of sliding, concrete slab thickness, moisture state of the supporting layer, interlayers, etc. were used in each study.

All the tests attempted to simulate the movement of a concrete slab caused by uniform temperature or moisture changes. The experimental procedures consisted of applying a horizontal force to a slab placed on a supporting layer. From all these studies, it has been determined that the primary factors influencing the sliding test results include:

- Base layer—the material, texture, and moisture content of the base layer have a direct effect on the friction factor.
- Magnitude of the horizontal displacement—according to Kelley (1939), the coefficient of friction versus displacement curve closely approximates a parabola.
- Number of load applications—friction-displacement curves for the first load cycle are different than those obtained from subsequent load applications.
- Slab thickness—a weak dependence exists between slab thickness and friction factors.

In addition, Ioannides and Salsili-Murua (1988) presented an analysis of the experimental data for different types of supporting layers and interface materials, including unbound bases and treated bases with or without friction reducers. They presented a number of tables and graphs with friction factor values for different supporting layers. Based on their analysis, the range of friction factors obtained from experimentation were the highest for concrete slabs resting on CTBs without friction reducers (40 to 50) and lowest for concrete slabs resting on natural subgrades (0.5 to 1).

A theoretical study of pavement-base interface friction was presented by both Bradbury (1938) and Kelley (1939). According to them, the maximum concrete axial stresses due to friction could be represented as:

$$\sigma_f = \beta \mu W \Lambda \qquad (4)$$

where:

σ_f = maximum stress due to friction, psi
Λ = maximum distance from “fixed point,” in
β = dimensionless friction reduction factor

Kelley (1939) proposed two methods to determine β. Bergstorm (1950) proposed that β varies as a function of another dimensionless number, ψ, which can be approximated as follows:

$$\psi = (D/2\Lambda)/(\alpha\nabla T) \quad (5)$$

where:

D	=	assumed displacement, in
α	=	coefficient of thermal expansion (CTE) of the concrete, in/in/^{o}F
∇T	=	temperature drop, ^{o}F

Iwama (1964) further improved on Bradbury and Kelley's method by suggesting the use of experimental data for estimating β in equation (4).

Another theoretical approach to modeling friction was taken by Van Cauwelaert (1986) for multi-layer pavement systems. This method modifies the elastic multi-layer analysis through the introduction of a dimensionless multiplication factor, k, which characterizes the displacement transfer at the interfaces of two adjacent pavement layers. A generalized representation of the concept is presented in equation (6):

$$u_i = k u_{i+1} \quad (6)$$

where:

u_i	=	horizontal displacement at the bottom of the upper layer, in
u_{i+1}	=	horizontal displacement at the top of the lower layer, in

Full slip occurs when $k=\infty$ and full bond when k=1.

All the aforementioned analytical approaches are empirical and have no theoretical substantiation.

Wimsatt and McCullough (1989) summarized the frictional study performed at the Center for Transportation Research at the University of Texas in the late 1980s by Wesevich et al. (1987). During this study, a standardized method, called the "push-off" test, was developed to characterize concrete slab-base sliding friction. Push-off tests were conducted on a flexible base (asphalt aggregate with inherent cement agents), an asphalt-stabilized base with bond-breaker, a cement-stabilized base, a lime-treated clay subbase, and an untreated unbound base. The results of the push-off tests were represented as bi-linear curves that fit the stress-displacement relationships. This representation of slab-base friction is widely used today by researchers and software programs (e.g., HIPERPAV [Ruiz et al., 2001]).

Using the friction data generated by Wesevich et al. (1987), a computer program was developed to compute tensile stresses in the concrete slab caused by slab-base friction and to recommend a maximum joint spacing for concrete slabs constructed on different types of base layers.

Tarr et al. (1999) performed field tests of concrete pavements constructed on a lean concrete base (LCB). The purpose of this testing was to investigate the effect of the interaction between pavement layers under loading on concrete slab strains for several different cases of interface treatment. Static loads were induced using a 20-kip dual wheel single axle truck positioned adjacent to the strain gauge location. The researchers observed that, due to friction, absolute values of stresses computed from observed strains at the top and bottom concrete slab surfaces were not equal except for the case with a double layer of polyethylene used as an interlayer. Higher bottom tensile concrete stresses corresponded to a lower interface stress reduction. Stresses computed from measured strains were compared with numerical calculations using the ILSL2 program (now ISLAB2000) for unbonded and fully bonded conditions. Tarr et al. concluded that the theoretical stress computations agreed very well with the experimental data.

Rasmussen and Rozycki (2000) introduced a one-dimensional approach for slab-base interaction under axial loading. A one-dimensional analytical model was developed on the basis of the push-off test results published by Wimsatt and McCullough (1989). To analyze the response of concrete slabs under temperature and shrinkage strains, Rasmussen and Rozycki made the following assumptions:

- Concrete behaves as a linear elastic material.
- Model considers only uniformly distributed through-slab shrinkage and temperature change.
- Model ignores the base deformation under friction forces (assumption of infinite rigidity of base material). (This assumption is the most questionable for tie bar design because real base stiffness may be low, especially in the case of unbound base.)
- The restraint stresses from the base are assumed to be represented by the following bi-linear function:

$$\tau_f = \begin{cases} Ku_c \ \ if \ \ 0 < |u_c| \le \delta_f \\ C\dfrac{u_c}{|u_c|} \ \ if \ \ \delta_f \le |u_c| \end{cases} \qquad (7)$$

where:

u_c = concrete slab axial displacement, in

τ_f = restraint stress, psi

δ_f = maximum sliding, in

K = slope of the stress-displacement curve, lb/in^3

C = maximum friction, psi

The basis of the model is governed by the one-dimensional equilibrium equation. The one-dimensional finite difference method is used for the solving equilibrium equations. The Rasmussen and Rozycki (2000) one-dimensional model was incorporated into the HIPERPAV program (Ruiz et al., 2000).

A similar one-dimensional model was presented by Zhang and Li (2001). They used a semi-analytical method for solving the equilibrium equation. They suggested that their model also can be used when restraint stresses develop in a slab from a source other than those arising from slab-base friction (e.g., tie bars in jointed plain concrete pavements [JPCP]).

Many researchers have used commercial finite element packages (e.g., ABAQUS, ANSYS) for three-dimensional analysis of JPCP. Masada et al. (1996) presented the results of a three-dimensional ABAQUS analysis of JPCP. Using interface elements, the interaction between concrete slabs and the base was modeled. The interface element gave the model the capability to solve the partial contact between curled slabs and the base and to examine the influence of slab-base friction. The data from the ABAQUS modeling were in reasonable agreement with the results from pavement programs (KENSLAB, ILLI-SLAB and JSLAB) and Bradbury's analytical solution. The model was used to conduct parametric studies on curling and thermal-expansion stresses, to study the effect of superposition of both stresses, and to address the effect of uniform temperature changes on joint opening. The effect of the friction factor on tensile curling stress was found to be minimal. Curling stresses tended to increase with an increase in slab thickness. In the case of uniform thermal-expansion, maximum stresses increased with an increase in the frictional parameter.

Nishizava et al. (2001) used a bi-linear model for simulating slab-base interaction. For improving convergence for the case of slab-base separation (due to curling), they modified the model by including a so-called "transition zone," which allows a smooth change to the interface spring stiffness. This model is incorporated into a three-dimensional pavement analysis program, PAVE3D.

A three-dimensional finite element program for the analysis of concrete pavements, EverFE2.2, allows the specification of either perfect bond between the slab and base (no slip and no separation) or free separation of the slabs and base under tensile contact stresses (Davids et al., 2003). To capture slab-base shear transfer, a zero-thickness interface element was incorporated in the program. The element's constitutive relationship is based on the theory proposed by Rasmussen and Rozycki (2000). The bi-linear constitutive relationship defines the relationship between the interface shear stress and the relative slip between the slab and the base. For very large values of the interface shear stiffness, this model approaches Coulomb friction with a very large friction coefficient, and for very small values of shear stiffness it is equivalent to a

frictionless interface. The program's new features are detailed in the referenced paper, along with the findings of a sensitivity analysis. Davids et al. (2003) considered the effect of slab-base shear transfer under different combinations of uniform shrinkage and temperature loading (uniform distribution and temperature gradients) and concluded the following:

> The need for three-dimensional analysis (instead of one- or two-dimensional) when simulating both thermal gradients and shrinkage is evident: even under uniform shrinkage, the slab-base shear stresses acting at the bottom of the slab result in the slab-base separation and a nonuniform distribution of the stresses over the slab thickness because of the eccentricity of the shear stress respective to the center gravity of the slab.

STEEL-CONCRETE BOND MODELS

Many experimental, analytical, and semi-analytical models of shear transfer between concrete and steel rebars have been developed. Generally speaking, all the approaches consider relationships between a relative displacement between concrete and steel (bond slip) and bond stresses. However, based on how these models treat the bond stress distribution along the concrete/steel interface, they can be broadly divided into two categories: (1) those that relate the "average" bond condition along the concrete/steel interface and rebar slip and (2) those that consider the variation of the bond condition along the rebar and its relationship with slip. The difference between the two approaches obviously lies in the assumptions of bond distribution along the embedded steel surface.

An example of a model that fits into the second group is the one developed by Abe et al. (1990). They developed a non-linear one-dimensional equation for stress-slip for continuously reinforced concrete pavement (CRCP) analysis. Further, Olesen (2002) presented a tri-linear bond-slip curve between a concrete specimen and an embedded rebar. Test results for local stress-slip were presented by Kankam (1997).

In the current practice of finite element modeling, various bond stress-slip models of the first group generally are employed. To account for the effect of the bond stress and bond slip, spring elements at nodal points along the rebar simulate steel-concrete contact. The relationships between the bond stress and bond slip employed in these numerical modeling studies usually are based on pull-out test data obtained in a laboratory.

The literature review shows that, under static, monotonically increasing loads (e.g., in a pull-out test), the main factors that affect bond behavior are the concrete strength, yield strength of steel bar, bar size, and surface condition of bars. In a pull-out test, two types of bond failures are typical: direct pull-out of the bar and splitting of the concrete cover when the cover of confinement is insufficient.

Eligehausen et al. (1983) investigated the bond stress-slip relationship over a very large range of slip. They suggested a typical bond stress-slip diagram as a sequence of linear segments, as shown in Figure 2. Eligehausen et al. (1983) explained the figure as follows:

- Up to a certain value of bond stress τ_1, the concrete-steel bond is due to chemical adhesion of the cement on the surface of the steel bar and practically no slip takes place. Typical values of τ_1 range from approximately 72.5 psi to 145 psi (0.5 MPa to 1.0 MPa).
- For $\tau \geq \tau_1$ adhesions breaks down and bond is provided by friction and by mechanical interlock between the bar and concrete. Due to these interlock forces, at a stress level $\tau = \tau_2$ (which is a function of the tensile strength of concrete) bond cracks form. At approximately the same time, separation of concrete from reinforcement bar takes place in the region of primary (flexural) cracks. This separation causes an increase in the circumference of the concrete surface previously in contact with the bar and, as a result, circumferential tensile stresses develop. These stresses, in combination with the radial component of the force carried by the ribs, lead to splitting cracks.
- At the stress $\tau = \tau_3$ the splitting cracks propagate up to the external face of the member and, if there is not enough confinement, bond is destroyed and a splitting failure occurs. In the case of significant confinement, the bond stress can reach higher values τ_{max}.
- The descending branch of the bond stress-slip diagram ($\Delta \leq \Delta_{max}$) corresponds to a complete deterioration of concrete between adjacent ribs and for $\Delta \geq \Delta_4$, the moderate amount for residual bond stress τ_4.
- The stress τ_4 can remain practically constant for high values of slip. The value of the slip Δ_4 almost coincides with the spacing of the ribs. The only remaining mechanism of the bond transfer is friction at the cylindrical failure surface.

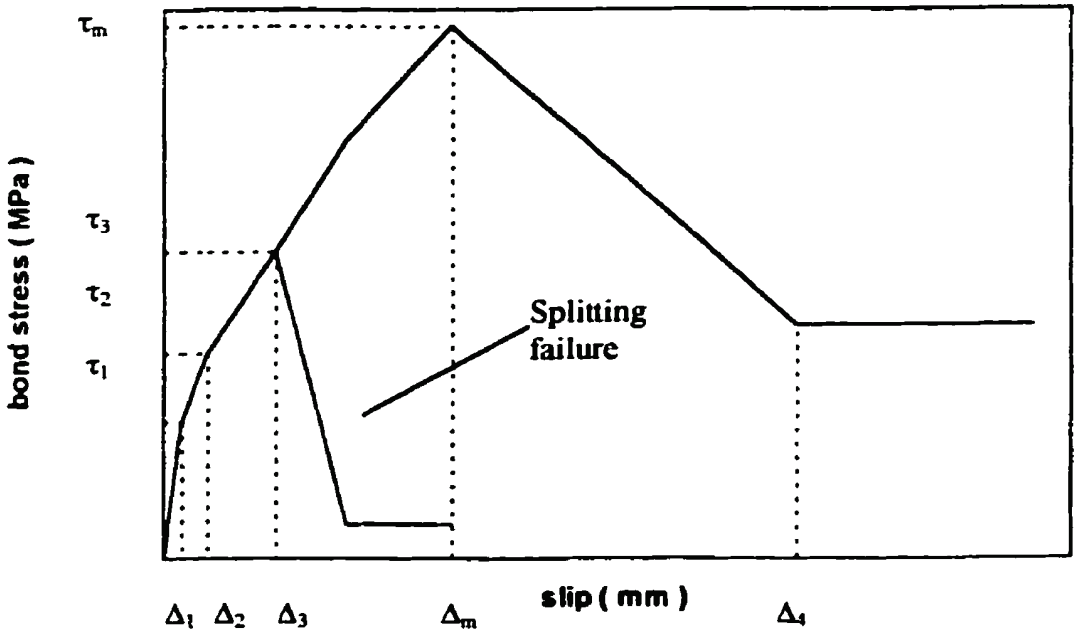

Figure 2. Bond stress-slip relationship (from Eligehausen et al. [1983]).

Kachlakev et al. (1996) presented a new bond test procedure that minimizes the effect of Poisson's ratio. Reinforced concrete specimens of various strengths were tested to evaluate the robustness of the procedure. Typical results from the testing were published. The range of the estimated bond stress was between 340 psi and 980 psi for rebars embedded in concrete with compressive strength ranging from 3,400 psi and 7,800 psi. The performance of each rebar also was described with a dimensionless ratio, termed the *mobilization of yield resistance*.

Ahlborn and DenHartigh (2002) compared the experimentally defined bond strength with the empirical equation established by Orangun et al. (1977). They considered the load to cause a free-end displacement of 2 mils as the criterion of bond strength failure. Results of their test allowed the estimation of pull-out shear stiffness.

In pavement analysis of reinforced concrete, different types of linear and bilinear bond-slip relationships are used.

Seong-Min Kim et al. (1998) performed parametric studies of CRCP to analyze the impact of steel/concrete shear, using both linear and bi-linear relationships. Their study concluded that linear bond-slip relationships cause larger concrete stresses than bi-linear relationships.

Linear models of steel-concrete interaction were implemented in PAVE3D and EverFE2; CRCP-10 (Seong-Min Kim et al., 2000) used a linear model for both dowel and tie bar modeling. In this case, steel-concrete shear interaction may be characterized by one parameter—pull-out modulus. A large value of this modulus corresponds to a high degree of bond.

TIE BAR DESIGN

As mentioned previously in this report, conventional tie bar design methods use SDT for estimating the required tie bar size, spacing, and embedded length. Figure 3 and Figure 4 present plots of the required tie bar spacing for a 10-in-thick, 12-ft-wide concrete slab with embedded Grade 40 and Grade 60 steel, respectively, using the SDT. The range of friction coefficients considered was 2.5 to 8.9. The end points of this range represent the coefficient of friction values recommended in the MEPDG (AASHTO, 2008) for aggregate and CTBs.

An FHWA Technical Advisory on concrete pavement joints (FHWA, 1990) presents a table of the maximum recommended tie bar spacing (reproduced here as Table 1). The table from this document considers tie bar size (#4 or #5), steel grade (40 or 60), distance to free edge (10 through 24 ft), and concrete slab thickness (9 through 12 in) as variables.

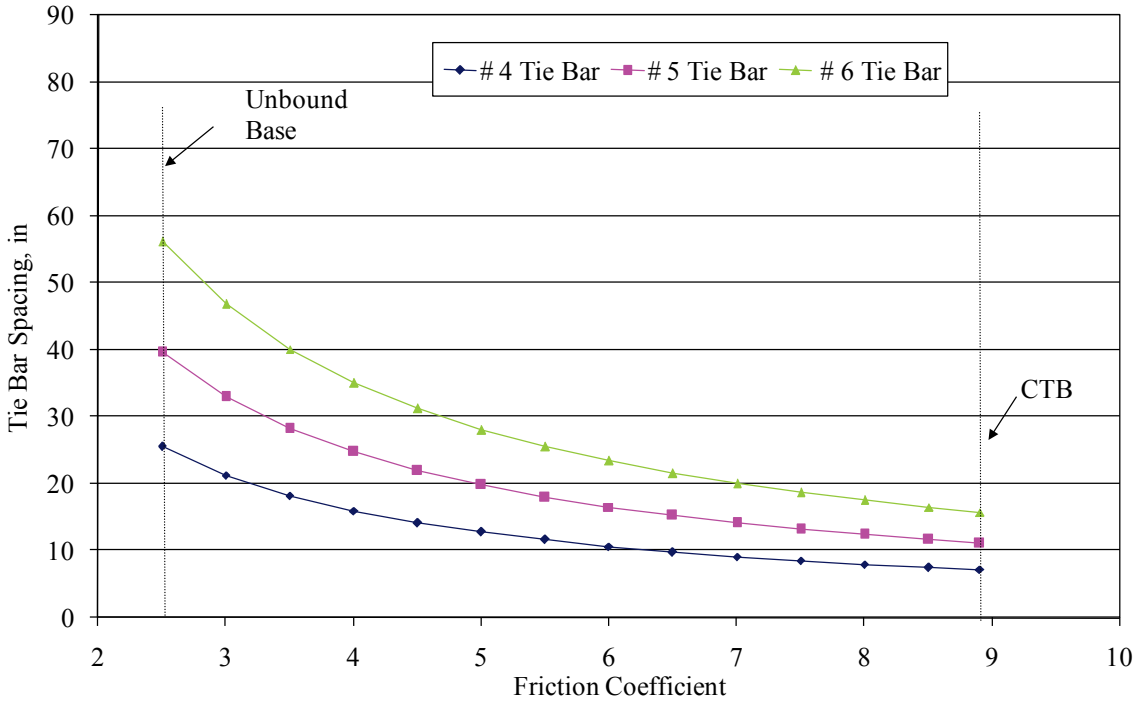

Figure 3. Tie bar spacing per the SDT vs. friction coefficient for Grade 40 steel.

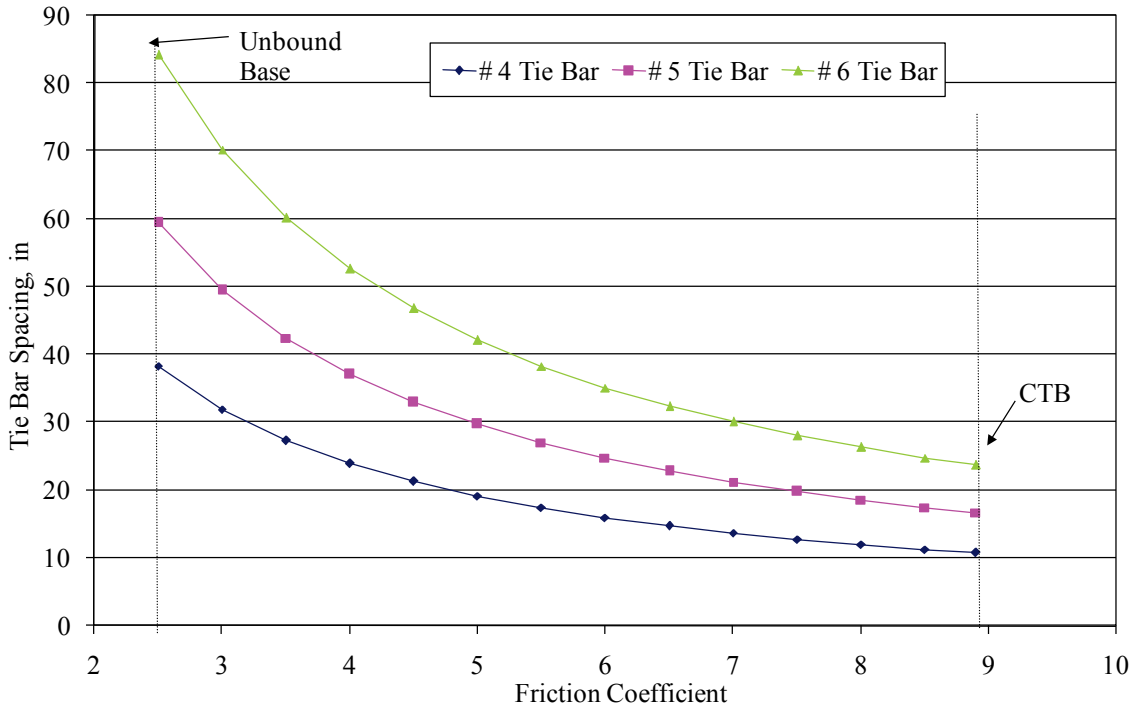

Figure 4. Tie bar spacing per the SDT vs. friction coefficient for Grade 60 steel.

Table 1. FHWA maximum tie bar spacing recommendations per the SDT (from FHWA, 1990).

H_{PCC}, in	#4 Bar								#5 Bar							
	Grade 40				Grade 60				Grade 40				Grade 60			
	Distance to Free Edge, ft				Distance to Free Edge, ft				Distance to Free Edge, ft				Distance to Free Edge, ft			
	10	12	16	24	10	12	16	24	10	12	16	24	10	12	16	24
9	26	22	16	11	40	34	25	16	42	35	26	17	48	48	39	26
10	24	20	16	10	36	30	23	14	38	31	24	16	48	47	35	23
11	22	18	14	9	34	27	21	14	34	29	21	14	48	43	31	21
12	20	16	13	9	30	25	19	13	31	26	20	13	47	39	29	20

The New York State Department of Transportation (NYSDOT) pavement design manual (Bendana et al., 1992) also suggests using the subgrade drag equations as the basis for tie bar design. On the basis of this theory, and with the assumption of using Grade 60 steel and a working stress equaling two-thirds the yield strength of steel, the manual presents design plots for tie bar spacing (see Figure 5). The assumed friction coefficient values are not indicated in the manual.

The Florida DOT pavement design manual (FDOT, 2006) tie bar design tables also are based on the SDT but with the following assumptions:

- Total embedded length—25 in for #4 bar and 30 in for #5 bar.
- Tie bar allowable working stresses—30,000 psi (Grade 40 steel).
- Coefficient of friction—1.5.

Using these assumptions, the required tie bar spacings for various combinations of concrete slab thicknesses, distance to free edge, and tie bar diameters were computed and used for design (see Table 2 and Table 3).

Table 2. Florida DOT maximum tie bar spacing for a #4 bar per the SDT (from FDOT, 2006).

H_{PCC}, in	Distance to Free Edge, ft		
	12	14	24
6	24	24	24
7	24	24	22
8	24	24	19
9	24	24	17
10	24	24	15
11	24	24	14
12	24	22	13
13	24	21	12
14	22	19	11
15	21	18	10

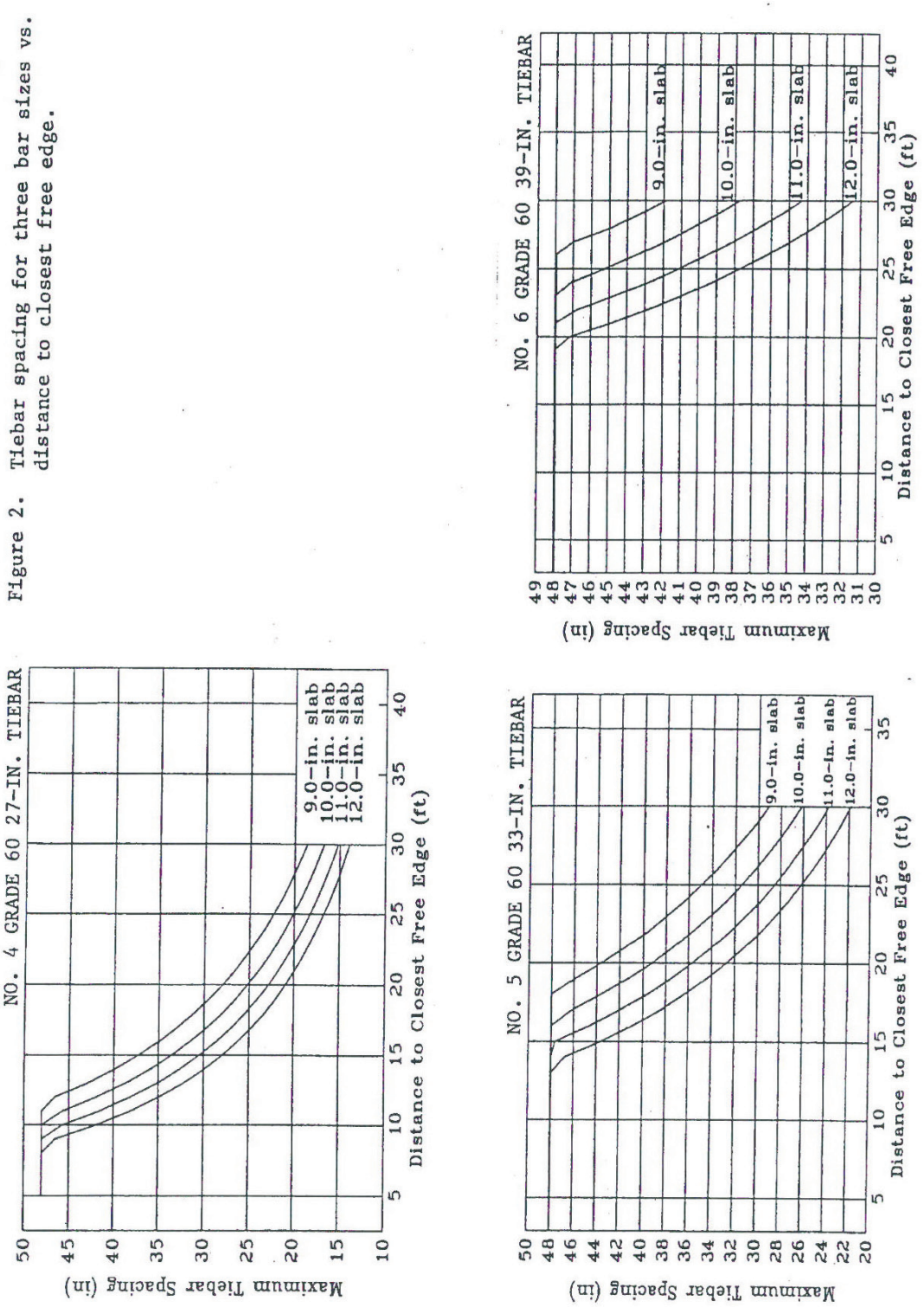

Figure 5. NYSDOT tie bar spacing for three bar sizes per the SDT (from Bendana et al., 1992).

Table 3. Florida DOT maximum tie bar spacing for a #5 bar per the SDT (from FDOT, 2006).

H_{PCC}, in	Distance to Free Edge, ft		
	12	14	24
6	38	38	38
7	38	38	35
8	38	38	31
9	38	38	27
10	38	38	24
11	38	38	22
12	38	35	20
13	38	32	19
14	35	30	17
15	33	28	16

One common deficiency of all the aforementioned approaches, which is also true of the underlying SDT they employ, is their failure to account for the range of pavement loading in the process of defining the required steel content.

CHAPTER 3. IDENTIFICATION OF FIELD SECTIONS OF INTEREST AND FIELD TESTING

Under this study, researchers collected two types of in-service pavement information related to tie bars. The first type involved gathering anecdotal evidence to (1) identify typical longitudinal joint performance issues that might be predominately attributable to improper tie bar design or construction and (2) determine if tying greater-than-recommended pavement widths increases the likelihood of longitudinal cracking. The second type of information gathered involved the measurement of the longitudinal joint responses in terms of joint opening and joint LTE as a function of cyclical temperature changes.

FIELD REPORTS: LONGITUDINAL JOINT FAILURE MODES AND IMPACT OF TYING MULTIPLE LANES/SHOULDERS ON PAVEMENT DISTRESS

Information on in-service pavement sections that met the following characteristics was sought:

- Category 1 Sites: Pavement sections for identifying longitudinal joint failures primarily attributable to improper tie bar design, construction, or both:
  - The pavement section should have been in service for 10 years or more.
  - The section must have tie bars as part of the original design or rehabilitation.
  - The longitudinal joints within the section should have experienced failures.
- Category 2 Sites: Pavement sections for determining the impact of tying multiple lanes on pavement distress:
  - The pavement section should have been in service for 10 years or more.
  - Sites should have more than three lanes/shoulders tied together.

The purpose of this effort was to:

1. Establish the distresses that could occur at longitudinal joints due to inadequate design or placement of tie bars. This information was used later to establish our recommended tie bar design criteria.
2. Establish any plausible linkage between tying a large number of lanes together and longitudinal cracking distress in pavements.
3. Establish the state of the practice among several agencies with regard to tie bar design.

The information gathered for this activity was obtained through telephone interviews with highway agency and industry personnel who were highly experienced with

concrete pavement design and construction practices related to tie bars. A limited number of site visits also were conducted to observe and record distresses.

Data Collection and Observations

The following information was gathered on the identified sites:

- Number of lanes and concrete shoulders and their widths.
- Longitudinal cracking – extent and location.
- Longitudinal joint "settlements" or shear failures.
- Construction date.
- Truck traffic.
- Longitudinal joint width observation.
- Pavement structural details.
- Tie bar design details.
- Transverse joint design details.

The results of the individual telephone interviews are summarized in Table 4.

As can be noted, the information gathered covered 10 States and 24 sites. Figure 6 through Figure 8 present some longitudinal joint distresses observed at sites in Colorado. The following are some of the key observations based on an examination of the data gathered:

- Excessive openings (Figure 6) and faulting (Figure 7) appear to be the predominant modes of longitudinal joint failures, with the former being more prevalent.
    - The widths of the excessive joint openings often were greater than 1 in, and in some extreme cases they were as much as 4 in.
    - Longitudinal joint faulting greater than ½ in was observed in some locations.
- In some instances, slippage between adjacent slabs has occurred (see Figure 8).
- The longitudinal joint performance was found to be highly variable on the sites studied. Joint performance sometimes ranged from poor to excellent along the same roadway with seemingly similar lane configurations, geometry, and tie bar design, pointing to placement or material variability.
- Of all the sites experiencing joint distress that could be attributed to some aspect of tie bar design or construction, the prevalent tie bar diameter was 5/8 in (or #5 bars). The next most commonly occurring bar diameter was ½ in (or #4 bars). Only one site, which used a ¾ in bar diameter (or #6 bars), experienced a higher than expected longitudinal joint opening. Additionally, typical tie bar spacings were at 30-in centers, but a few sites had tie bar spacings of 24 or 48 in.

Table 4. Longitudinal joint-tie bar system and multi-lane concrete pavement investigation.

State	Site Location (Site Category)	No. of Tied Lanes & Concrete Shoulders (Total tied width)	Construct-ion Date	Traffic Volume	Longitudinal Joint Width	Pavement Structural Details	Tie Bar Design Details	Transverse Joint Spacing	Distresses
CO	Broadway, south of C-470, Douglas Co (Category 1 & 2)	3-12 ft lanes + 8ft. tied shoulder (44 ft)	1981	Average Daily Traffic (ADT) = 34,500	3 to 4 in	7 in JPCP over existing subgrade	#4 bars at 30 in interval	15 ft centers	Longitudinal cracks, minor corner breaks, patches, and settlement
CO	Wildcat Reserve Parkway, south of Grace Blvd (Category 1& 2)	5-12 ft lanes + 2-10 ft shoulders (80 ft)	2002	ADT = 141,447	1 to 2 in at some locations	6-7 in JPCP over natural subgrade	#4 bars at 30 in Interval	15 ft	Severe cracking, excessive longitudinal settlement
CO	Quebec Blvd., north of Timberline (N.B) (Category 1 & 2)	7-12 ft lanes + 2 - 8 ft tied shoulders (100 ft)	1990	ADT= 29,475	1 to 2 in at some locations	6-7 in JPCP over natural subgrade	#4 bars at 30 in interval	15 ft	Longitudinal cracks, minor corner breaks, patches, and settlement
CO	Quebec Blvd., south of Collegiate (N.B) (Category 1 & 2)	7-12 ft lanes + 2 -8 ft tied shoulders (100 ft)	1990	ADT= 29,475	1 to 2 in at some locations	6-7 in JPCP over natural subgrade	#4 bars at 30 in Interval	15 ft	Moderate longitudinal cracking, corner breaks
CO	SH 119, south of US 287 (Category 1)	2-12 ft lanes, curb & cutter (24 ft)	1983	ADT = 32,300 (%Trucks = 5.2)	1 to 2 in	8 in JPCP over class 6 materials (DGAB)	#5 bars at 30 in Interval	random at 12 to 20 ft	Moderate longitudinal cracking, corner breaks
CO	Quebec Blvd., north of Ashburn Lane (S.B) (Category 1 & 2)	3-12 ft lanes + 8 ft shoulder (44 ft)	1990	ADT= 29,475	1 to 2 in at some locations	6-7 in JPCP over natural subgrade	#4 bars at 30 in Interval	15 ft	Longitudinal cracking, corner spalling
CO	US 287, north of Fort Collins (Category 1)	1-12 ft NB + 10 ft shoulder (22 ft)	1991	ADT = 7,600 (%Trucks = 15.1)	Over 1 in	9 in JPCP over DGAB	#5 bars at 30 in Interval	15 ft	Minor distresses
CO	University Ave., west of Quebec (WB) (Category 1 & 2)	7-12 ft lanes + 2 - 8 ft tied shoulders (100 ft)	1989	ADT= 30,996	2 in at some locations	6-7 in JPCP over natural subgrade	#4 bars at 30 in Interval	15 ft	Longitudinal cracking, spalling,
CO	I-25, MP 152-153 (Category 1)	2-12 ft lanes SB + 10 ft & 4 ft tied shoulders (38 ft)	1987	ADT= 71,600 (%Trucks = 11.7)	1 in	7 in unbonded JPCP/chip seal/8 in JPCP	#5 bars at 30 in. interval	15 ft	Full depth longitudinal cracking, corner breaks, patches and settlement

DGAB = dense graded aggregate base.

Table 4. Longitudinal joint-tie bar system and multi-lane concrete pavement investigation, continued.

State	Site Location (Site Category)	No. of Tied Lanes & Concrete Shoulders (Total tied width)	Construct-ion Date	Traffic Volume	Longitudinal Joint Width	Pavement Structural Details	Tie Bar Design Details	Transverse Joint Spacing	Distresses
IL	I-39 near El Paso (Category 1)	2-12 ft lanes SB + AC shoulder (24 ft)	1992	Average Daily Truck Traffic (ADTT) = 6,550	Approx. 1 in	10 in CRCP/4 in permeable CTB (PCTB)	#5 bars at 30 in interval	N/A	Longitudinal cracks, settlement, patching
IL	I-80 near Morris (Category 1)	2-12 ft lanes EB + 10 ft tied shoulder (34 ft)	1993	ADTT = 11,500	1 in	11.5 in CRCP/4 in PCTB	#5 bars at 24 in interval	N/A	Longitudinal cracks, settlement, patching
KS	K96 North of Yoder (Category 1)	2-12 ft lanes with 10 ft and 4 ft tied shoulders (38 ft)	1998	ADT =6,216 (%Trucks = 16.4)	1 to 2 in	10 in JPCP/cement or lime treated base	#5 bars at 30 in interval	15 ft	Moderate longitudinal cracking and spalling, faulting
KS	K-96 at Greenwich Rd ramp (Category 1)	2-12 ft. lanes with 10 ft and 4 ft tied shoulders (38 ft)	1993	ADT= 19,850 (%Trucks = 5.1)	1 to 2 in	10 in JPCP/cement or lime treated base	#5 bars at 30 in interval	30 ft	Moderate longitudinal cracking and spalling
MO	SH 71 NB ramp to I-470 EB (Category 1)	2-12 ft. lanes + 2 -10 ft. tied shoulders (44 ft)	2003	N/A	3 to 7 in	14 in JPCP/24 in rock base	#6 at 30 in, may be missing	15 ft	Fill subsidence
NV	US 95 (Category 1)	4-12 ft lanes + 4ft and 10 ft concrete shoulders (34 ft)	1985-1990	Equivalent Single Axle Load (ESAL) = 15-20 million	2 in	10 in JPCP/CTB	#4 bars at 30 in interval	random at 12, 13, 16 & 18 ft	Corner breaks, transverse and longitudinal cracking
PA	SR 0080, Seg. 2283, Columbia County (Category 1)	2-12 ft lanes with 4 ft and 10 ft shoulders (38 ft)	1993	ADT= 15,452 (%Trucks = 30)	Normal	13 in JPCP/4 in unbound drainable base/4 in No. 2A unbound subbase	#5 bars at 30 in interval	15 ft	Minimal transverse cracking and joint spalling

Table 4. Longitudinal joint-tie bar system and multi-lane concrete pavement investigation, continued.

State	Site Location (Site Category)	No. of Tied Lanes & Concrete Shoulders (Total tied width)	Construct-ion Date	Traffic Volume	Longitudinal Joint Width	Pavement Structural Details	Tie Bar Design Details	Transverse Joint Spacing	Distresses
PA	SR 0081, Seg. 0775, Dauphin County (Category 1)	2-12 ft lanes with 4 ft and 10 ft shoulders (38 ft)	1995	ADT= 30,646 (%Trucks = 28)	Normal	14 in JPCP/4 in granular base/10 in rubbilized concrete/11 in granular subbase	#5 bars at 30 in interval	15 ft	No cracking distress.
SD	I-29, north of Brookings & south of Watertown (Category 1)	2-12 ft lanes, + 4 ft and 10 ft shoulders (38 ft)	1978	ADT = 3,385 (%Trucks = 22)	¾ to 1 in	9½ in JPCP/3 in lime treated base	#5 bars at 48 in interval	random at 13 to 19 ft	D-Cracking, corner breaks, minor transverse cracking
SD	US 16 at milepost 40, near Hill city (Category 1)	2-12 ft lanes + 4 ft and 10 ft shoulders (38 ft)	1985	ADT = 5,200 (%Trucks = 9.1)	¾ in	8 in JPCP/ 8 in granular base (Dowel Retrofit)	#5 bars at 48 in interval	random at 13 to 19 ft	Minor transverse and longitudinal cracking
SD	SD 12 at milepost 263-274 (Category 1)	2-12 ft lanes + 2 -11 ft tied shoulders (46 ft)	1974	ADT = 2,583 truck = 484	Normal	7in JPCP/4 in lime-treated gravel	Unknown	random at 13 to 19 ft	Some faulting, extensive longitudinal cracking
SD	SD 10 in Britton (Category 1)	2-12 ft lanes + 4 ft and 10 ft shoulders (38 ft)	2004	ADT = 2,243 (%Trucks = 7.7)	Normal	8 in. JPCP/ 8 in granular base (Dowel retrofit)	Unknown	random at 13 to 19 ft	Minor transverse and longitudinal cracking
UT	I-80 near Foothill Blvd. (Category 1)	2-12 ft lanes with asphalt shoulders (24 ft)	1966	AADTT = 10,000 (approx)	4 in	7 in JPCP/ 8 in unbound base	Unknown	random spacing at 11 to 17 ft	Broken slabs, corner breaks, faulting (corrected by grinding in 2003)

Table 4. Longitudinal joint-tie bar system and multi-lane concrete pavement investigation, continued.

State	Site Location (Site Category)	No. of Tied Lanes & Concrete Shoulders (Total tied width)	Construct-ion Date	Traffic Volume	Longitudinal Joint Width	Pavement Structural Details	Tie Bar Design Details	Transverse Joint Spacing	Distresses
VA	Route 460 Appomattox by-pass, near the town of Appomattox in Lynchburg (Category 1 & 2)	3-12 ft lanes + 2 -10 ft tied shoulders (48 ft)	1993	ADT = 13,000 (%Trucks = 10)	Normal	9 in. JPCP/4 in. AASHTO #57 PCTB/6 in soil cement	#5 bars at 30 in Interval	15 ft	No longitudinal cracks
WY	I-80, MP 20-28 (Category 1)	2-12 ft lanes WB + 10ft and 4 ft tied shoulder (38 ft)	1988	ADT = 6,300 (% Trucks = 48)	1 to 1½ in	10½ in. JPCP over hot-mix asphalt (HMA) base	#4 bars at 24 in interval	Random at 16, 18, 15 & 14 ft	Minor distresses

Figure 6. Excessive joint openings on Broadway Avenue (left) and Howe Street (right) in Douglas County, Colorado.

Figure 7. Longitudinal joint faulting on I-25 (left) and Wildcat Reserve Parkway (right) in the Denver area.

Figure 8. Slab slippage due to inadequate design or placement of tie bars between adjacent lanes on Broadway Avenue in Douglas County, Colorado.

- The total tied widths for the projects included in the survey ranged from 22 ft (one lane with a tied shoulder) to 100 ft (seven lanes with tied shoulders). Longitudinal cracking was noted on pavements of varying widths and was not necessarily confined to those with greater-than-recommended pavement widths tied together.

It is clear that the current state of the practice for tie bar design (i.e., to use #5 bars at 30-in centers) is not adequate to prevent excessive joint openings in all cases. Inadequate design or poor construction practices are plausible causes for several of the observed joint failures. The distress information collected via the telephone interviews and site visits was not to a level of detail that allowed definite conclusions to be drawn regarding the role of tying several lanes together on propagating longitudinal cracking. Although it might have been a contributing factor, based on past research performed by Colorado DOT which nominated all the 100 ft wide pavements surveyed, many other pavement site, design or construction factors (e.g., shallow saw cuts, malfunctioning of vibrators, poor compaction and swell potential of the subgrade) could have contributed to the observed cracking (Ardani et. al, 2003). The investigation of these factors to ascertain the exact causes of the distress for the pavements surveyed was beyond the scope of this research effort. However, considerations to mitigate stress build-up from uniform contraction of tied concrete slabs are discussed in Chapter 6 of this report.

FIELD TESTING TO DETERMINE LONGITUDINAL JOINT RESPONSE

As was noted earlier, excessive joint opening and the resultant loss of load transfer is the dominant mechanism by which longitudinal joints fail. Therefore, a deeper understanding of this aspect of joint behavior is important. It is surmised that joint openings are driven largely by environmental forces such as cyclical temperature changes and pavement shrinkage (other factors, such as foundation movements on slopes, can influence this behavior, but they are not considered herein). One of the major challenges in advancing theoretical modeling of tie bars is a lack of field data to understand the impact of environmental factors on longitudinal joint openings and load transfer. In this study, the movements and LTE of longitudinal joints were measured simultaneously as a function of temperature change on in-service highway pavements in three different locations. Each location had multiple sites representing different JPCP slab thicknesses, tie bar configurations, base types, and slab widths. The measurements at each location were recorded over several hours, starting in the early morning, when the joint is open the widest, and proceeding until mid-afternoon, when the joint is fully locked. Although this was a short-term monitoring study and did not consider the seasonal impacts on joint openings, it nevertheless helped establish trends which were useful in shaping the analytical modeling approach and design methodology developed.

Site Selection

An ideal site to conduct the testing for this project was determined as one which affords side-by-side comparison of longitudinal joint performance of pavements with and without tie bars at lane-lane and lane-shoulder joints built on a variety of base types. The long-term pavement performance (LTPP) Specific Pavement Studies 2 (SPS-2) national and supplemental experimental sections in some States come close to satisfying these criteria. However, considering several practical project-related factors, such as prevailing weather patterns during the window of opportunity available to the researchers for testing (cool nights and warm days are desirable for joint opening measurements), traffic volumes and operational issues at the sites to be tested, the willingness of highway agencies to participate and provide logistical and traffic control support, availability of crews for traffic control and costs of testing, and so on, the project team could test three sites that accommodated the ideal site criteria inasmuch as possible. The sites tested were:

- The Arizona LTPP SPS-2 experiment on I-10 east of Pheonix, AZ.
- Missouri DOT Highway 412 east of Kennet, MO.
- Colorado DOT US 40 east of Hugo, CO.

Descriptions of the testing performed at each site are presented later in this section.

Data Collection Plan

The following information was collected at each site:

- Falling Weight Deflectometer (FWD) deflection measurements at the lane/shoulder or lane/lane joint at various times during the day. In most instances, it was only possible to test the lane/shoulder joint due to traffic control issues.
- Width of the longitudinal joints at various times during the day (coinciding with the deflection measurements).
- Subsurface concrete temperature at different depths (1 in below the surface, mid-depth of concrete layer, and 1 in from the bottom of the concrete layer) at various times during the day (also coinciding with the deflection measurements).

In addition, a MIT Scan device was used at all sites to locate the tie bars. At the Colorado site, it also was used to detect the position and alignment of the tie bars.

Anywhere from 3 to 15 rounds of testing were conducted at each site.

Test Methods

Falling Weight Deflectometer Testing

The FWD testing for this project involved configuring the device to perform longitudinal joint LTE testing. For this purpose, a side sensor was specially configured to measure deflections across the longitudinal joint. The deflection testing was completed by placing the load plate tangential to the longitudinal joint and applying the load on one side of the joint (usually at the edge of the outside or driving lane). The resulting deflections at the center of load plate and across the joint were measured and recorded to compute the deflection LTE. The standard LTPP load sequence for rigid pavement testing, shown in Table 5, was followed:

Table 5. LTPP FWD loading sequence for longitudinal joint LTE testing.

FWD Drop Position Number	#of Drops	Target Load, lb	Acceptable Range, lb
2	4	9,000	8,100 to 9,900
3	4	12,000	10,800 to 13,200
4	4	16,000	14,400 to 17,600

Figure 9 and Figure 10 show the FWD positioned to test longitudinal joint LTE at the lane-shoulder joint. The Dynatest FWD equipment was used at the Arizona and Missouri test sites, and JILS equipment was used at the Colorado site because Colorado DOT conducted all the FWD testing at that site.

Longitudinal Joint Movement Measurement

Joint movement measurements were taken in general accordance with the LTPP Seasonal Monitoring Program: *Instrumentation Installation and Data Collection Guidelines* (FHWA, 1994). The guidelines involve drilling ½-in diameter holes on both sides of the joint at mid-length and near the ends of the joint, placing ½-in high modulus steel snap rings in the holes below the pavement surface, and measuring the joint movement using a digital caliper. Figure 11, taken from the referenced LTPP guidelines, illustrates a typical snap ring set up at a joint.

For this project, joint movements were measured at each location with a +/- 0.39 mils precision electronic digital caliper. The snap rings improve repeatability and accuracy of the measurement by providing a sharp edge for the caliper jaws to touch each time a measurement is taken. The reported joint movement is the average value of the three measurements from the mid-length and near the ends of the joint. Carbon blocks of known widths were used as standards and were checked with the calipers periodically to ensure calibration.

Figure 9. FWD configured for longitudinal joint LTE testing.

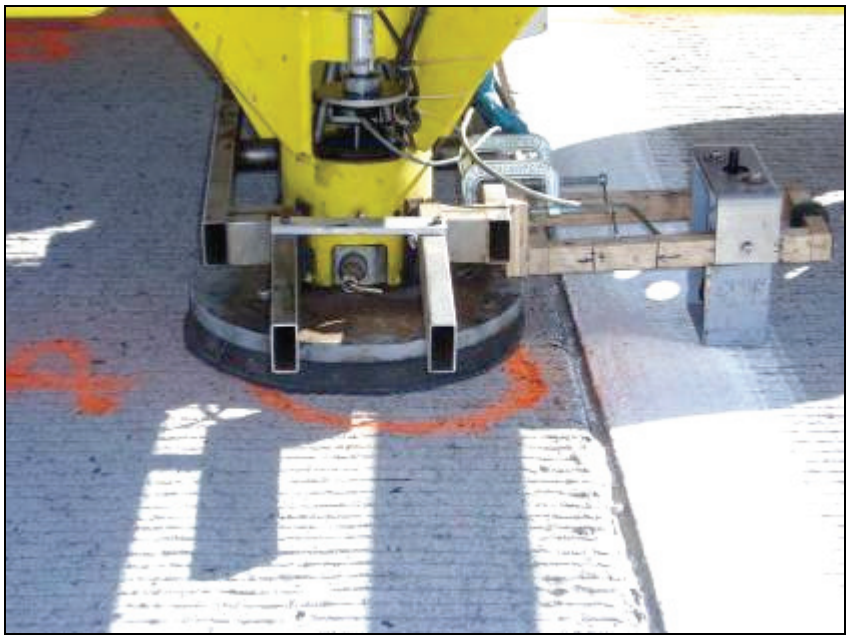

Figure 10. Close-up of FWD load plate and side sensor.

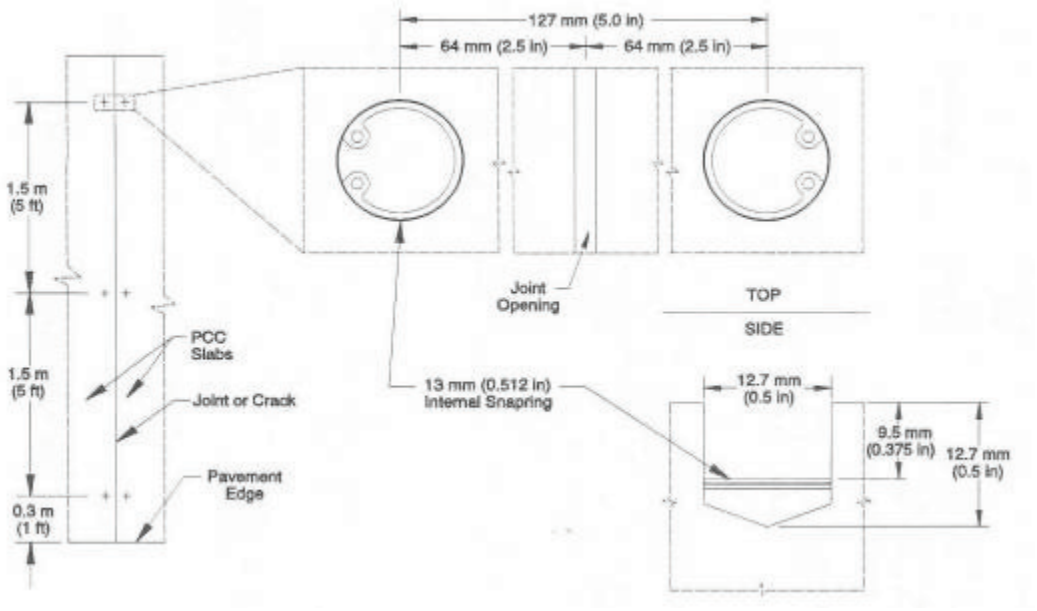

Figure 11. Schematic of a snap ring testing set up across a joint in a concrete pavement.

Pavement Temperature Measurement

For pavement temperature monitoring during testing, three ½-in diameter holes were drilled for each joint location near the center of the concrete slab at the depths indicated in the section titled "Data Collection Plan." After drilling was completed, the holes were cleared of dust and 0.07 oz of mineral oil measured with an oral syringe was dispensed into them to provide thermal conductivity between the pavement and the temperature probe. Temperatures were taken with a +/- 0.18 °F k-type digital probe at the same time the joint measurements were taken. The mid-depth temperature was used for data analysis. The top and bottom slab temperatures were used for error checking the mid-depth slab temperatures.

MIT Scan Testing

MIT Scan testing was conducted to determine the tie bar position relative to the longitudinal joint being tested. The MIT Scan measuring process involves setting rails on the joint to be scanned, entering the pavement information such as concrete thickness and tie bar size into the on-board computer, and then pulling the unit along the joint. During testing, the device emits a weak, pulsating magnetic signal and detects the transient magnetic response signal induced in the metal tie bars. Methods of tomography are used to determine the position and/or alignment of the tie bars. This information is used in the field to guide FWD testing and also can be used for analysis (as was done at the Colorado site). Figure 12 illustrates MIT Scan testing of a transverse joint for dowel bar detection.

Figure 12. Pulling the MIT Scan device along the rail system.

Site-by-Site Summary of Field Testing, Test Data, and Observations

Arizona Test Site

As indicated earlier, the Arizona test site is from the LTPP SPS-2 study. The eight test sections located at this test site are in the eastbound lanes of rural Interstate 10, east of Phoenix. Figure 13 shows the section details. These sections have been open to traffic since 1993 (approximately 15 years of service at the time of testing).

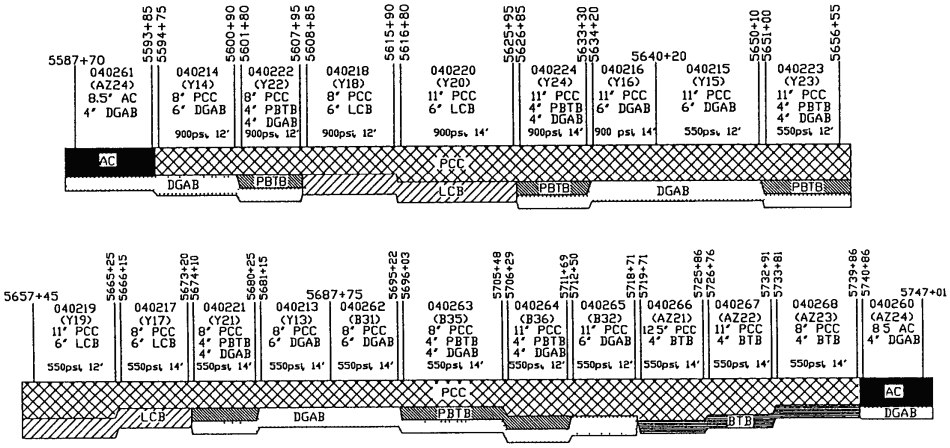

AC = asphalt concrete; PCC = portland cement concrete; PATB = permeable ashpalt-treated base; BTB = bituminious treated base

Figure 13. Layout of the Arizona LTPP SPS-2 section identifying the section extents, cross-section, lane widths, and concrete strength.

Joint movement measurement and FWD testing were initially conducted on sections 214. 215, 218, 219, 223, 267, and 268 in January 2008. In March 2008 sections 214 and 218 were revisited to collect additional joint movement data because the first round resulted in highly suspect data (joint movements in excess of 2 mm). During this visit, joint movements on section 222 were also collected. No corresponding FWD data were collected for these sections. For these field visits, the Arizona DOT provided traffic control. Details of each section tested are presented in Table 6. As can be noted, the tied longitudinal joints between the two eastbound lanes (lane/lane joint) were tested for the majority of the sections. On some sections, the untied joint between the lane and the outside shoulder also was tested for comparison purposes. The LTE and joint movement data as a function of temperature from this site are presented in Figure 14 and Figure 15. Figure 16 presents a plot of longitudinal joint LTE versus joint movement.

Table 6. Arizona SPS-2 section details.

SPS-2 section ID, Lane Width	Concrete Thickness	Base	Tied or untied joint/Tie Bar Details	Joint tested	Joint distresses
04214, Standard	8 in	DGAB	Untied	Lane/shoulder	Lane/Shoulder Faulting >0.75 in; Joint opening >1-in; Interconnectig surface cracking
04215, Standard	11 in	DGAB	Tied/#5 bars, 24 in long @30 in spacing	Lane/lane	No distress
04218, Standard	8 in	LCB	Untied	Lane/shoulder	Minor loss of adhesion
04219, Standard	11 in	LCB	Tied/#5 bars, 24 in long @30 in spacing	Lane/lane	No distress
04222, Standard	8 in	PATB	Untied	Lane/shoulder	No distress
04223, Standard	11 in	PATB	Tied/#5 bars, 24 in long @30 in spacing	Lane/lane	No distress
04267, Widened	11 in	BTB	Tied/#5 bars, 24 in long @30 in spacing	Lane/lane	No distress
04268, Widened	8 in	BTB	Tied/#5 bars, 24 in long @30 in spacing	Lane/lane	No distress

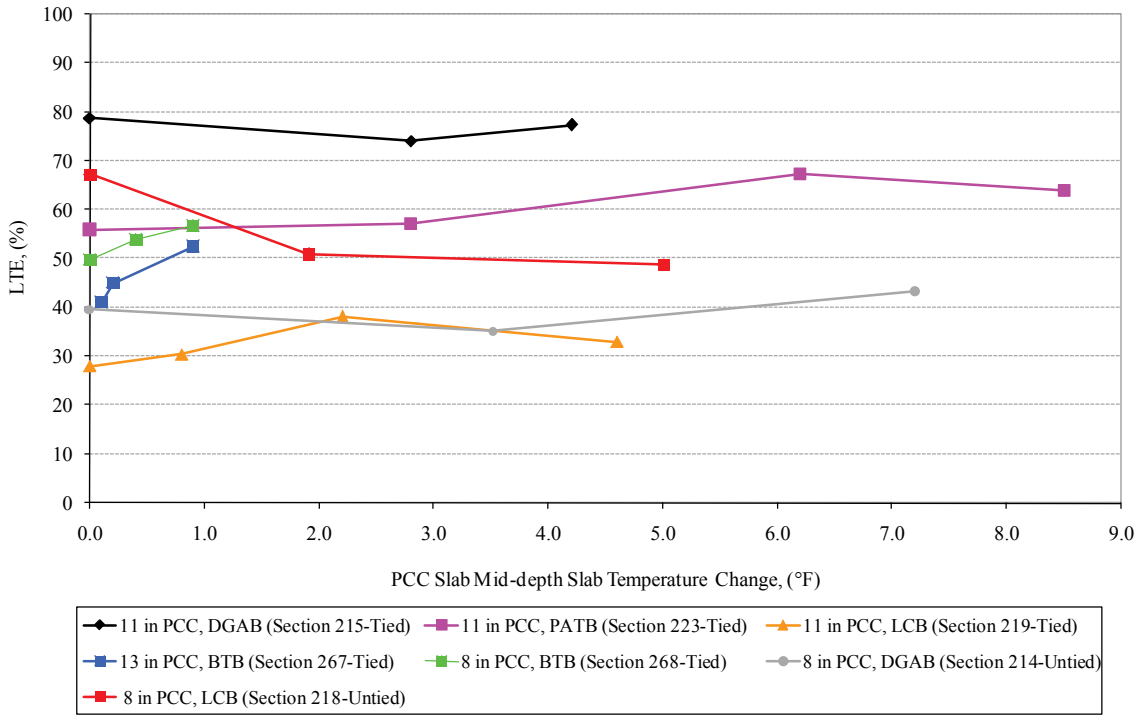

Note: LTE data not collected for section 222.

Figure 14. Arizona SPS-2 longitudinal joint LTE versus temperature.

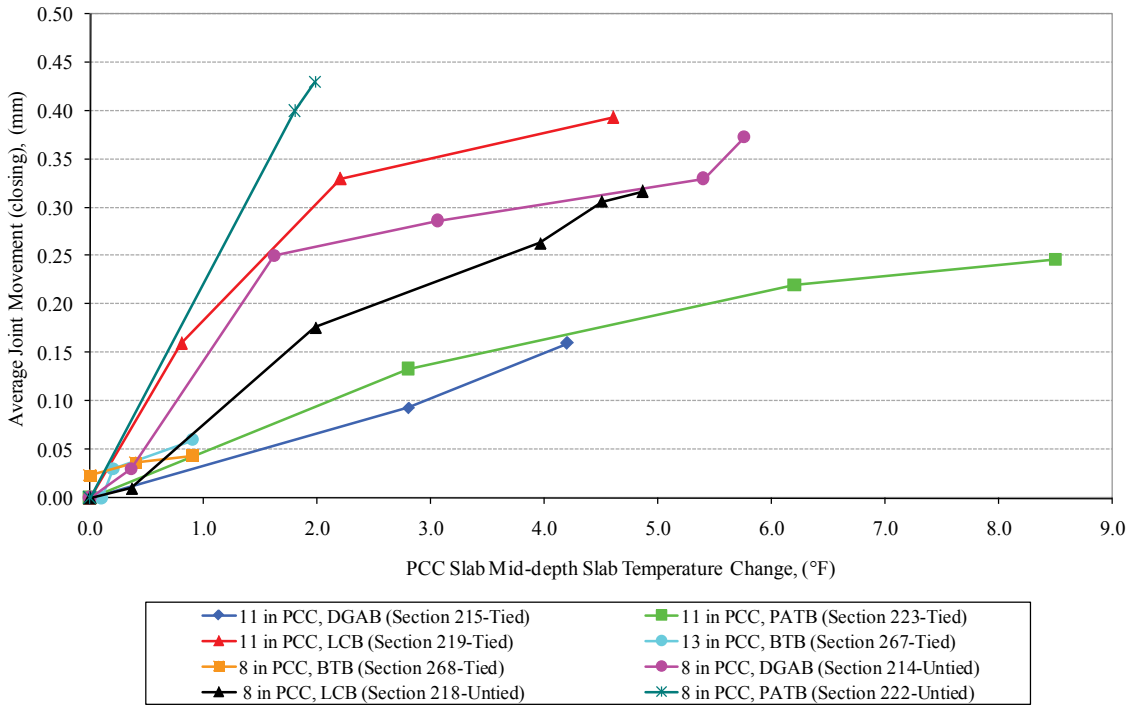

Figure 15. Arizona SPS-2 longitudinal joint movement versus temperature.

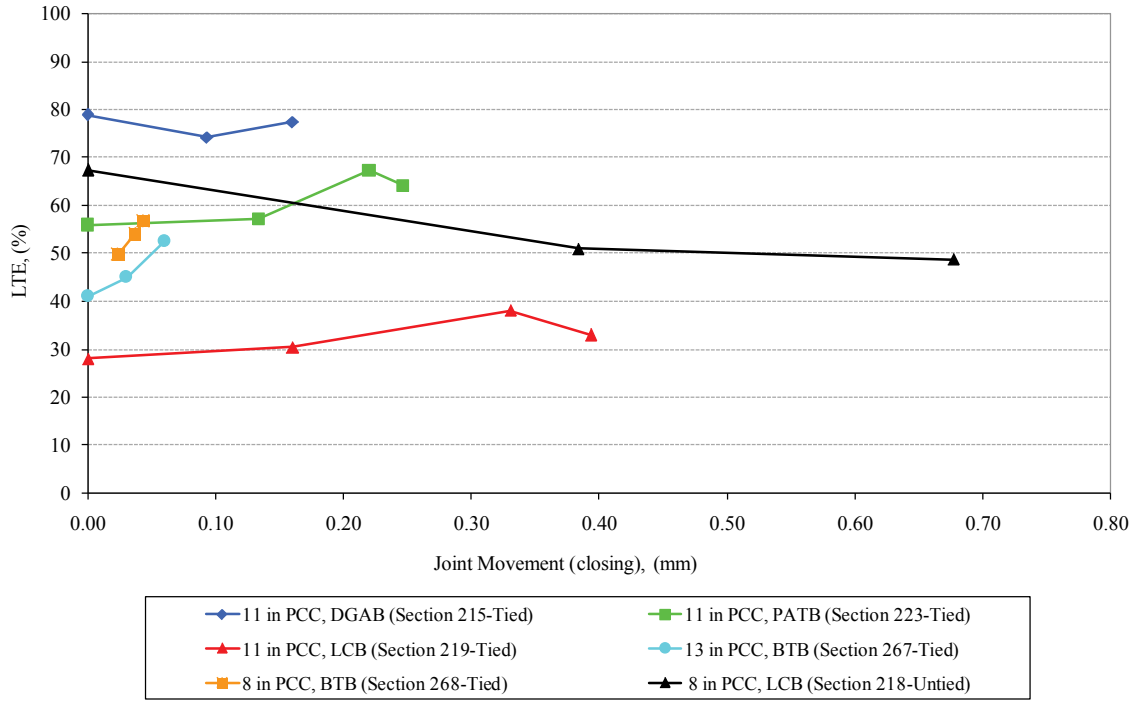

Figure 16. Arizona SPS-2 longitudinal joint LTE versus joint movement.

As can be noted from the data presented, the joint movements and LTE were measured over a relatively narrow range of mid-depth slab temperature change (8.5 °F). The ambient temperature change over the monitoring period was approximately 20 °F. The following general observations can be made from the collected data:

- An analysis of the long-term LTE data (Figure 14) suggests the following:
  - LTE does not change significantly as a function of temperature for any section.
  - In general, untied joints exhibit lower deflection LTE, as expected (in the range of 40 to 50 percent), than tied joints (in the range of 50 to 80 percent). Section 219, which is a tied joint and perhaps the strongest cross-section, showed the lowest LTE of all sections. The causes for this anomalous finding were not investigated.
- An analysis of the joint movement data (Figure 15) suggests the following:
  - As expected, the untied longitudinal joints generally show greater movement than the tied joints. The maximum joint movement recorded was approximately 0.018 in for the untied longitudinal joint on Section 222 for a mid-slab temperature change of only 2 °F. The least joint movement recorded was 0.010 in for the tied longitudinal joint on Section 215 for a mid-slab temperature change of 8.5 °F. The exception to this general trend was Section 219, which is a tied joint that exhibited greater than expected joint movement.
  - The untied joints generally show greater sensitivity to changes in temperatures in terms of joint movements (greater slope on the joint movement versus temperature change plot) than untied joints.
  - Within the untied sections, the section with the PATB recorded the greatest movement and the LCB the least over the same range of temperature change. The DGAB section's joint movement was bracketed by these two sections. If it is assumed that the PATB section is the most pliant (least stiff) of all sections, this pattern falls along expected lines.
  - Judging from the data for Sections 267 and 268, the slab thickness appears to have a very small impact on joint movement.
- No appreciable trends were noted between LTE and joint movement.

Missouri Test Site

Two test sections on Missouri rural highway 412 (westbound) east of the town of Kennett were selected for testing. The sections were less than 5 years old at the time of testing. One of the sections was designated as a control section and consists of two 12-ft wide lanes, 12 in thick with a 10-ft wide tied (#6 tie bars at 30-in spacing) outside shoulder tapered from 12 in at the lane to 6 in at the outer edge. The other section was designated as a test section and was approximately 100 ft away from the control section and of the same slab width, but only 10 in thick with an untied 6-in thick concrete shoulder. Both pavement sections were built on a DGAB.

The joint movement and LTE testing was conducted in March of 2008; Missouri DOT provided traffic control. A total of four lane-shoulder joints were tested—two each from the control and test sections. All the joints were tightly closed and exhibited no lane-shoulder drop-off or faulting. The MIT Scan was used to determine tie bar locations during data collection. Figure 17 shows the Missouri site with the FWD positioned for testing.

Figure 17. FWD testing of one of the sections at the Missouri test site.

The LTE and joint movement data as a function of temperature from this site are presented in Figure 18 and Figure 19. Figure 20 presents a plot of longitudinal joint LTE versus joint movement.

As can be noted from the data presented for the Missouri site, the joint movements (closing) and LTE were measured over a moderate range of cyclical mid-depth slab temperature change (14 °F). The ambient temperature change over the monitoring period was approximately 25 °F. The following general observations can be made from the collected data:

- An analysis of the LTE data (Figure 18) suggests the following:
  - LTE does not change significantly as a function of temperature for any section.
  - As expected, the untied joints exhibited lower deflection LTE (in the range of 30 to 60 percent) than the tied joints (in the range of 80 to 98 percent). This is a significant difference, considering that the pavement sections were relatively new.

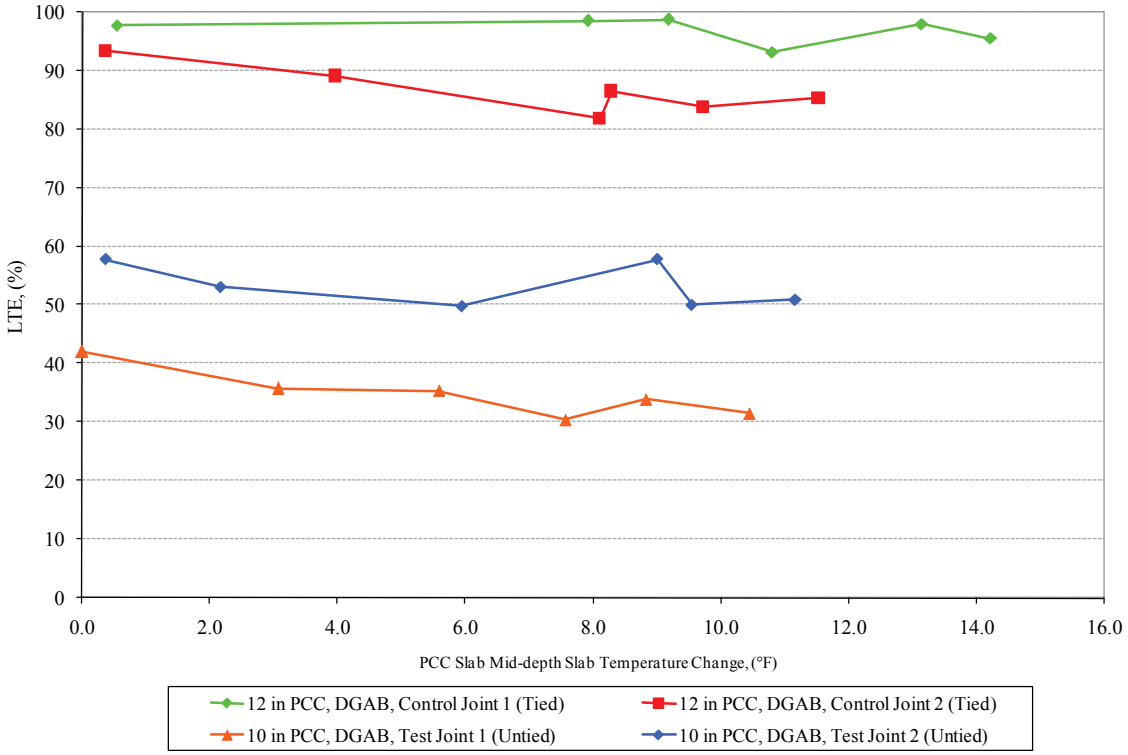

Figure 18. Missouri test site longitudinal joint LTE versus temperature.

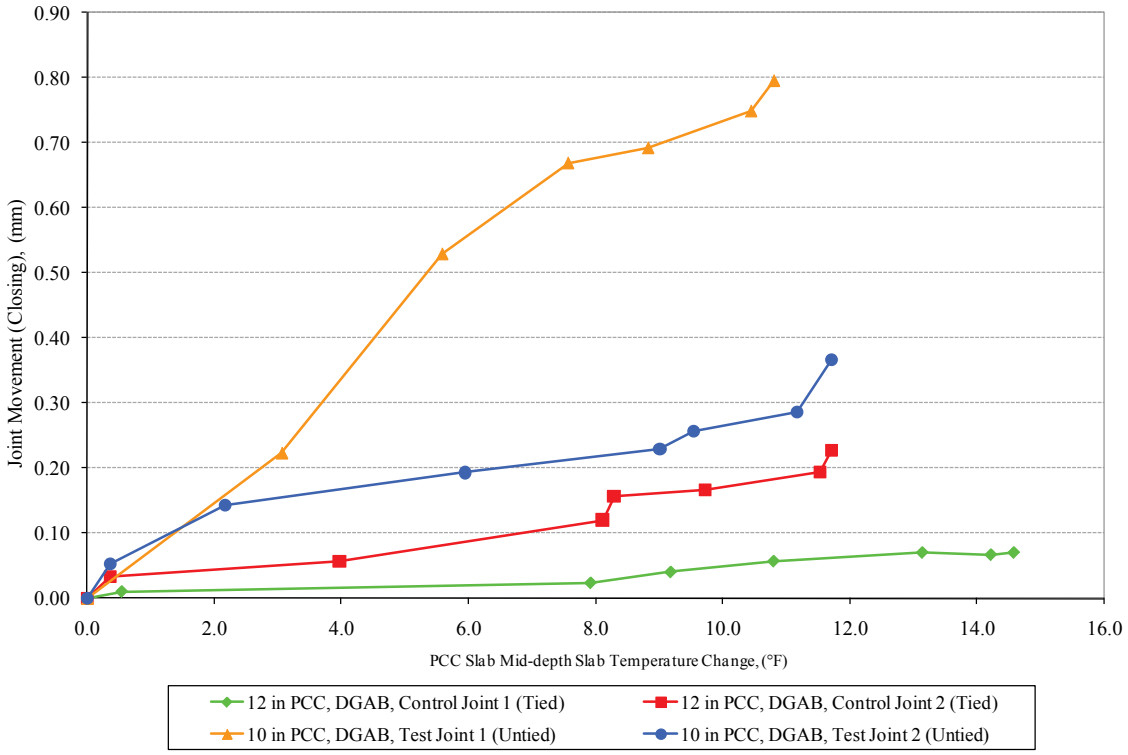

Figure 19. Missouri test site longitudinal joint movement versus temperature.

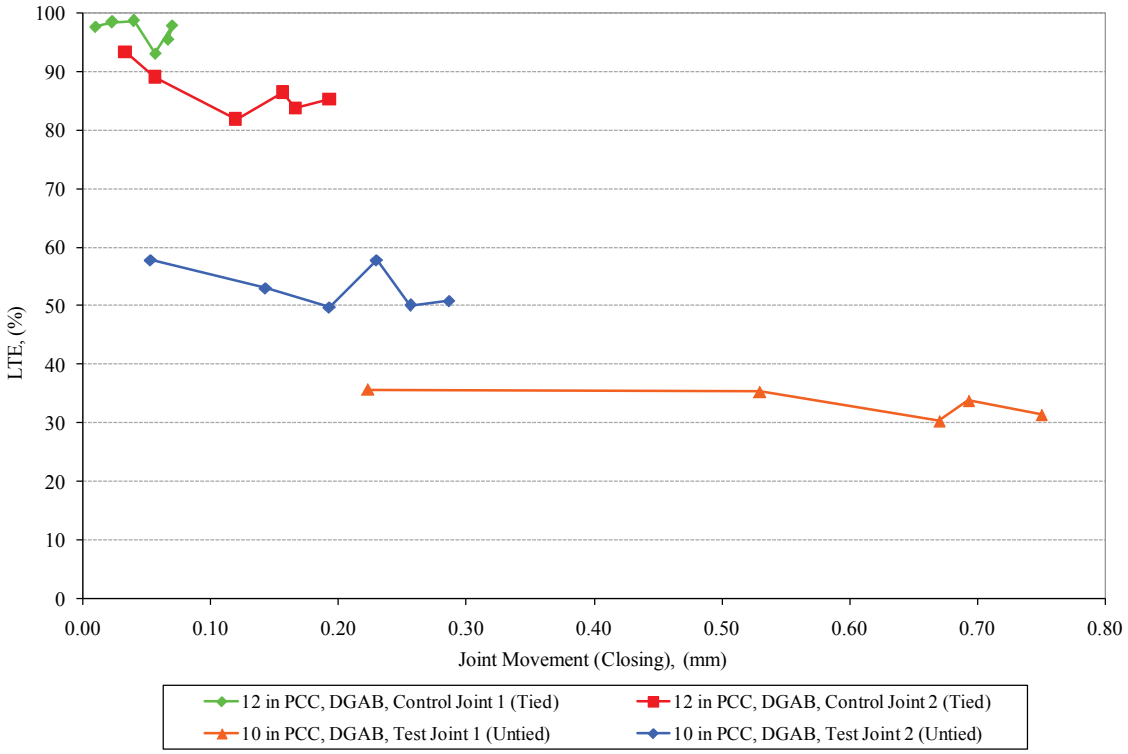

Figure 20. Missouri test site longitudinal joint LTE versus joint movement.

- An analysis of the joint movement data (Figure 19) suggests the following:
  - The untied joints show higher rates of joint movement with temperature and also have higher total joint movements when compared to the tied joints. For example, Test Joint 1 (untied) had a total joint movement of approximately 0.031 in at a temperature change of 11 °F, compared to approximately 0.009 in for Control Joint 2 (tied).
- No appreciable trends were noted between LTE and joint movement.

Colorado Test Site

Testing was conducted on the lane/lane tied joint (# 5 bars, 30 in long placed at 30 in centers) between the two westbound lanes on US 40 just east of the town of Hugo in September 2008. The pavement section consisted of a 9.5-in JPCP, a 7- to 10-in ATB , and a 10-in silty sand subbase. The pavement lane width was 12 ft, and the slab length was 15 ft. Figure 21 shows an overall view of the site and a view of a typical slab layout.

Figure 21. Overall view of the Hugo, Colorado, site and an image showing three temperature holes drilled in the center of the slab and paint marks along the longitudinal joint for FWD positioning.

Three well performing longitudinal joints identified as Control Joints A, B, and C and three joints which opened 1 to 1.5 in designated as Test Joints A, B, and C were selected for testing. Figure 22 shows Control Joint A with a low-severity crack above a tie bar, typical of all joints in the control section. Also shown is Test Joint B with a 1.25-in joint opening and detached sealant.

The MIT Scan was used at this location to determine the tie bar alignment. Tests showed that the mean depth to the tie bars was 3.1 in the Control Joints, shallower than the mid-thickness depth of 4.75 in. Figure 23 shows the alignment of the bars in Control Joints A, B, and C. The MIT Scan also produced blank contour images (not shown) of all three test joints and the MIT scans for these test joints indicated that the tie bars were moderately to severely misaligned.

The LTE and joint movement data as a function of temperature from this site are presented in Figure 24 and Figure 25. Figure 26 presents a plot of longitudinal joint LTE versus joint movement.

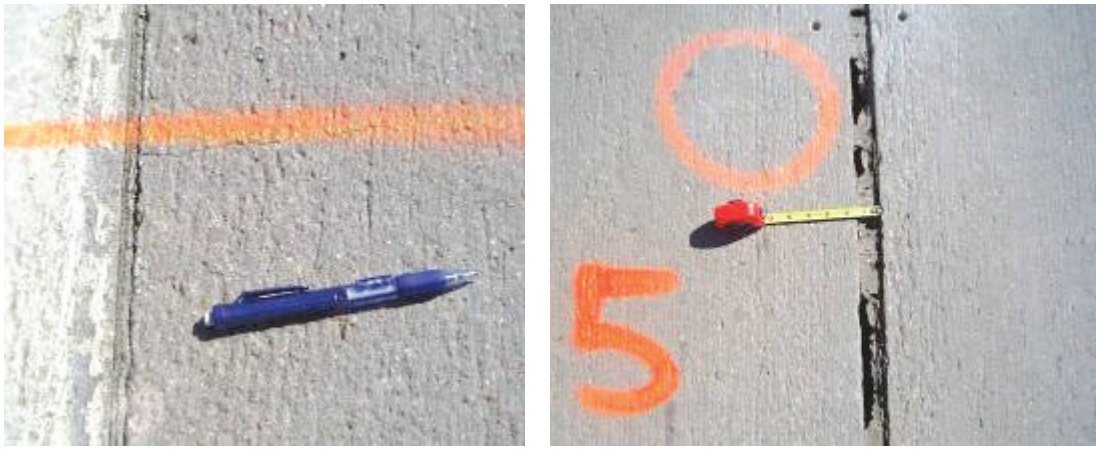

Figure 22. Control Joint A (left) with low-severity crack above a tie bar and Test Joint B (right) open 1.25 in, showing the detached sealant at the Colorado testing site.

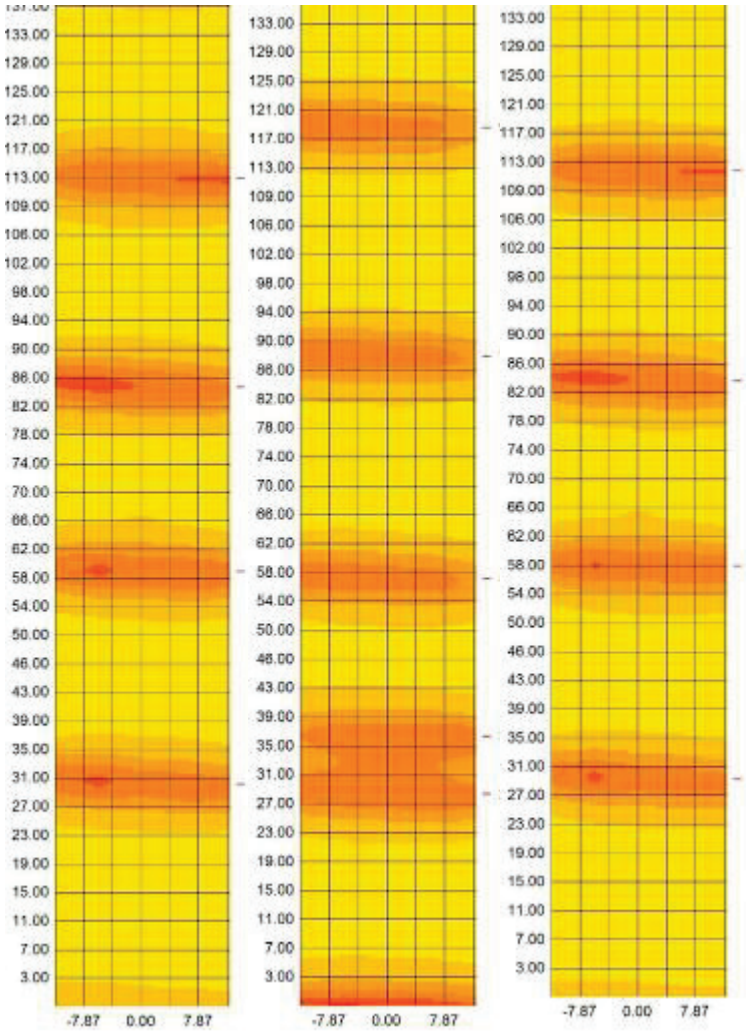

Figure 23. MIT Scan contour images of Control Joints A, B, and C (left to right).

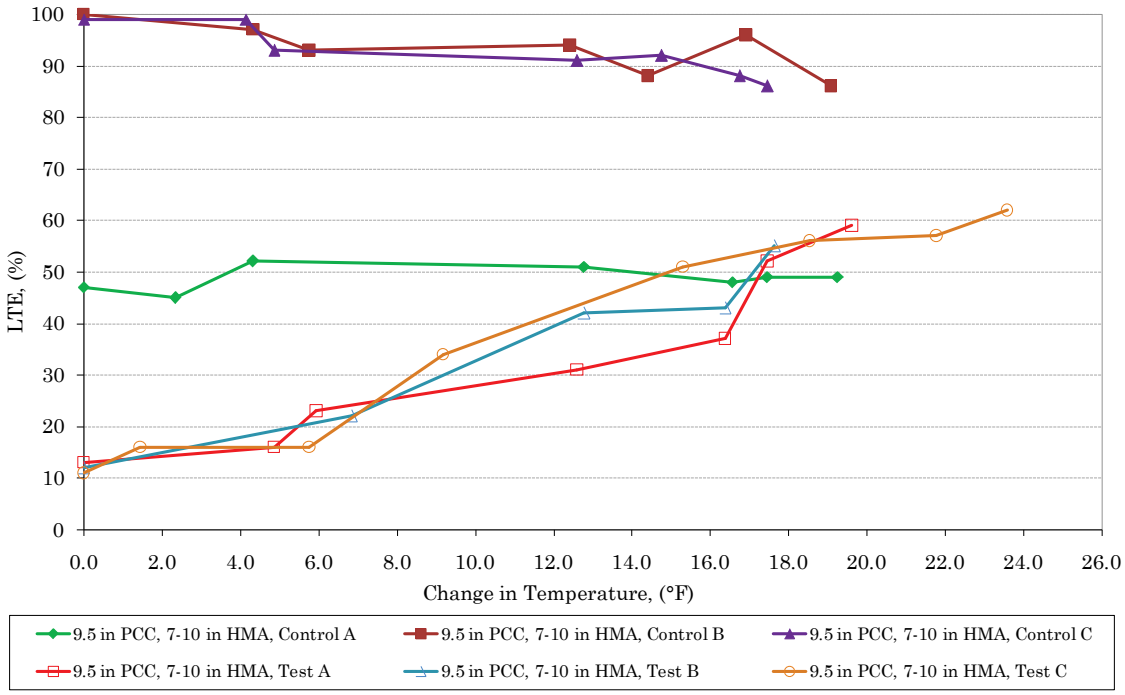

Figure 24. Colorado site longitudinal joint LTE versus temperature.

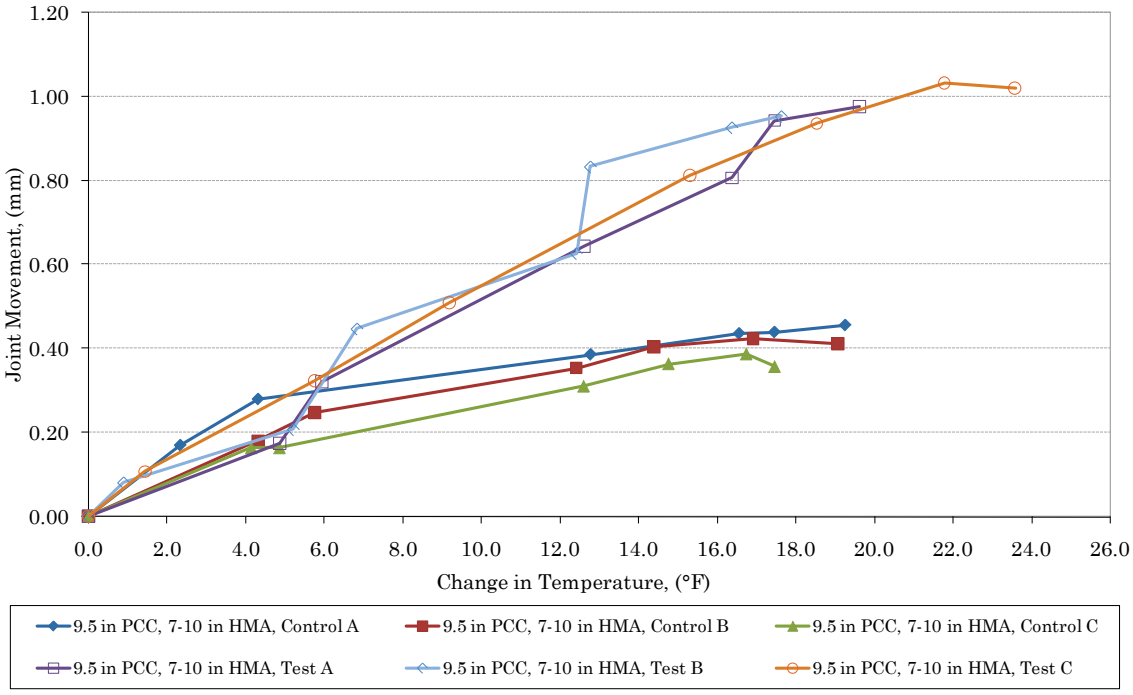

Figure 25. Colorado site longitudinal joint movement versus temperature.

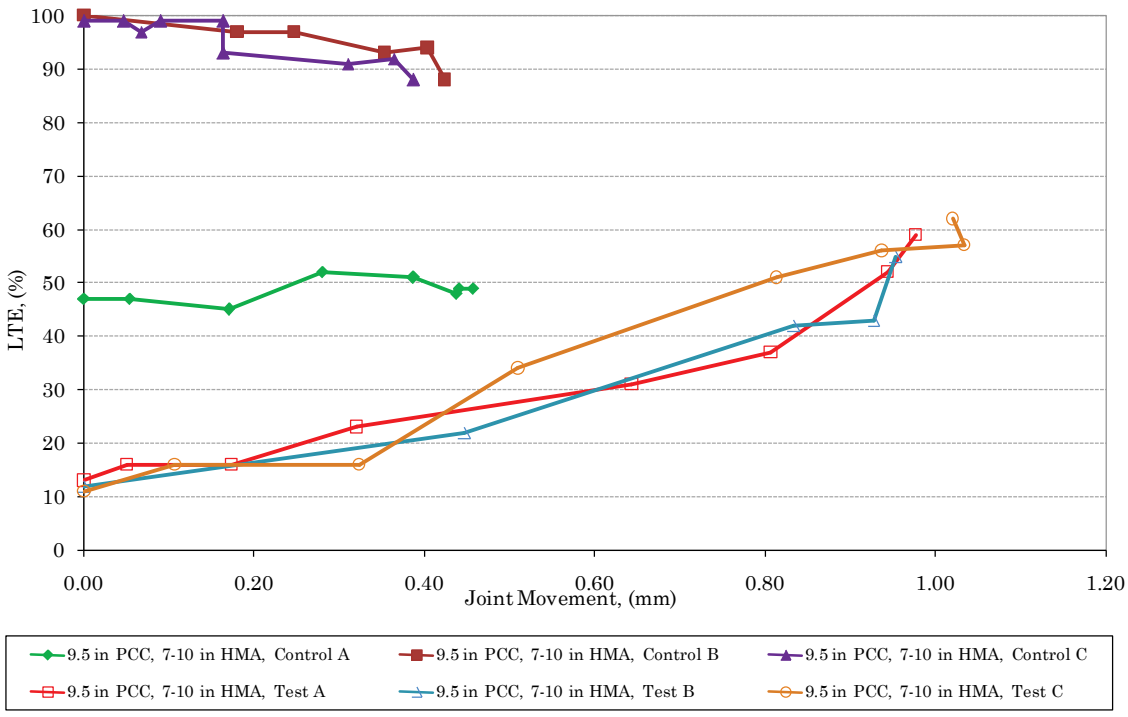

Figure 26. Colorado site longitudinal joint LTE versus movement.

As can be noted from the data presented for the Colorado site, the joint LTE and movement data were collected over a significant temperature range (the mid-depth temperature changed by approximately 24 °F during testing). The ambient temperature change over the monitoring period was approximately 35 °F. The following observations can be made from the collected data:

- An analysis of the LTE data (Figure 24) suggests the following:
  - LTE does not change significantly as a function of temperature for the tied joint (control). However, the LTE increased as the joint closed from an open position for the untied (test) joints, suggesting that aggregate interlock was becoming re-engaged as the joint closed.
  - As expected, the untied joints exhibited lower deflection LTE (ranging from 10 to 60 percent) than the tied joints (50 to 98 percent). This suggests that, in cooler months, the untied joints provide no edge support to the pavement in these test sections.
- An analysis of the joint movement data (Figure 25) suggested the following:
  - The untied joints showed higher rates of joint movement with temperature and also had higher total joint movements when compared to the tied joints. The untied joints moved nearly 0.040 in for a mid-depth concrete slab temperature change of 24 °F, compared to approximately 0.4 mm or 0.016 in movement of the tied joints for a temperature change of nearly 20 °F.

- No appreciable trends were noted between LTE and joint movement for tied joints, but a strong correlation was detected for untied joints.

Summary of Field Testing Observations

The movements of well performing tied joints are small, even when the pavement temperature changed appreciably during any given day. In addition, the joint LTE of well performing joints was high and was not affected appreciably due to the joint movements. Consequently, it can be deduced that the impact of cyclical changes in pavement temperature (or, by extension, seasonal changes in moisture and temperature) on joint performance can be mitigated if the tie bars can be designed to ensure a tight joint.

Construction-related problems came to the fore at one site, which readily explained the unsatisfactory performance of the longitudinal joints.

A factor that may have some impact on joint response is tie bar misalignment (horizontal, vertical or combined). Note that Test Joints A, B, and C, where tie bars could not be detected with the MIT Scan device, showed inferior joint performance compared to a control joint. However, before definitive conclusions can be established vis-a-vis tie bar misalignment and joint movements, a more detailed study needs to be performed.

CHAPTER 4. DEVELOPMENT OF THE MECHANISTIC-EMPIRICAL TIE BAR DESIGN PROCEDURE

INTRODUCTION

This chapter describes the technical development of the proposed M-E tie bar design procedure, as well as providing step-by-step guidance for using the procedure. The M-E based design is applicable to JPCP, CRCP, and jointed reinforced concrete pavements (JRCP) for highways.

This new design procedure is based on fundamental mechanistic principles and uses the ISLAB2005 finite element software (Gotlif et al., 2006) as the basic structural model.

ASSUMPTIONS AND DEFINITIONS

The M-E tie bar design procedure for longitudinal joints is based on the following assumptions:

- The longitudinal joints are held tightly together by deformed steel tie bars.
- The stresses in the steel tie bars are held to the yield stress or less (based on a safety factor as needed) for all designs.
- The joint opening in the maximum opening condition is very low; thus, aggregate interlock will assist in providing significant long-term LTE of the longitudinal joint. (Note that joint opening is not a direct failure criterion).
- Stress in the tie bars is the result of two major components: 1) contraction of the concrete slabs due to the temperature drop from the set temperature and 2) drying shrinkage.
- The number of lanes and shoulders that can be tied together is a function of the allowable transverse tensile stress in the concrete slab. This tensile stress must be limited to avoid the occurrence of longitudinal cracking.

In addition, the procedure was developed with an eye toward using inputs that are practical and easy to obtain.

DESCRIPTION OF THE ANALYTICAL MODEL AND THE RESPONSE DATABASE

The first step in developing the M-E tie bar design procedure was to use an analytical model to develop a database of critical yield stress solutions for several combinations of loading, materials, and pavement structural design inputs. The second step involved using the database as a basis for developing tie bar size and spacing recommendations for a variety of scenarios.

Model Description

The ISLAB2005 model was used to develop the tie bar design database. The concrete pavement with a tied longitudinal joint was modeled as a two-layered slab system on a Winkler foundation (see Figure 27). Further, the slabs are connected to each other using linear elastic springs as shown in the figure. This representation of the system of slabs and slab support is a fundamental shift from the SDT, which models a single slab and assumes that it rests on a rigid base. The assumption of a rigid layer for the base has many important consequences, which will be discussed in later sections of this report.

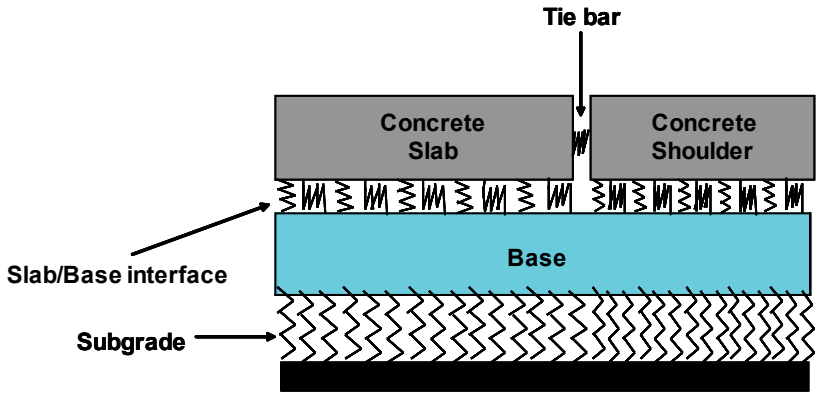

Figure 27. ISLAB2005 model of longitudinal joint and tie bar.

The following input parameters must be defined for the ISLAB2005 finite element concrete pavement model:

- Model geometry.
- Concrete properties.
- Base properties.
- Concrete/base interface parameters.
- Subgrade properties.
- Tie bar design.
- Environmentally-induced strains (both thermal and drying shrinkage strains).
- Finite element mesh.

These input requirements are described in detail in the following sections.

Model Geometry

The analysis of the longitudinal joint involved modeling a single 15-ft slab along the direction of traffic. Two, three, four, five, and six lanes/shoulders were modeled in the direction perpendicular to traffic flow. The width of each lane/shoulder was assumed to be 12 ft for a standard section and 14 ft for widened slab section.

A concrete layer thickness of 10 in and a base layer thickness of 6 in were used to simplify the solution scheme and without loss of generality (there is a weak dependence of thickness of either layer on steel stress in the tie bars).

Concrete Properties

The concrete material (modeled as a linear elastic material in ISLAB2005) assumed the following properties:

- Elastic modulus—4,000,000 psi.
- Poisson's ratio—0.2.
- Unit weight—a fictitious unit weight value was used to ensure that the concrete slab and base did not separate during response calculation (i.e., only axial movement was permitted).
- CTE— 5.5 in/in/^{o}F.

Base Properties

The base material (also modeled as a linear elastic material in ISLAB 2005) assumed the following properties:

- Elastic modulus—mid-range values recommended in the MEPDG (AASHTO, 2008) were used for the following base materials:
  - Unbound base – 50,000 psi.
  - Soil cement base – 500,000 psi.
  - PCTB – 750,000 psi.
  - CTB – 1,000,000 psi.
  - LCB – 2,000,000 psi.
  - ATB – 1,000,000 psi (a higher than normal value was adopted because critical conditions for tie bar stress occur in cold weather when the asphalt modulus is high).
- Poisson's ratio:
  - 0.25 for treated bases.
  - 0.35 for unbound bases.

Slab/Base Interface Parameters

The slab-base interface for tie bar design should allow for both direct compression and sliding. For this reason, this interface was modeled using two sets of springs—one in the vertical direction (Totsky model) and one in the horizontal direction (based on the modified Coulomb friction model).

Totsky Model

The Totsky model was incorporated in the ISLAB2000 program to address the layer separation problem (Khazanovich et al., 2000). This approach models a multi-layered pavement system constructed on the subgrade as a series of plates and springs. The plate elements model the bending, whereas the springs accommodate the direct compression in such a system.

The contact pressure between the slab and base is related to the relative vertical displacement of the layers through:

$$\sigma_{press} = k_v \Delta w \tag{8}$$

where:

σ_{press} = normal pressure stress between slab and base, psi
Δw = difference of vertical displacement, in
k_v = stiffness of vertical interlayer springs, lb/in^3

According to Khazanovich (1994), the interlayer vertical stiffness may be defined as:

$$k_v = \frac{1}{1/k_{PCC} + 1/k_{Base}} \tag{9}$$

where:

$$k_{PCC} = \frac{2E_{PCC}(1-\mu_{PCC})}{H_{PCC}(1-\mu_{PCC}-2\mu_{PCC}^2)} \tag{10}$$

$$k_{Base} = \frac{2E_{Base}(1-\mu_{Base})}{H_{Base}(1-\mu_{Base}-2\mu_{Base}^2)} \tag{11}$$

E_{PCC} = concrete elastic modulus, psi
μ_{PCC} = concrete Poisson's ratio, dimensionless
H_{Base} = base thickness, in
E_{Base} = base elastic modulus, psi
μ_{Base} = base Poisson's ratio, dimensionless

For a concrete pavement, portions of the bottom surface of the concrete slab may separate from the top surface of the base. If curling deformation takes into account this phenomenon, the vertical spring coefficient is assumed to be a function of the vertical displacement difference as follows:

$$k_v = \begin{cases} k_v \ \ if \ \ \Delta w > 0 \\ \\ 0 \ \ if \ \ \Delta w < 0 \end{cases} \qquad (12)$$

Modified Coulomb Friction Model

The modified Coulomb friction model included in ISLAB2005 is an extended version of the classical Coulomb friction model (see Figure 28). This model states that the contact surfaces do not slide over each other if the shear stress magnitude is less than the coefficient of friction multiplied by the pressure stress between the two surfaces. ISLAB2005 allows the user to assign a shear stress limit so that, regardless of the normal pressure stress, sliding will occur if the magnitude of the shear stress reaches this limiting value.

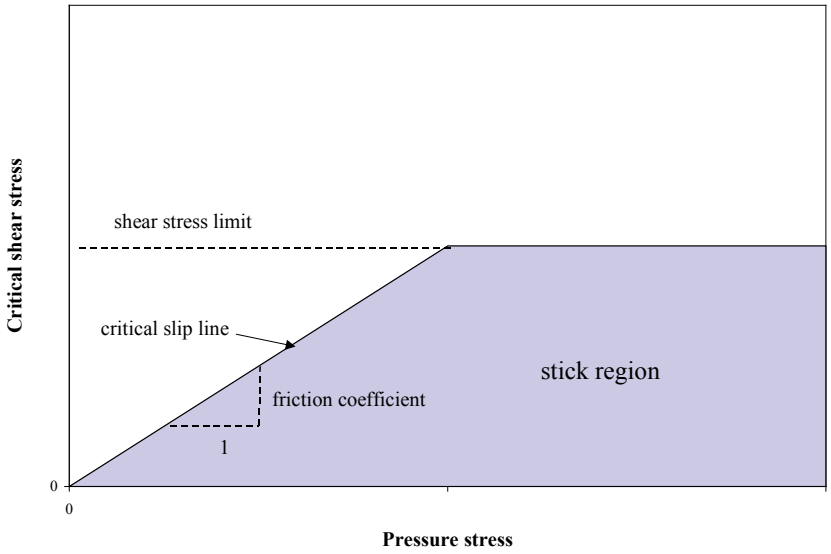

Figure 28. Coulomb slab-base friction model parameters.

In the ISLAB2005 program, there is no slab-base shear transfer when separation occurs between these two layers.

The displacements at the bottom surface of the concrete slab and the top surface of the base are related to the friction stress as follows:

$$\sigma_{hor} = k_h \Delta u \qquad (13)$$

where:

σ_{hor} = shear stress between the contact surfaces of the slab and base, psi

Δu = difference of horizontal displacement of the contact surfaces, in

k_h = stiffness of horizontal interlayer springs, lb/in^3

And the interlayer horizontal stiffness may be defined as:

$$k_h = \begin{cases} k_{h0} \ \ if \ \ |\sigma_{hor}| < \sigma_{cr} \ \ and \ \ k_v > 0 \\ \sigma_{cr} / |\Delta u| \ \ if \ \ |\sigma_{hor}| = \sigma_{cr} \ \ and \ \ k_v > 0 \\ 0 \ \ if \ \ k_v = 0 \end{cases} \quad (14)$$

where:

k_{h0} = stiffness of the slab/support layer interface in the stick region simply referred to stiffness in stick, lb/in^3

σ_{cr} = critical stress; min (k_{fr}, σ_{press}, σ_{ult}), psi

k_{fr} = friction coefficient, dimensionless

σ_{ult} = ultimate shear stress, psi

For the analysis performed herein, a specific case of the ISLAB2005 friction model was used. By assigning a very high value of interface friction coefficient and realistic values of shear stress limit and stiffness in stick for specific base types, the ISLAB2005 friction model has been converted into a bi-linear spring model described by two parameters—steady state frictional stress (taken as the ultimate shear stress of the slab/base interface for the purpose of this study) and the stiffness in stick. This is similar to the treatment of the slab/base interface in the HIPERPAV program (Ruiz et al., 2001).

The following values were adopted for the parameters of the bi-linear slab/base interface spring model in the ISLAB2005 factorials:

- Steady-state frictional stress
  - 15 psi for CTB, LCB, soil-cement, and PCTB.
  - 6 psi for ATB.
  - 2 psi for unbound base.
- Stiffness in stick
  - 15,000 lb/in^3 for CTB, LCB, soil-cement, and PCTB.
  - 240 psi/ in^3 for ATB.
  - 100 psi/ in^3 for unbound base.

These values were adopted from the HIPERPAV program (Ruiz et al., 2001).

Subgrade Property

A Winkler subgrade with a typical k-value of 200 psi/in was used.

Tie Bar Parameters

Guo's (1992) tie bar shear transfer model is implemented in ISLAB2005. This model treats the tie bar as a beam element and adjusts stiffness to account for bar-concrete interaction.

The vertical displacement at adjacent points on the two slabs is related to the vertical shear force transferred through the tie bar as follows:

$$F_{Dw} = k_s \Delta w_{TB} \quad (15)$$

where:

F_{Dw} = vertical shear force transferred through tie bar, lb
k_s = stiffness of shear vertical springs equivalent tie bar, lb/in
Δw_{TB} = difference of vertical displacement of adjacent slabs, in

To compute Guo's vertical spring shear stiffness, the following parameters must be defined:

- Tie bar diameter.
- Tie bar embedded length.
- Elastic modulus of steel (assumed to be 29,000,000 psi).
- Steel Poisson's ratio (assumed to be 0.3).
- Modulus of concrete support (assumed to be 500,000 psi/in).

In addition to shear transfer, ISLAB2005 considers a linear spring model for tie bar restraint in the direction along the length of the bar. The axial displacements at the points of the two adjacent slabs where the tie bars meet the concrete are related with the normal force transferred through the tie bar as follows:

$$F_{Dn} = k_p \Delta u_{TB} \quad (16)$$

where:

F_{Dn} = axial force transferred through tie bar, lb
k_p = pull-out stiffness of tie bar, lb/in
Δu_{TB} = change in joint opening, in

The stiffness of an equivalent spring in the axial direction (pull-out stiffness) may be identified directly from pull-out tests for a specific concrete strength, tie bar geometry, and steel properties.

For this study, the tie bar pull-out stiffness was estimated using an approach based on the CEB recommendations for analytical modeling of reinforced concrete elements (CEB-FIP, 1990). The following assumptions were made for modeling the pull-out behavior of tie bars embedded in concrete:

- The CEB pullout bond-slip model is used (see Figure 29). The first segment of the model is defined as follows:

$$\tau = \tau_{\max}\left(\frac{s}{s_1}\right)^{0.4} \quad \text{for } 0 \le s \le s_1 \tag{17}$$

where:

τ	=	bond stress, psi
s	=	free edge slip, in
s_1	=	free edge slip at τ_{max}, in

Characteristic values of s_1 (24 mils) and τ_{max} (940 psi) were assumed based on CEB recommendations.

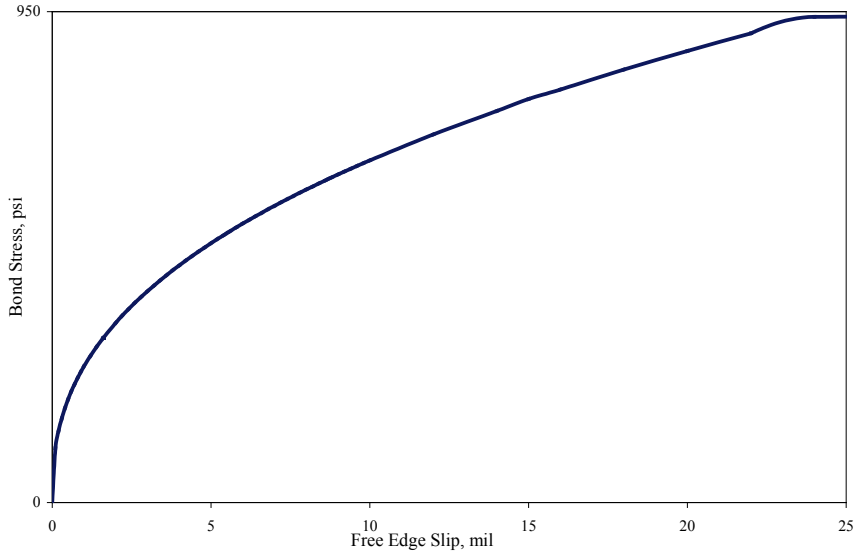

Figure 29. CEB bond model for a tie bar in concrete.

- With the assumption of the uniform bond stress distribution along the tie bar, equation (17) may be rewritten for pull-out force:

$$F = F_{\max}\left(\frac{s}{s_1}\right)^{0.4} \tag{18}$$

where:

$$F = \tau 0.5\pi D_{TB} L_{TB} \tag{19}$$

$$F_{\max} = \tau_{\max} 0.5\pi D_{TB} L_{TB} \tag{20}$$

D_{TB}	=	tie bar diameter, in
L_{TB}	=	tie bar length, in

Note that embedment length was assumed to be one-half of L_{TB} in the proposed design methodology.

- The limit value of pull-out force depends on the tie bar cross section and yield stress of steel:

$$F_{\lim} = 0.25\pi D_{TB}^2 f_y \quad (21)$$

Note that in equation 21, no factor of safety was applied to the steel yield strength, f_y in the M-E approach. Since the proposed M-E approach is more comprehensive in its treatment of the various factors that affect steel stresses (e.g., slab, base, and slab/base interface properties, tie bar properties, and environmentally-induced movements) and is based on better analytical modeling tools, it was surmised that adding a factor of safety would result in overly conservative designs.

- Using equations 17 through 21, values of free edge slip corresponding to the beginning of yield may be defined as:

$$s_{\lim} = s_1 \left(\frac{F_{\lim}}{F_{\max}} \right)^{2.5} \quad (22)$$

The ratio of limit pull-out force to limit slip may be used for defining the spring stiffness for tie bar modeling in ISLAB2005. The process is illustrated in Figure 30 for a #5 tie bar. Two steel grades (Grades 40 and 60) and three tie bar lengths (24, 30, and 36 in) were considered in developing the figure.

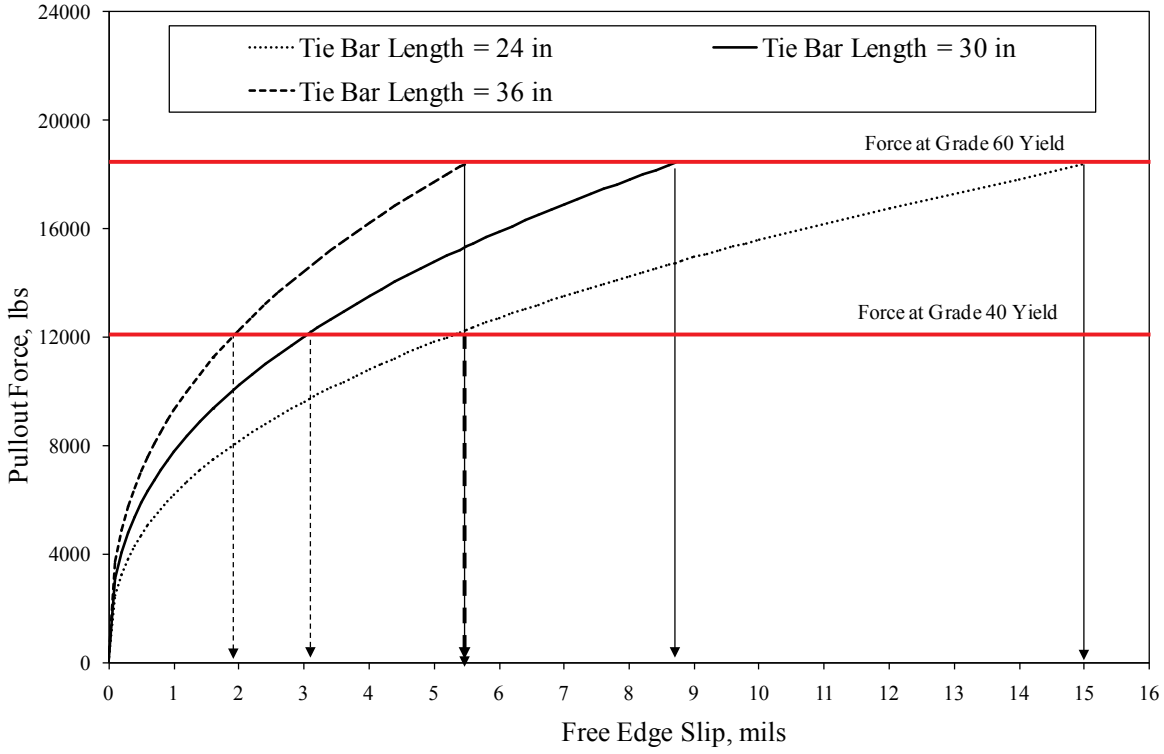

Figure 30. Pullout force vs. free edge slip for a #5 tie bar of three different lengths.

Table 7 presents calculated values of pull-out forces, bond stresses, and free edge slips for different tie bar sizes, grades, and lengths.

Table 7. Bond properties for #4, #5, and #6 tie bars.

Tie Bar #	Total Tie Bar Length, in*	Force at Steel Yield, lbs		Bond Stress at Steel Yield, psi		Free Edge Slip at Steel Yield, mil	
		Grade 40	Grade 60	Grade 40	Grade 60	Grade 40	Grade 60
4	24	7,875	11,775	417	625	3.1	8.7
	30	7,875	11,775	333	500	1.8	5.0
	36	7,875	11,775	278	417	1.1	3.1
5	24	12,266	18,398	521	781	5.5	15.1
	30	12,266	18,398	417	625	3.1	8.7
	36	12,266	18,398	347	521	2.0	5.5
6	24	17,663	26,494	625	938	8.7	23.8
	30	17,663	26,494	500	750	5.0	13.6
	36	17,663	26,494	417	625	3.1	8.7

*Note: Embedment length was assumed to be one-half of the total tie bar length.

Defining Equivalent Temperature and Drying Shrinkages

Two environmental conditions are used to define movements in the concrete slabs that set up critical stress conditions in the proposed M-E tie bar design procedure: contraction of the slab due to a uniform temperature drop and contraction of the slab due to drying shrinkage. The quantification of the environmental factors driving these movements and the procedure to compute the thermal and shrinkage related strains due to them are discussed in this section.

Temperature Related Strains

The uniform temperature drop used for design purposes is estimated as the difference between the concrete temperature at set, T_{constr}, and the mean minimum monthly temperature for a given project location, T_{min}. The estimation of these parameters is discussed in the following paragraphs. From these two parameters, the concrete thermal strain, $\varepsilon_{thermal}$, due to a uniform temperature drop is computed as:

$$\varepsilon_{thermal} = \alpha * (T_{constr} - T_{\min}) \quad (23)$$

Estimation of T_{constr}. The concrete set temperature can be estimated from the expected construction monthly ambient temperature and cementitious materials content using the following equation from the MEPDG (AASHTO, 2008):

$$T_{constr} = CC\left[-0.015917 + \left(0.001416 + \frac{1}{CC}\right) * MMT - 0.000006 * MMT^2\right] \quad (24)$$

where:

CC = cementitious materials content, lb/yd^3

MMT = mean ambient monthly temperature for the month of construction, °F

Estimation of T_{min}. The mean monthly ambient temperature of the coldest month of the year for a project location can be determined from historical climatic records. Table A-1 in Appendix A provides the historical average monthly temperatures for 100 U.S. cities. As can be noted, the coldest month is typically January for nearly all cities.

Mean Drying Shrinkage Strains

The mean drying shrinkage strain in the concrete slab, $\varepsilon_{sh,m}$, is estimated using equation 25. This strain depends on concrete material properties, relative humidity (RH) at the project site, and the age of the slab at the time when shrinkage calculations are desired. An age of 1-year was selected for all shrinkage calculations in the proposed method because a majority of drying shrinkage in the slab is expected to have occurred by this age. Further, since moisture content also varies with concrete depth, a thickness weighted mean drying shrinkage strain is used to obtain one characteristic and uniform drying shrinkage strain for the slab's cross section.

$$\varepsilon_{sh,m} = \varepsilon_{sh,b} + \left(\varepsilon_{sh,t} - \varepsilon_{sh,b}\right) \cdot \frac{h_d}{H_{PCC}} \tag{25}$$

where:

$\varepsilon_{sh,m}$ = mean shrinkage strain at 1 year, microstrain
$\varepsilon_{sh,b}$ = shrinkage strain at the bottom surface of the concrete slab at 1 year, microstrain
$\varepsilon_{sh,t}$ = shrinkage strain at the top surface of the concrete slab at 1 year, microstrain
h_d = thickness of the shrinkage zone (e.g., the driest portion of the slab, near the surface), set equal to 2 in

The computation of each of these parameters is described in the following paragraphs. For typical concrete pavements, the mean drying shrinkage strain is approximately between 200 and 300 microstrain.

Estimation of Drying Shrinkage Strain at the Top of the Concrete Slab. This quantity can be estimated as:

$$\varepsilon_{sh,t} = \varepsilon_{su} \cdot S_t \cdot S_{mean} \tag{26}$$

where:

ε_{su} = ultimate shrinkage [estimated based on equation (27)]

$$\varepsilon_{su} = C_1 \cdot C_2 \cdot \varepsilon_{ts} \tag{27}$$

where:

ε_{ts} = typical shrinkage strain, recommended value is 650 microstrain

C_1 = cement type factor: 1.0 for Type I cement, 0.85 for Type II cement, and 1.1 for Type III cement

C_2 = type of curing factor: 1.0 if cured with wet burlap and 1.2 if cured by curing compound

S_t = time factor for drying shrinkage of slab [estimated from equation (28)]

$$S_t = \frac{Age}{n + Age} \tag{28}$$

where:

Age = Concrete age, days since placement, set at 1 year (365 days), days

n = time to develop 50 percent of ultimate shrinkage strain, days (recommended American Concrete Institute value = 35 days)

S_{mean} = mean relative humidity factor of the surface being investigated measured over the course of 1 year at the project site, as determined by equation (29).

$$S_{mean} = \begin{cases} 3 - 0.03 \cdot RH_i \ \ if \ \ RH_i > 80\% \\ 1.4 - 0.01 \cdot RH_i \ \ if \ \ 30 < RH_i < 80\% \\ 1.1 \ \ if \ \ RH_i \le 30\% \end{cases} \tag{29}$$

where:

RH_i = ambient average yearly RH at project site, percent, available in Table A-1 in Appendix A.

Drying Shrinkage Strain at the Bottom of the Concrete Slab. This quantity can be estimated as:

$$\varepsilon_{sh,b} = \varepsilon_{su} S_t S_{mean} \tag{30}$$

The MEPDG default relative humidity of 90 percent should be used to compute S_{mean} at the bottom of the concrete slab. Note that this always will result in a S_{mean} of 0.3.

Total Free Strain Due to Temperature Drop and Drying Shrinkage

The total equivalent free strain, ε_{Eq}, due to a uniform temperature drop and drying shrinkage can be defined as:

$$\varepsilon_{Eq} = \varepsilon_{thermal} + \varepsilon_{sh,m} \tag{31}$$

Defining the Finite Element Mesh

Four-noded rectangular flat shell elements were used in the ISLAB2005 program for discretizing the slabs and base of the concrete pavement for various slab/lane configurations. Finite element models for different numbers of tied lanes considered for the analysis are presented in Figure 31 through Figure 33.

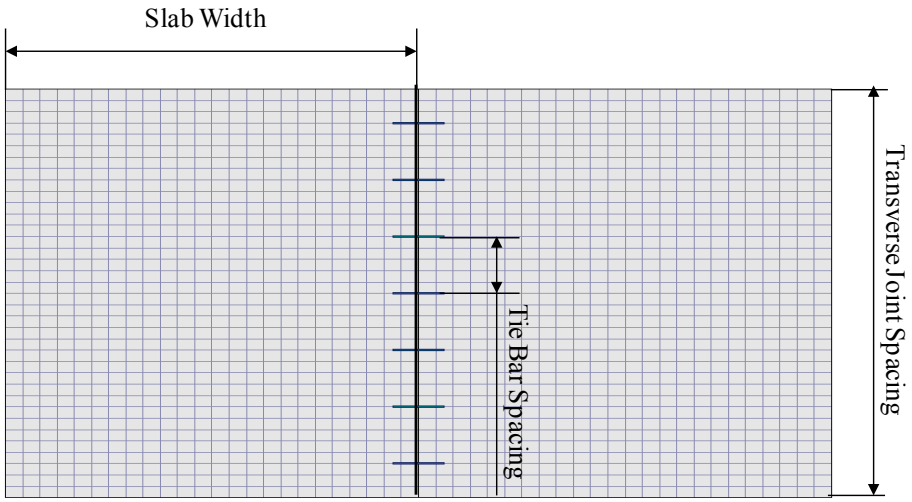

Figure 31. ISLAB2005 model of two tied 12-ft concrete lanes.

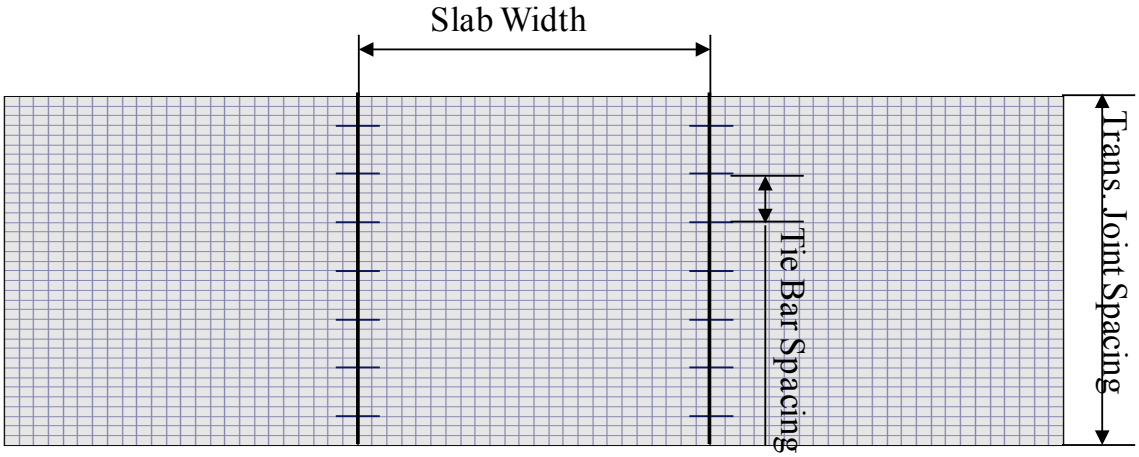

Figure 32. ISLAB2005 model of three tied 12-ft concrete lanes.

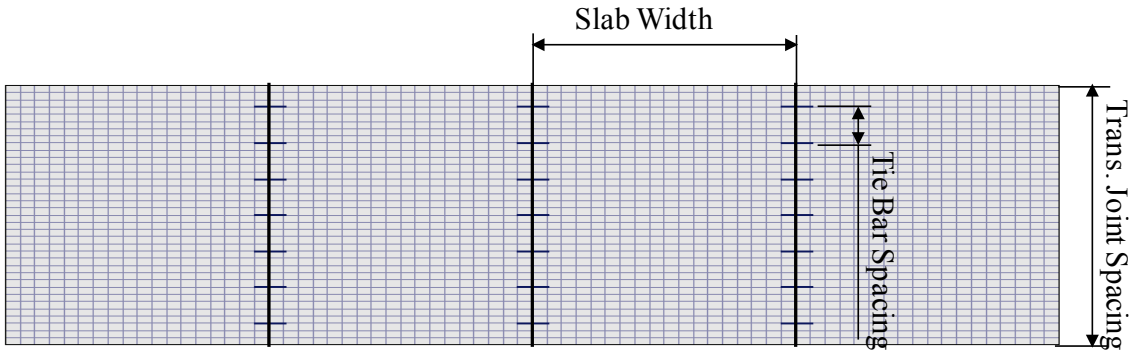

Figure 33. ISLAB2005 model of four tied 12-ft concrete lanes.

ISLAB2005 Program Execution and Database Generation

Using the various model parameters and their ranges of values and the meshing described in the previous section, the ISLAB2005 program was executed for different combinations of tie bar dimensions, tied lane configurations, and pavement cross-section details (including slab/base interface definitions) to generate a database of solutions. The outputs of interest for each combination of parameters were the displacements of the slab edges on either side of the critical longitudinal joint in the direction perpendicular to traffic (i.e., contraction of the slabs). Critical joint openings were calculated as the difference between the displacements of slab edges. The computed joint opening was divided by 2 and compared to the free edge slip for a given tie bar size and embedment length of L/2 shown in Table 7. If the one-half of the computed opening exceeded the free edge slip for a given tie bar, the assumption was that it will lead to excessive yield stress in steel. This information was utilized in developing the M-E tie bar design procedure.

TIE BAR DESIGN GUIDANCE

A series of design tables were prepared for two, three, and four tied standard width (12-ft) lanes and a widened (14-ft) lane placed on cement-stabilized (PCTB or CTB, soil cement, and LCB), ATB, and unbound bases. These design tables are included in appendices B through D. The step-by-step process for completing a successful design is illustrated below using an example.

Step 1. Obtain Design Inputs

- Location: Chicago, Illinois, USA.
- Geometry: Two traffic lanes, 12-ft wide and 15-ft long slabs, 10-in JPCP atop 6-in unbound base.
- Concrete CTE: $5.5*10^{-6}/^{o}F$.
- Concrete slab construction month: July.
- Cementitious materials content: 550 lb/yd^3.
- Cement type: Type I.
- Curing procedure: Application of curing compound.

Step 2. Estimate Design Temperature Drop and Thermal Strain

- The mean ambient temperature in July: 73 ^{o}F (taken from Table A-1 in Appendix A and based on location).
- Concrete set temperature, T_{constr}: 103 ^{o}F (estimated from equation 24 using mean ambient temperature at time of construction and cementitious materials content).

- Mean Minimum Monthly Temperature (January), T_{min}: 22°F (taken from Table A-1 in Appendix A and based on location).
- Total temperature drop: 103 °F – 22 °F = 81°F.
- Thermal strain, $\varepsilon_{thermal}$, due to a uniform temperature drop for the given concrete is: $5.5*10^{-6}$/F * 81 °F = 446 microstrain (from equation 23).

Step 3. Compute Drying Shrinkage Strain

- Calculate ultimate shrinkage strain, ε_{su}:
  - Typical shrinkage strain, recommended value 650 microstrain.
  - C_1 = Cement type factor = 1.0 for Type I cement (from equation 27).
  - C_2 = Type of curing factor = 1.2 because cured by curing compound (from equation 27).
  - Ultimate shrinkage ε_{su} = 650 * 1 * 1.2 = 780 microstrain (from equation 27).

- Calculate shrinkage strain at the top of the slab, $\varepsilon_{sh,t}$:
  - Ultimate shrinkage, ε_{su} = 780 microstrain.
  - Mean RH in Chicago: 71 percent (taken from Table A-1 in Appendix A and based on location).
  - Recommended value for the time to develop 50 percent of the ultimate shrinkage: 35 days.
    - S_t = 365/(35+365) = 0.9125 (from equation 28)
  - Mean relative humidity factor for RH of 71 percent, S_{mean}: 0.69 (from equation 29).
  - Shrinkage strain at the top of the slab, $\varepsilon_{sh,t}$ = 780 * 0.9125 * 0.69 = 491 microstrain (from equation 26).

- Calculate drying shrinkage strain at the bottom of the slab, $\varepsilon_{sh,b}$:
  - Ultimate shrinkage strain, ε_{su} = 780 microstrain.
  - Recommended time for shrinkage calculation: 365 days.
  - Minimum relative humidity factor for RH of 90 percent, S_{mean}: 0.3. (from equation 29).
  - Shrinkage strain at the bottom of the slab, $\varepsilon_{sh,b}$ = 780 * 0.9125 * 0.3 = 214 microstrain (from equation 30).

- Mean drying shrinkage strain, $\varepsilon_{sh,\,m}$, through the concrete slab:
  - Shrinkage strain at the bottom of the slab, $\varepsilon_{sh,b}$ = 214 microstrain.
  - Shrinkage strain at the top of the slab, $\varepsilon_{sh,t}$ = 491 microstrain.
  - Mean drying shrinkage strain, $\varepsilon_{sh,\,m}$ = 214 + (470-214)*2/10 = 265 microstrain (from equation 25).

Step 4. Compute Total Equivalent Free Strain in Concrete

Using equation 31, the total equivalent micro units of free strain, ε_{eq}, is:

- ε_{eq} = 446 + 265 = 711 microstrain.

Step 5. Determine Tie Bar Design from Standard Tables

Table 8 [also Table B-1] is an example of a design table prepared based on ISLAB2005 runs for selecting tie bar design criteria for two tied standard width traffic lanes on a 6-in unbound base subject to various free axial strains (same as Table B-1 in Appendix B). The table indicates that a total free microstrain of 711 units (see row for 750 microstrains) requires the following tie bar design:

- #4 tie bar, Grade 60 steel OR #5 tie bar, Grade 40 steel.
- 45-in spacing.
- 24-in total tie bar length (12 in embedment length).

Table 8. Tie bar design for two tied 12-ft lanes on 6-in unbound base.

Total Equivalent Free Strain, microstrain	Tie Bar Size Designation	Tie Bar Spacing, in	Total Tie Bar Length, in	Steel Grade
500	#4	45	24	40
550	#4/#5	45	24	60/40
600	#4/#5	45	24	60/40
650	#4/#5	45	24	60/40
700	#4/#5	45	24	60/40
750	#4/#5	45	24	60/40
800	#4/#5	45	24	60/40

This design will ensure that the yield stress in steel is below the yield strength of the steel to ensure the long-term integrity of the longitudinal joint.

CHAPTER 5. SENSITIVITY ANALYSIS OF THE M-E TIE BAR DESIGN AND COMPARISON WITH THE SUBGRADE DRAG THEORY

SENSITIVITY ANALYSIS OF THE ANALYTICAL MODEL USED TO DEVELOP THE TIE BAR DESIGN GUIDE

A parametric study was performed to illustrate the effects of design inputs on various responses of the ISLAB2005 analytical model. The baseline pavement design used for the sensitivity analysis was the following:

- Two tied 12-ft-wide lanes with transverse joints spaced at 15 ft.
- Concrete slab thickness, H_{PCC} = 10 in.
- Concrete modulus of elasticity, E_{PCC} = 4 million psi.
- Concrete CTE = 5.5×10^{-6} /°F (similar to limestone aggregate).
- Stabilized base thickness, h_{base} = 6 in.
- Base modulus of elasticity, E_{base} = 1 million psi (CTB).
- Slab/base interface, steady-state frictional stress, τ_0 = 15 psi; maximum slippage δ_0 = 1 mil.
- Tie bar diameter, D_{TB} = 0.625 in (#5 deformed bar).
- Tie bar length, L_{TB} = 24 in (12-in embedment length).
- Tie bar spacing, J_{TB} = 30 in.
- ε_{eq} = 500 microstrain produced by a uniform axial concrete temperature drop and equivalent drying shrinkage.

The following parameters were varied over a reasonable range, and the impact on longitudinal joint opening and stress in the steel tie bars was determined for non-tied and tied joints:

- Base type—CTB (baseline) and unbound for both non-tied and tied joints.
- Slab/Base Interface Friction—full friction for tied joint (baseline) and non-tied joint compared with analytical joint opening solution for a frictionless interface and an non-tied joint (this analytical solution gives the theoretical maximum joint opening possible for the given parameters and serves as a useful reference point to study the joint openings derived for all other cases).
- Concrete slab thickness—6, 8, 9, 10 (baseline), 11, 12, and 14 in.
- Base thickness—4, 5, and 6 in (baseline).
- Base modulus—0.5 million psi, 1 million psi (baseline), and 2 million psi.
- Lane width—12 (baseline) and 14 ft.
- Number of tie bars per joint for tied joints—3, 4, 6 (baseline), and 8.
- Number of tied lanes— 2 (baseline), 3, and 4.

Results of the sensitivity analysis (using the ISLAB2005 model) are presented in Figure 34 through Figure 49.

Figure 34 and Figure 35 present the effect of base type on the joint opening for non-tied and tied joints, respectively. It is clear from Figure 34 that the joint opening is greater for a non-tied concrete pavement joint on an unbound base than on a CTB due to the reduced modulus of elasticity and friction coefficient. However, as can be noted from Figure 35, the opposite is true for a tied joint. The resolution of equilibrium forces in a pavement with a tied joint explains this different trend when compared with a non-tied joint. At a tied joint, the slab movement due to environmentally-induced strains is restrained by the tie bar, the slab/base interface friction and the base modulus (or stiffness). As adjacent slab edges tend to pull away from the joint, the base, acting through its connections to the overlying slabs (through the tie bars and slab/base interface friction), tends to move towards the joint. Given this scenario, a less stiff base, such as an unbound base, can accommodate more of this opposing movement than a stiffer base. Thus, an unbound base can more effectively close the joint, resulting in a smaller joint opening for tied pavement joints. The relatively larger movement of an unbound base relieves a greater amount of stresses in the tie bar steel when compared to a section built on a CTB. For this reason, as shown in Figure 36, the tie bar stresses in concrete slabs over unbound bases are lower those on CTB (and other treated bases with higher moduli and higher slab/base interface friction).

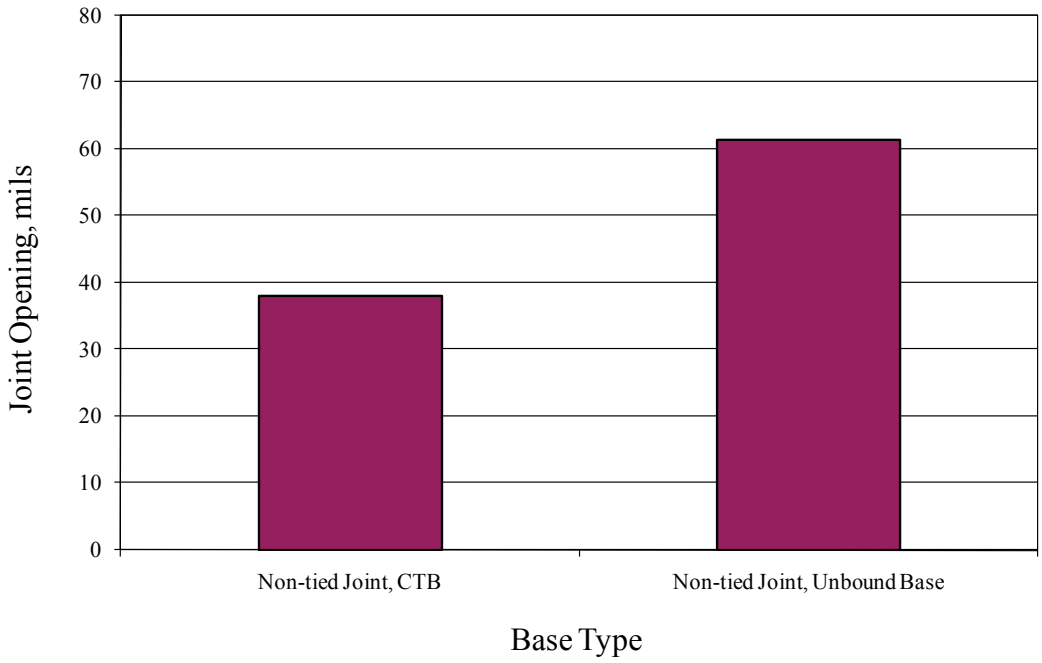

Figure 34. Effect of base type on joint opening for a non-tied joint.

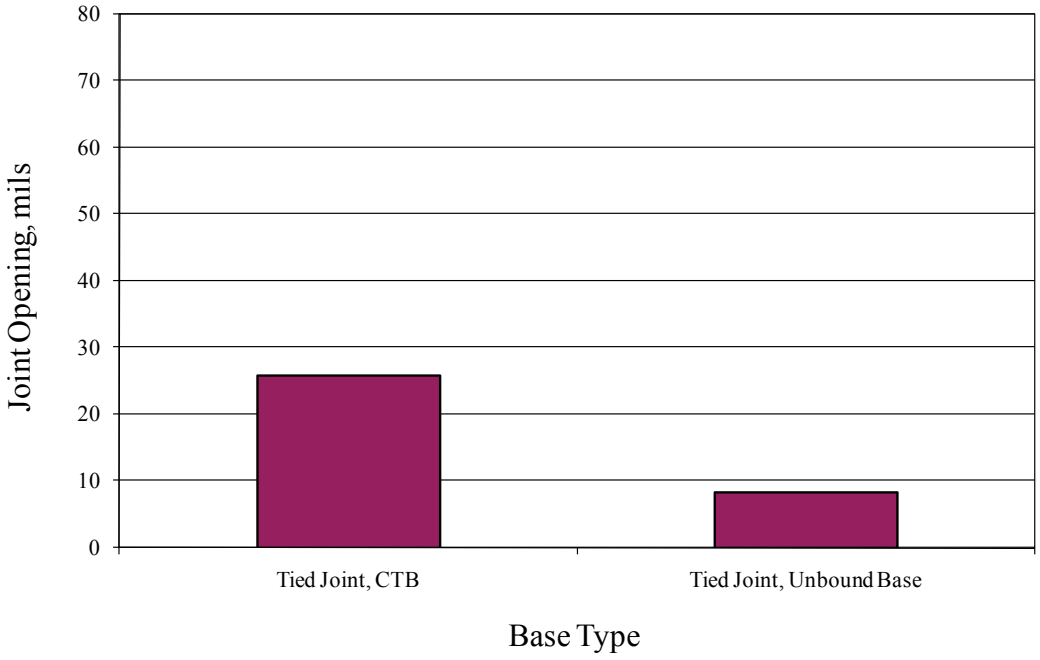

Figure 35. Effect of base type on steel stress for a tied joint.

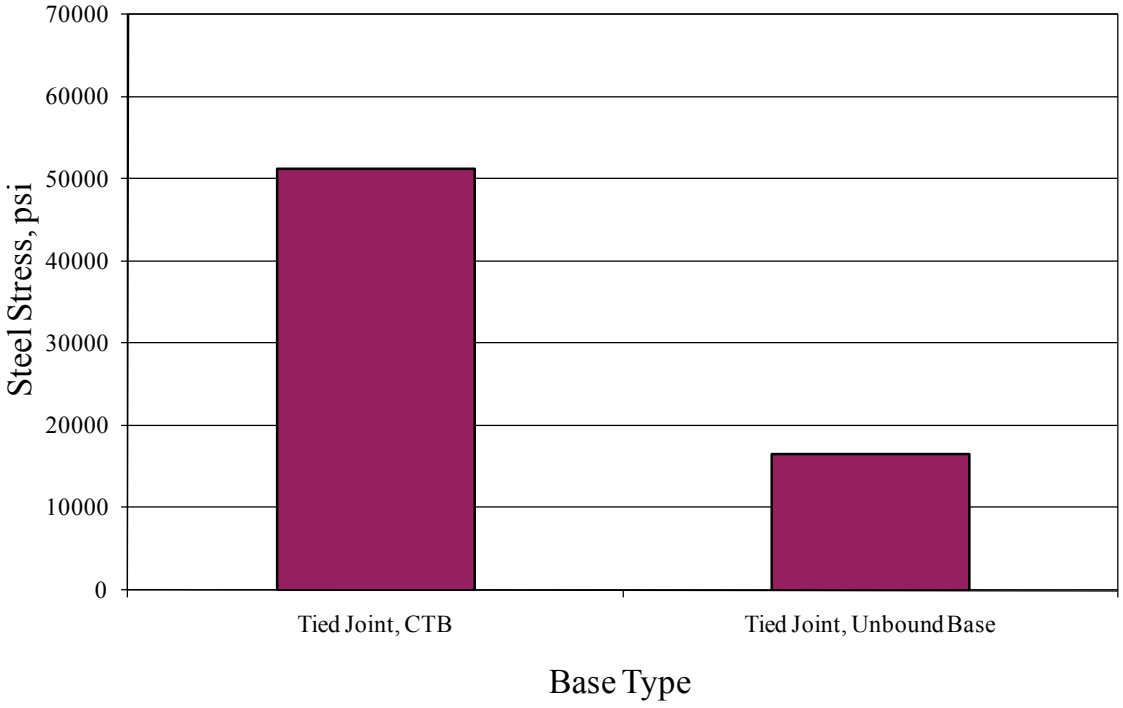

Figure 36. Effect of base type on steel stress in the tie bar for a tied joint.

Figure 37 presents the impact of slab/base interface friction and tie bar restraint on joint opening. The bar labeled "Non-tied Joint and Zero Friction" represents the theoretical maximum joint opening possible for the given parameters of interest. It can be noted from the bar marked "Non-tied Joint with CTB" that the joint opening reduces from the maximum value when restraint in the form of slab/base friction is introduced. The joint opening reduces further when an additional restraint in the form of tie bars is introduced, as illustrated by the bar marked "Tied Joint with CTB."

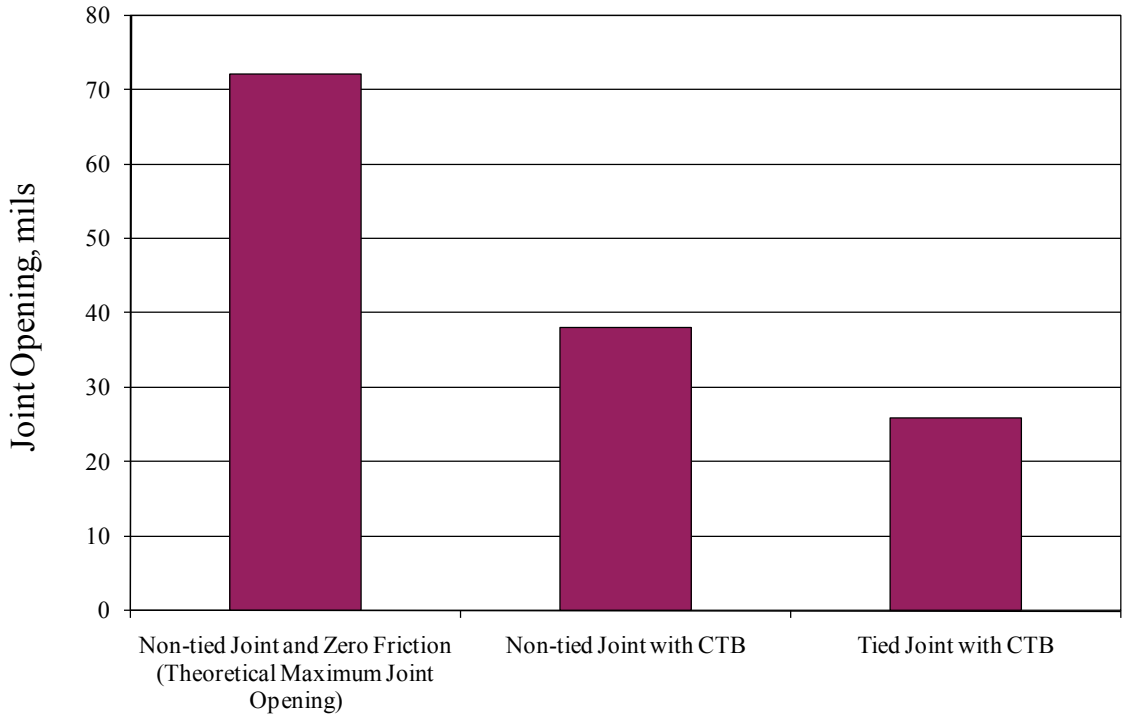

Figure 37. Effect of tie bars and base type on joint opening.

Figure 38 and Figure 39 show that concrete slab thickness has very little effect on either steel stress or joint opening.

From Figure 40 it can be noted that steel stress in the tie bar increases as the thickness of a CTB increases from 4 to 6 in. This is due to the increased resistance that a thicker base provides due to a higher stiffness. For the same reason, as shown in Figure 41, joint opening increases as the thickness of the base course increases from 4 to 6 in.

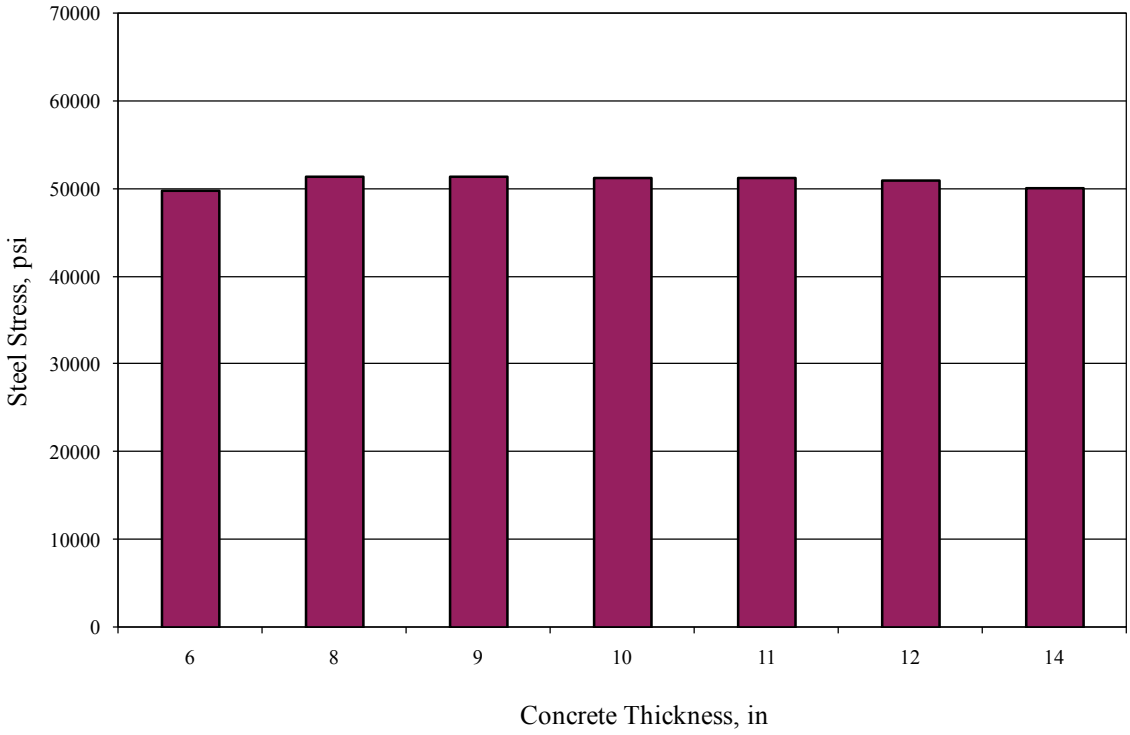

Figure 38. Effect of concrete thickness on steel stress in the tie bar.

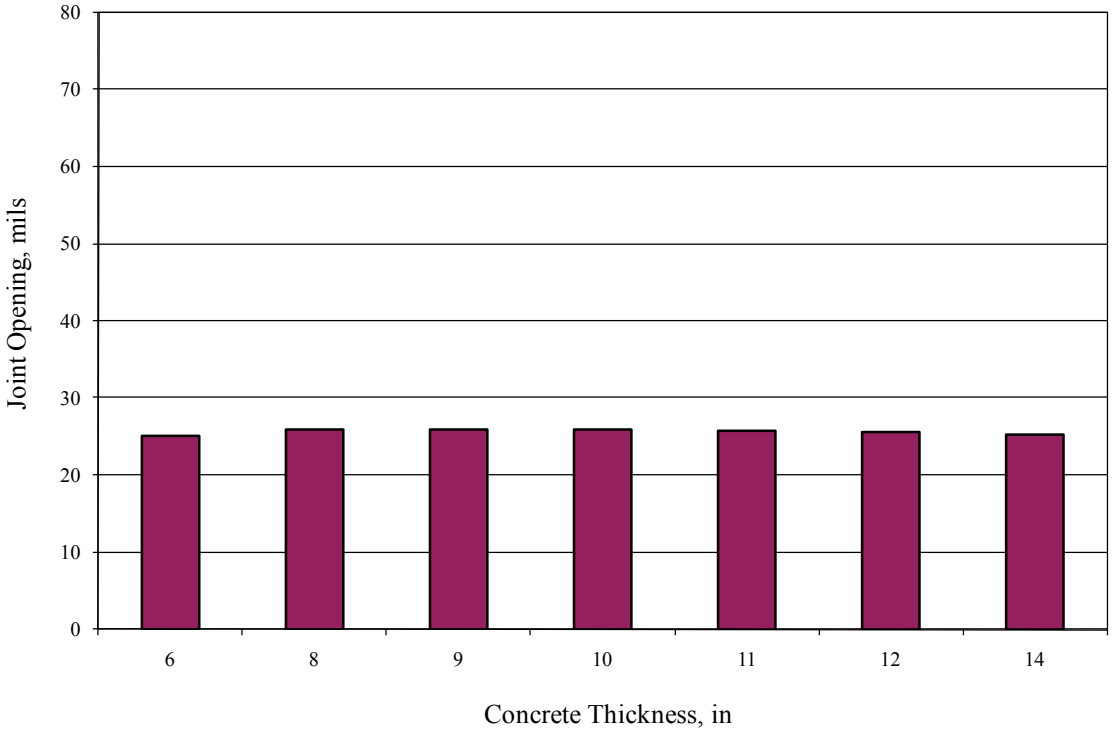

Figure 39. Effect of concrete thickness on joint opening.

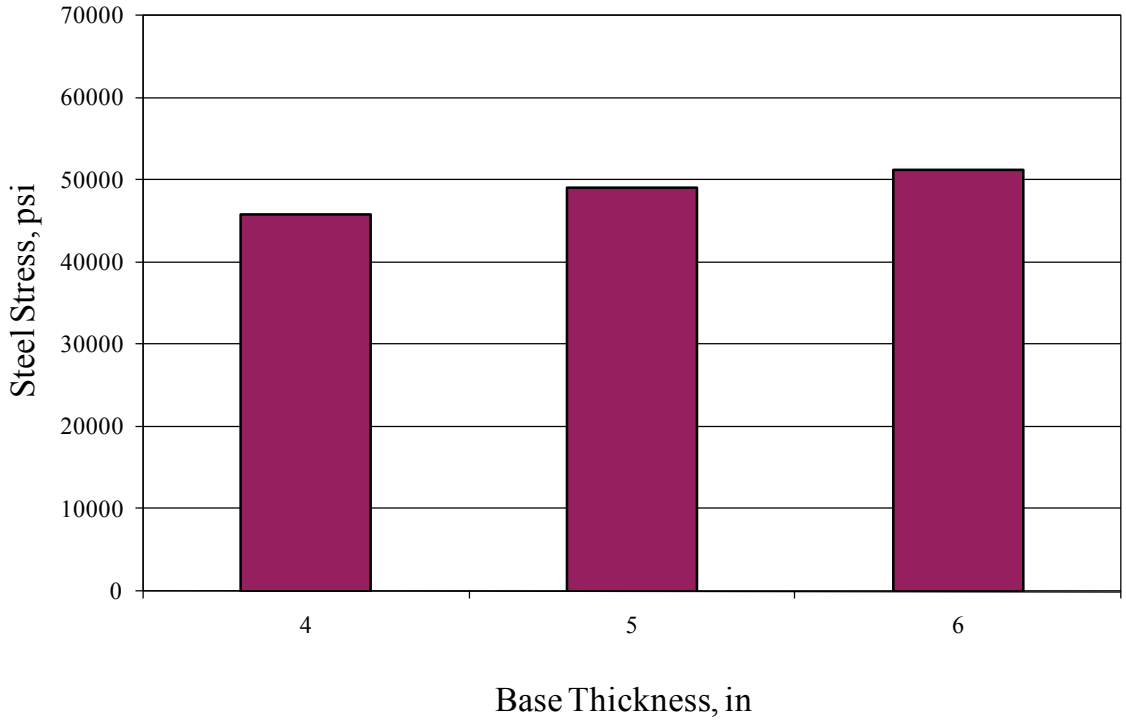

Figure 40. Effect of treated base thickness on steel stress in the tie bar.

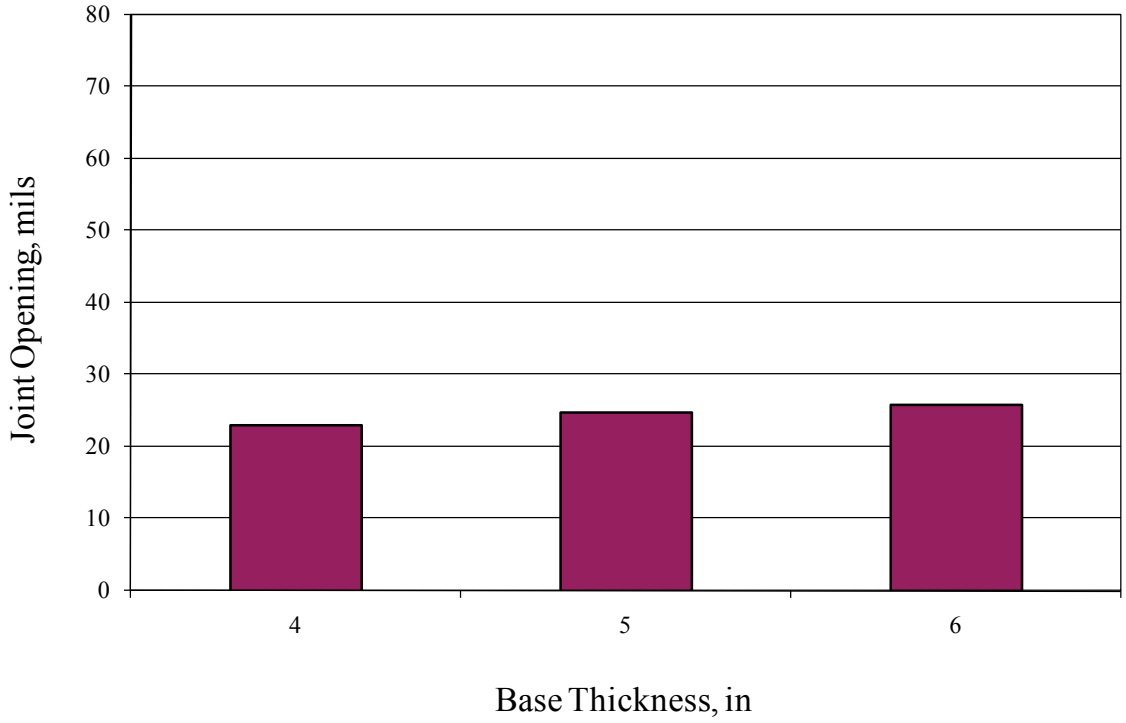

Figure 41. Effect of treated base thickness on joint opening.

From Figure 42 it can be noted that the steel stress in the tie bar increases as the base course modulus increases, due to the increased resistance at the slab-base interface. Figure 43 shows that the joint opening increases as the base course modulus increases, again due to the increased resistance. This may be due to the relief of the adjacent free edge of the two-lane pavement.

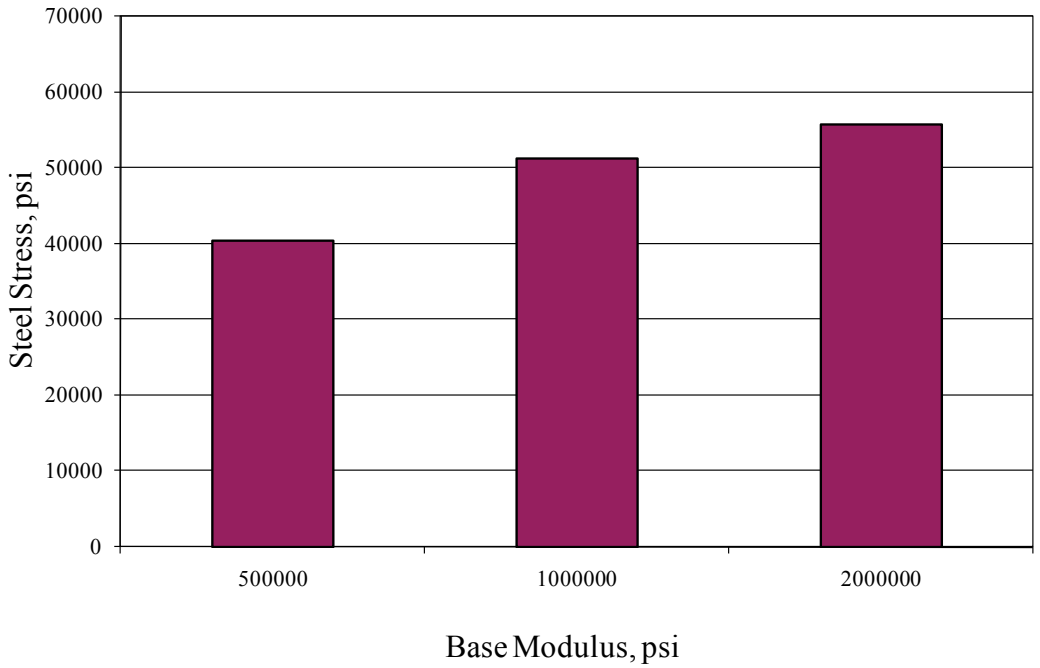

Figure 42. Effect of base elastic modulus on steel stress in the tie bar.

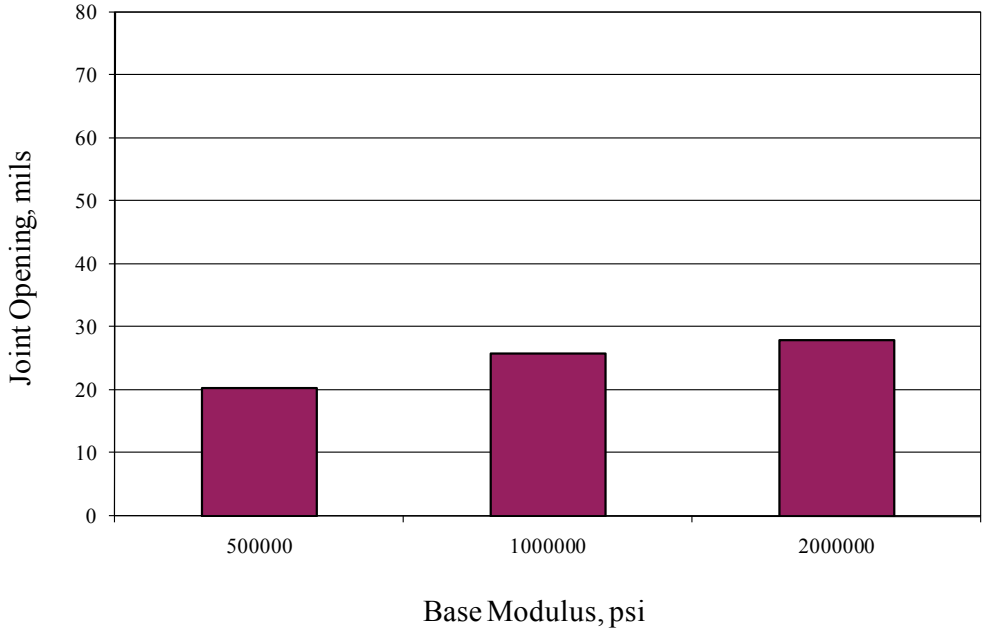

Figure 43. Effect of base elastic modulus on joint opening.

Figure 44 and Figure 45 illustrate that the steel stress in the tie bar and joint opening increase as the lane width increases from 12 to 14 ft.

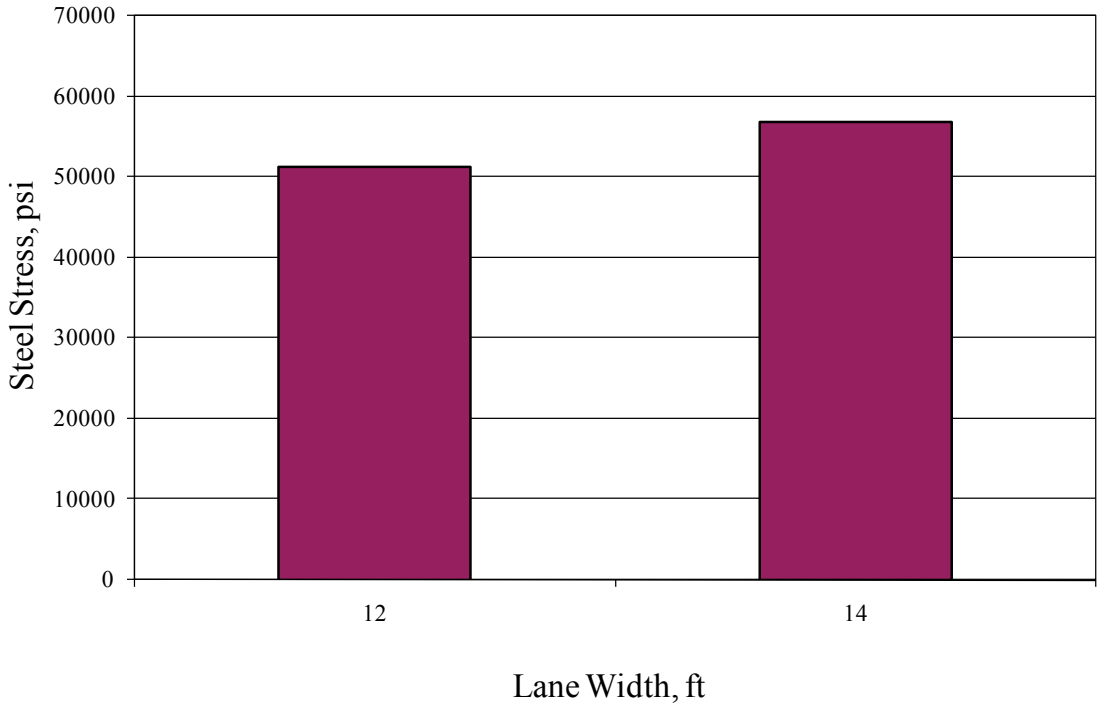

Figure 44. Effect of lane width on steel stress in the tie bar.

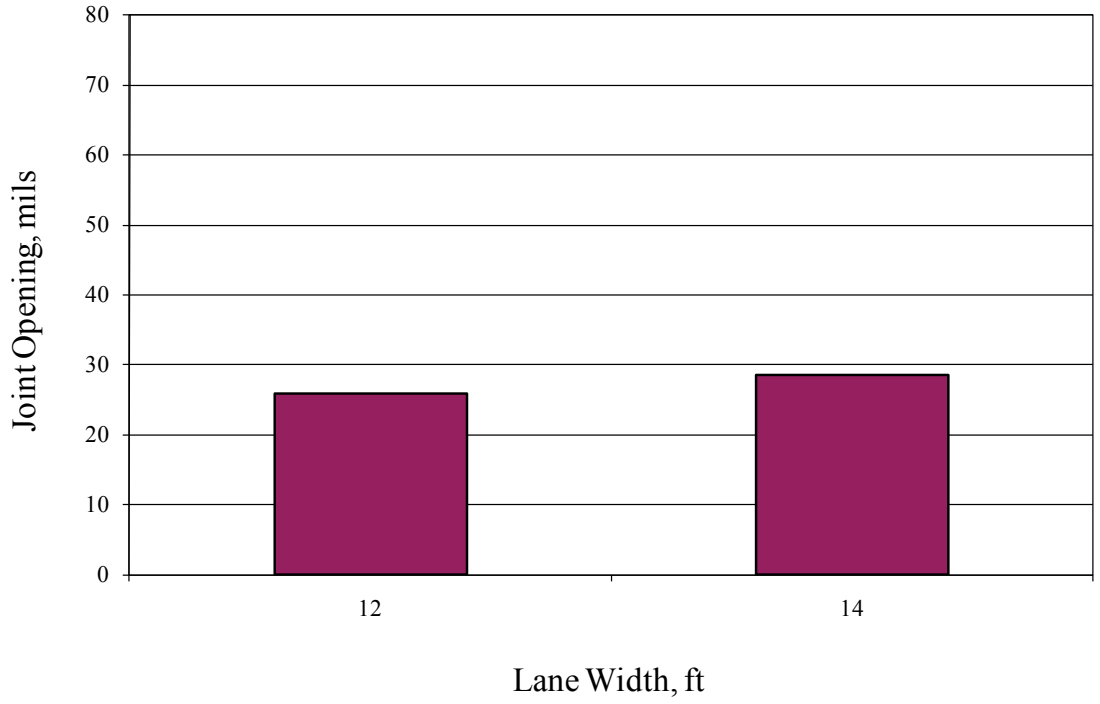

Figure 45. Effect of lane width on joint opening.

Figure 46 shows that the steel stress in the tie bar decreases as the number of #5 tie bars increases from three to six per 15-ft slab length. The greater amount of steel across the joint reduces the amount of stress in the steel. For the same reason, as shown in Figure 47, joint opening also decreases as the number of #5 tie bars increases.

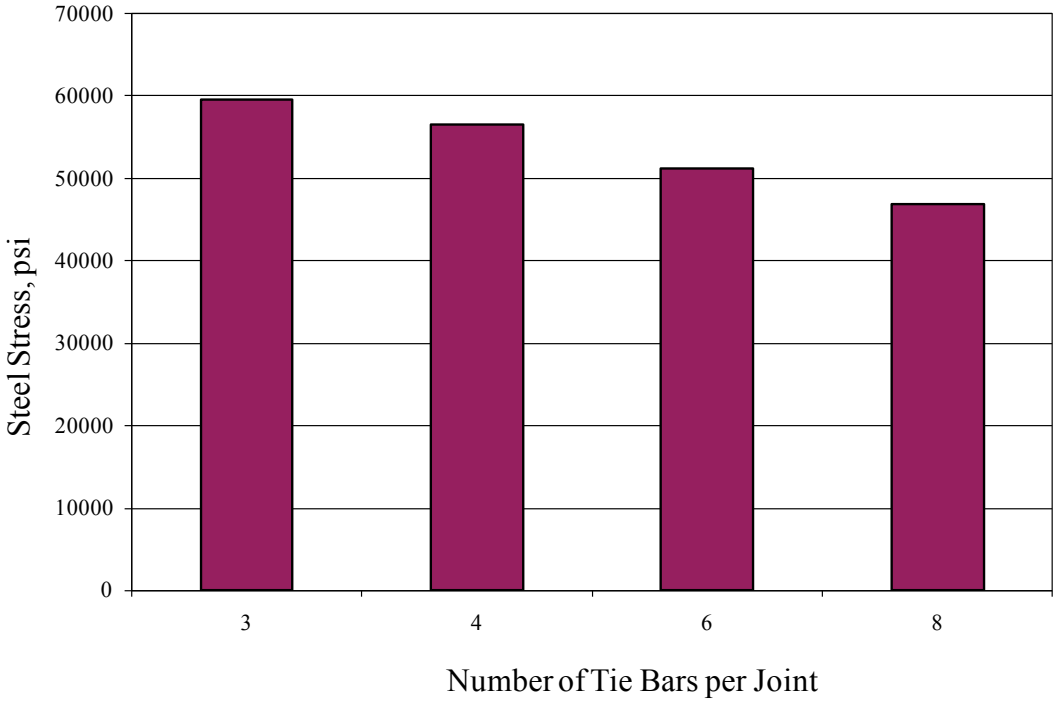

Figure 46. Effect of tie bar spacing on steel stress in the tie bar.

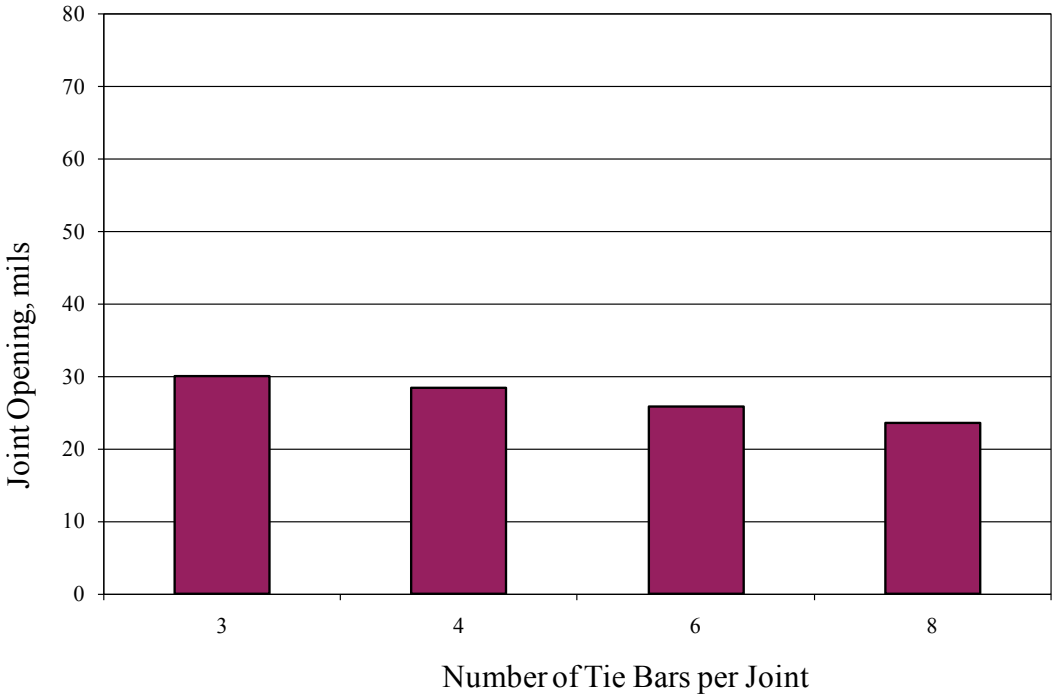

Figure 47. Effect of tie bar spacing on joint opening.

As can be noted from Figure 48 and Figure 49, when the tie bar spacing is held constant, the steel stress in the tie bar and joint opening increase as the number of tied lanes increases. This is due to the greater pull on the steel holding the longitudinal joints together.

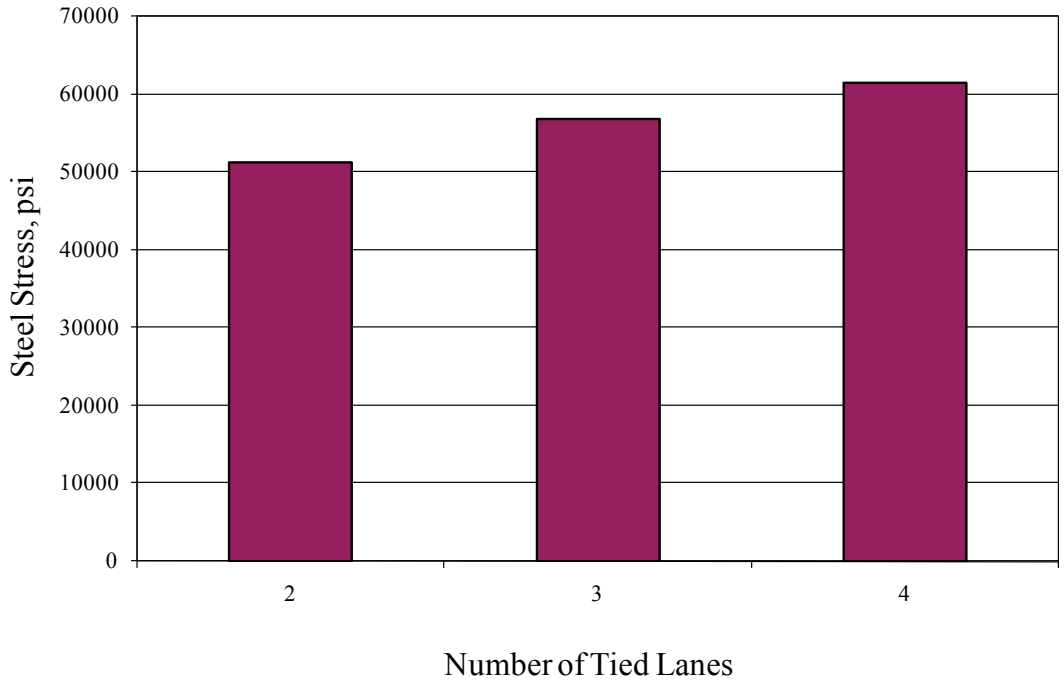

Figure 48. Effect of number of tied lanes on steel stress.

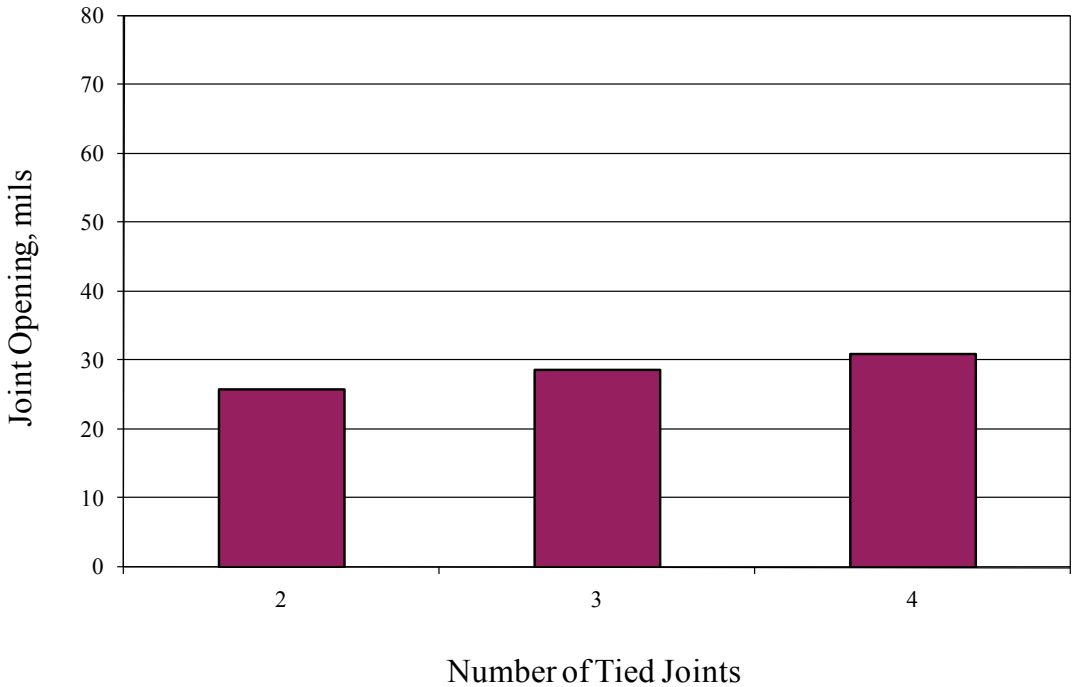

Figure 49. Effect of number of tied lanes on joint opening.

COMPARISON OF THE M-E TIE BAR DESIGN WITH THE SUBGRADE DRAG THEORY

The following comparison table was prepared to illustrate the results achieved with the M-E and the SDT-based 1993 AASHTO (AASHTO, 1993) procedures for tie bar design. Two locations were included for the comparison—Chicago and Las Vegas. The difference in tie bar spacing is used for comparison. The design constants used in the computations are as follows:

- 10-in JPCP with 15-ft transverse joint spacing.
- Base type
  - Unbound base course thickness: 6 in; base modulus = 50,000 psi.
  - Stabilized base (CTB or cold ATB): 6 in; base modulus = 1,000,000 psi.
- Traffic lane width: 12 ft.
- Concrete CTE: $5.5*10^{-6}$ in/in/^{o}F.
- Cementitious materials content: 550 lb/yd^3.
- Yield of steel tie bars: f_y = 60 ksi (Grade 60).
- Safety factor applied to f_y per AASHTO (AASHTO, 1993): 0.75 (applied only to the 1993 AASHTO tie bar design calculations; recall that as noted earlier no safety factor for f_y was used in the proposed M-E approach).
- #5 bar (diameter 0.625-in).
- Unit weight concrete: 0.0868 lb/in^3 (required only for the AASHTO method).
- Cement type: Type I cement (required only for the M-E method).
- Curing method: Curing compound (required only for the M-E method).
- Mean RH:
  - Chicago: 71 percent.
  - Las Vegas: 30 percent.
- Mean drying shrinkage for same concrete mixture:
  - Chicago: 265 microstrain.
  - Las Vegas: 327 microstrain.
- Temperature drop:
  - Chicago:
    - Construction month July, monthly ambient temperature = 73 ^{o}F.
    - Set temperature = 103 ^{o}F.
    - January mean temp = 22 ^{o}F.
    - Temperature drop = 81 ^{o}F.
  - Las Vegas
    - Construction month July, monthly ambient temperature = 91 ^{o}F.
    - Set temperature = 125^{o}F.
    - January mean temp = 47^{o}F.
    - Temperature drop = 78^{o}F.
- Total equivalent free strain in concrete:
  - Chicago: $5.5*10^{-6}$/^{o}F * 81 ^{o}F+ 265 = 711 microstrain.
  - Las Vegas: $5.5*10^{-6}$/^{o}F * 78 ^{o}F + 327 = 756 microstrain.

As can be noted from the discussion above, the design temperature drop was similar for both sites (81 ^{o}F versus 78 ^{o}F). The drying shrinkage was higher for Las Vegas (327 microstrain) than for Chicago (265 microstrain) due to the lower relative humidity. Table 9 presents the comparison of the tie bar design recommendations from the two procedures.

Table 9. A comparison of M-E and 1993 AASHTO tie bar design results for a 10-inch thick concrete pavement with Grade 60 tie bars.

Location	Base Type	Number of Tied Lanes	1993 AASHTO Tie Bar Design	M-E Tie Bar Design
Chicago	Unbound	2	#4 @ 48-in	#4 @ 45-in
		3	#4 @ 48-in	#4 @ 45-in
		4	#5 @ 37-in	#5 @ 45-in
		6	#6 @ 35-in	#5 @ 45-in
	CTB/Cold ATB	2	#4 @ 40-in	#6 @ 36-in
		3	#4 @ 40-in	#6 @ 36-in
		4	#5 @ 31-in	#6 @ 36-in
		6	#6 @ 30-in	#6 @ 36-in
Las Vegas	Unbound	2	#4 @ 48-in	#4 @ 45-in
		3	#4 @ 48-in	#4 @ 45-in
		4	#5 @ 37-in	#5 @ 45-in
		6	#6 @ 35-in	#5 @ 45-in
	CTB/Cold ATB	2	#4 @ 40-in	#6 @ 36-in
		3	#4 @ 40-in	#6 @ 36-in
		4	#5 @ 31-in	#6 @ 30-in
		6	#6 @ 30-in	#6 @ 30-in

The following can be noted based on the table:

- Effect of base type:
  - Both the AASHTO 1993 and M-E procedures result in very similar tie bar designs for Chicago and Las Vegas for unbound bases notwithstanding the differences in total equivalent free strains noted earlier.
  - Both procedures require more tie steel for CTB/cold ATB than an unbound base. However, the M-E design requires significantly more steel in terms of larger bar size or closer spacing for CTB or cold ATB due to the greater friction and greater modulus of these base types.
- Effect of number of lanes:
  - Both procedures require more tie steel as the number of lanes increase. However, the 1993 AASHTO is far more sensitive to number of lanes than the M-E design.

As an extension of this case study, the analysis above was repeated for concrete slab thicknesses of 6, 7, and 14 inches, respectively. The results are presented in Table 10 through Table 12.

Table 10. A comparison of M-E and 1993 AASHTO tie bar design procedures and project site parameters, concrete slab thickness = 6 in, Grade 60 steel.

Location	Base Type	#Lanes	1993 AASHTO Tie Bar Design	M-E Tie Bar Design
Chicago	Unbound	2	#4 @ 80-in	#4 @ 45-in
		3	#4 @ 80-in	#4 @ 45-in
		4	#5 @ 62-in	#5 @ 45-in
		6	#6 @ 59-in	#5 @ 45-in
	CTB/Cold ATB	2	#4 @ 67-in	#6 @ 36-in
		3	#4 @ 67-in	#6 @ 36-in
		4	#5 @ 52-in	#6 @ 36-in
		6	#6 @ 49-in	#6 @ 30-in
Las Vegas	Unbound	2	#4 @ 80-in	#4 @ 45-in
		3	#4 @ 80-in	#4 @ 45-in
		4	#5 @ 62-in	#5 @ 45-in
		6	#6 @ 59-in	#5 @ 45-in
	CTB/Cold ATB	2	#4 @ 67-in	#6 @ 36-in
		3	#4 @ 67-in	#6 @ 36-in
		4	#5 @ 52-in	#6 @ 25-in
		6	#6 @ 49-in	#6 @ 22-in

Table 11. A comparison of M-E and 1993 AASHTO tie bar design procedures and project site parameters, concrete slab thickness = 7 in, Grade 60 steel.

Location	Base Type	#Lanes	1993 AASHTO Tie Bar Design	M-E Tie Bar Design
Chicago	Unbound	2	#4 @ 68-in	#4 @ 45-in
		3	#4 @ 68-in	#4 @ 45-in
		4	#5 @ 53-in	#5 @ 45-in
		6	#6 @ 50-in	#5 @ 45-in
	CTB/Cold ATB	2	#4 @ 57-in	#6 @ 36-in
		3	#4 @ 57-in	#6 @ 36-in
		4	#5 @ 44-in	#6 @ 36-in
		6	#6 @ 42-in	#6 @ 30-in
Las Vegas	Unbound	2	#4 @ 68-in	#4 @ 45-in
		3	#4 @ 68-in	#4 @ 45-in
		4	#5 @ 53-in	#5 @ 45-in
		6	#6 @ 50-in	#5 @ 45-in
	CTB/Cold ATB	2	#4 @ 57-in	#6 @ 36-in
		3	#4 @ 57-in	#6 @ 36-in
		4	#5 @ 44-in	#6 @ 30-in
		6	#6 @ 42-in	#6 @ 25-in

Table 12. A comparison of M-E and 1993 AASHTO tie bar design procedures and project site parameters, concrete slab thickness = 14 in, Grade 60 steel.

Location	Base Type	#Lanes	1993 AASHTO Tie Bar Design	M-E Tie Bar Design
Chicago	Unbound	2	#4 @ 48-in	#4 @ 45-in
		3	#4 @ 48-in	#4 @ 45-in
		4	#5 @ 37-in	#5 @ 45-in
		6	#5 @ 25-in	#5 @ 45-in
	CTB/Cold ATB	2	#6 @ 88-in	#6 @ 36-in
		3	#6 @ 88-in	#6 @ 36-in
		4	#6 @ 44-in	#6 @ 36-in
		6	#6 @ 29-in	#6 @ 36-in
Las Vegas	Unbound	2	#4 @ 48-in	#4 @ 45-in
		3	#4 @ 48-in	#4 @ 45-in
		4	#5 @ 37-in	#5 @ 45-in
		6	#5 @ 25-in	#5 @ 45-in
	CTB/Cold ATB	2	#6 @ 88-in	#6 @ 36-in
		3	#6 @ 88-in	#6 @ 36-in
		4	#6 @ 44-in	#6 @ 30-in
		6	#6 @ 29-in	#6 @ 30-in

It can be noted from the data in these tables that the 1993 AASHTO tie bar design procedure is sensitive to the thickness of the slab while the M-E procedure is relatively insensitive. The M-E procedure requires higher amounts of steel for thinner pavements when compared to the 1993 AASHTO procedure but lower amounts of steel for thicker pavements.

CHAPTER 6. IMPACT OF MULTIPLE TIED LANES AND SHOULDERS ON SLAB STRESSES

INTRODUCTION

How many traffic lanes and concrete shoulders can be tied together without risking longitudinal cracking? Currently, the only information available to answer this question comes from specific project sites where several lanes have been tied together and no cracking has developed. Although there has not been a single case documented where longitudinal cracking has occurred solely due to tying too many lanes together, the rule of thumb typically calls for a maximum of three or four lanes/shoulders, or less than about 50 ft. While this answer may sound sufficient, it has led to some major problems where non-tied longitudinal joints have opened significantly, leading to wide opening of the non-tied joints and creating a scenario in which continued maintenance is required to fill the gaps to avoid safety concerns. Thus, this is a major question that needs to be answered for reliable design.

The ISLAB2005 finite element model developed for this study provides an ideal way to represent the horizontal slab-to-slab structure that can be tied together with deformed steel tie bars. The model was used to compute tensile stress in the slab that might lead to longitudinal cracking when more than two lanes are tied together due to the applied total equivalent free strains discussed earlier.

ILLUSTRATION OF CRITICAL TENSILE STRESSES IN CONCRETE SLABS WHEN MULTIPLE LANES ARE TIED TOGETHER

Figure 50 through Figure 53 were prepared using the ISLAB2005 tie bar model to illustrate the tensile stresses that develop in a concrete slab constructed on a CTB due to an applied total equivalent axial free strain, ε_{eq}, of 800 microstrain applied perpendicular to the direction of traffic. The definition of ε_{eq} is presented in Chapter 4. As expected, the critical tensile stress due to this type of slab "loading" occurs in the center of the centermost tied slab. This stress, if high enough, may lead to longitudinal cracking. The tie bar configurations for all of these designs were acceptable, meaning the steel yield stress was not exceeded. The average tensile stress through the slab increased significantly, however, as the number of lanes increased from two (tensile stress of about 200 psi) to five (tensile stress of about 375 psi). However, as shown in Figure 54, the critical stress did not increase significantly after three lanes.

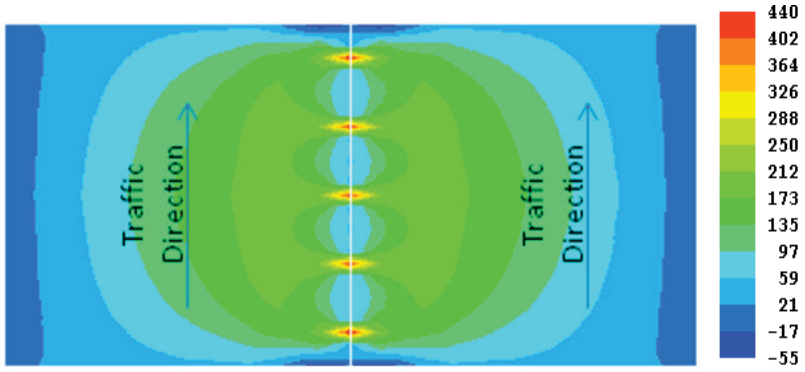

Figure 50. Tensile concrete stresses; two tied concrete pavement lanes on 6-in CTB, ε_{eq} = 800 microstrain in the direction perpendicular to traffic.

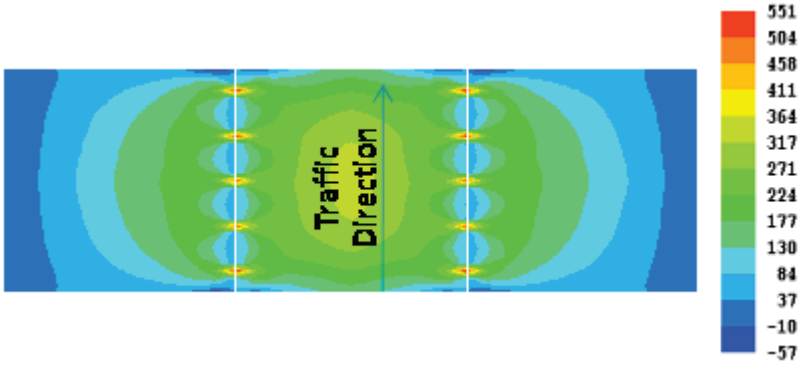

Figure 51. Tensile concrete stresses; three tied concrete pavement lanes on 6-in CTB, ε_{eq} = 800 microstrain in the direction perpendicular to traffic.

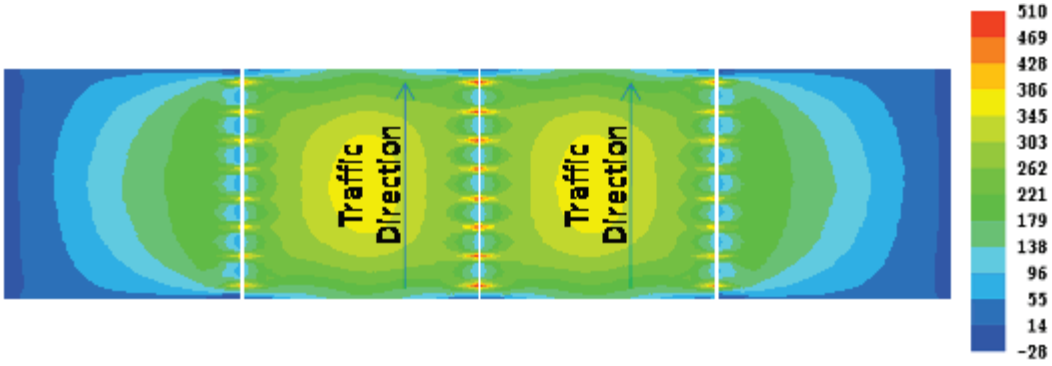

Figure 52. Tensile concrete stresses; four tied concrete pavement lanes on 6-in CTB, ε_{eq} = 800 microstrain in the direction perpendicular to traffic.

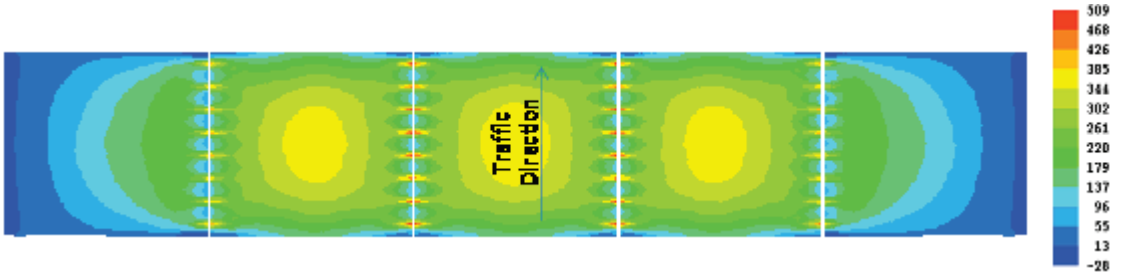

Figure 53. Tensile concrete stresses; five tied concrete pavement lanes on 6-in CTB, ε_{eq} = 800 microstrain in the direction perpendicular to traffic.

Figure 54. Tensile stress in the concrete slab built over a CTB vs. the number of tied lanes/shoulders.

Table 13 through Table 17 were prepared to show the values of tensile stress in the concrete slab for different numbers of tied lanes and varying amount of ε_{eq} applied to the slabs. These tables and Figure 50 through Figure 54 illustrate the following points:

- Slab tensile stresses caused by a uniform temperature drop and drying shrinkage of the concrete are significant and need to be considered in design.
- Adding traffic lanes increases the slab tensile stresses, which are transverse to the direction of traffic and generally located in the center of the central critical lane.
- Three lanes have higher stresses than two lanes because of the pull from the additional lane. Previous tie bar design procedures did not consider this, instead using only the shortest distance to a free edge as the basis for design.
- These stresses level out and do not increase significantly after more than three traffic lanes and/or shoulders are tied together.
- An unbound base course shows the lowest tensile stresses. For this design case, an unlimited number of lanes/shoulders can theoretically be tied together without risk of longitudinal cracking.
- Stabilized bases greatly increase the tensile stress in the slab. The higher the base modulus and slab-base friction, the greater the tensile stress in the concrete slabs. The most critical case is the LCB, where the elastic modulus was assumed to be about 2 million psi.

Table 13. Maximum tensile stresses in a 10-in concrete slab on a 6-in unbound base.

Total Equivalent Free Strain, microstrain	Number of Tied Lanes				
	2	3	4	5	6
800	20 psi	34 psi	36 psi	36 psi	36 psi

Table 14. Maximum tensile stresses in a 10-in concrete slab on a 6-in soil cement base.

Total Equivalent Free Strain, microstrain	Number of Tied Lanes				
	2	3	4	5	6
500	131 psi	147 psi	148 psi	148 psi	148 psi
600	151 psi	179 psi	179 psi	179 psi	179 psi
700	163 psi	208 psi	209 psi	209 psi	209 psi
800	175 psi	238 psi	240 psi	240 psi	240 psi

Table 15. Maximum tensile stresses in a 10-in concrete slab on a 6-in PCTB.

Total Equivalent Free Strain, microstrain	Number of Tied Lanes				
	2	3	4	5	6
500	152 psi	188 psi	191 psi	192 psi	192 psi
600	166 psi	225 psi	228 psi	228 psi	228 psi
700	180 psi	259 psi	266 psi	266 psi	266 psi
800	185 psi	292 psi	301 psi	301 psi	301 psi

Table 16. Maximum tensile stresses in a 10-in concrete slab on a 6-in CTB or cold ATB.

Total Equivalent Free Strain, microstrain	Number of Tied Lanes				
	2	3	4	5	6
500	163 psi	229 psi	235 psi	237 psi	237 psi
600	177 psi	267 psi	279 psi	279 psi	279 psi
700	185 psi	302 psi	319 psi	319 psi	319 psi
800	191 psi	336 psi	375 psi	375 psi	375 psi

Table 17. Maximum tensile stresses in a 10-in concrete slab on a 6-in LCB.

Total Equivalent Free Strain, microstrain	Number of Tied Lanes				
	2	3	4	5	6
500	177 psi	284 psi	304 psi	307 psi	307 psi
600	189 psi	326 psi	373 psi	*	*
700	197 psi	374 psi	*	*	*
800	206 psi	430 psi	*	*	*

*No tie bar design could be determined for these design situations using #6 and smaller tie bars. Such sections, however, could be handled using larger diameter tie bars and/or closer tie bar spacing.

DESIGN RECOMMENDATIONS

Based on the information presented, the following design recommendations can be made:

- **Unbound base course.** The magnitude of tensile stress for an unbound base course is so small that it is doubtful if longitudinal cracking would ever occur, no matter how many lanes and shoulders were tied together. Thus, the recommendation is that at least six lanes/shoulders could be tied together without significant build up of tensile stresses from thermal and drying shrinkages.
- **Cement and asphalt stabilized base courses**. The magnitude of tensile stress for stabilized base increases with the modulus of elasticity of the material and friction parameter. For example, the stresses shown in Table 18 were computed for the modulus associated with each base type for four tied lanes (total width of 48 ft) and 600 microstrains of total equivalent free strain.

Table 18. Summary of base type, modulus of elasticity, friction parameter, and maximum concrete pavement tensile stress.

Base Type	Base Elastic Modulus, psi	ISLAB2005 Friction Parameter	4 Tied Lane/Shoulders Maximum Tensile Stress, psi
Unbound Aggregate	50,000	100 psi/in	36
Soil Cement Base	500,000	15,000 psi/in	179
PCTB	750,000	15,000 psi/in	228
CTB & ATB	1,000,000	15,000 psi/in	279
LCB	2,000,000	15,000 psi/in	373

- The major question is what level of stress is acceptable without posing too great a risk for longitudinal slab cracking. Using stress as the criterion is not sufficient because the strength of the concrete can vary considerably. This can be overcome by utilizing the ratio of tensile stress to tensile strength as the

criterion. The indirect tensile strength can be determined using AASHTO T198 (ASTM C496) test protocol. It can also be determined from standard correlations with concrete flexural or compressive strength.

1. Determine the indirect tensile strength of the concrete via laboratory testing at 28 days, or use the following estimated relationships with other types of strength:

    a. Indirect Tensile Strength = Modulus of Rupture * 2/3
    b. Indirect Tensile Strength = $10*[\text{Compressive Strength}]^{0.5} * 2/3$

    Similar to the MEPDG, use the mean tested strengths here, not the minimum specification strength.
2. Compute the ratio of tensile stress to indirect tensile strength. If this ratio exceeds a critical value, the design is unacceptable. A critical ratio less than 1.0 is needed, perhaps in the range of 0.75 since fatigue is not an issue. Critical values of this ratio will need to be established based on field projects that have performed with or without longitudinal cracking.
3. If the stress/strength ratio exceeds the critical value, redesign the pavement by changing the base course or reduce the number of lanes tied together.

Table 19 shows a sample calculation of the stress/strength ratio.

Table 19. Concrete stress to strength ratio for concrete pavement on a 6-in CTB or cold ATB.

Free Strain, microstrain	Number of Tied Lanes				
	2	3	4	5	6
500	163/450=0.36	0.51	0.52	0.53	0.53
600	0.39	0.59	0.62	0.61	0.61
700	0.41	0.67	0.71	0.71	0.71
800	0.42	0.75	0.83	0.83	0.83

Assumes that the mean 28-day compressive strength for a project is 4,500 psi, so estimate of the indirect tensile strength is $10 * (4500)^{0.5} * 2/3 = 450$ psi. Stress values are taken from Table 16.

It is obvious that the stress calculation shows that the tensile stress in the concrete slab does not increase appreciably after three slabs are tied together. Practically every highway agency allows three lanes to be tied together regardless of base type. Thus, it could be argued that, given the fact that three or even four slabs tied together over stabilized bases are not that unusual, and these have not shown longitudinal cracking, the same recommendation for unbound bases could be given for stabilized bases. Further validation is required to resolve this question.

CHAPTER 7. SUMMARY, CONCLUSIONS, AND RECOMMENDATIONS

SUMMARY AND CONCLUSIONS

A major objective of this study was to develop a new methodology for the design of longitudinal joints in concrete pavements placed on different types of bases. The research effort involved the following aspects:

- A literature review of past theoretical and experimental studies on friction between the concrete pavement slabs and base and bonding between steel and concrete.
- Field investigations of tied multi-lane concrete pavements in 10 States.
- Field measurements of joint opening and LTE as a function of temperature changes.
- Development of an M-E tie bar design procedure based on finite element modeling.
- Sensitivity analysis of the effect of various design parameters on longitudinal joint openings and steel stresses.
- Comparison of the M-E based tie bar design solutions with the 1993 AASHTO SDT-based approach for multi-lane pavements.
- Investigation of the impact of multiple tied lanes on slab stresses due to uniform environmentally-induced strains in the slab.
- Development of supplementary tie bar design tables for different base types and environmental loading conditions.

The proposed M-E tie bar design procedure was based on the premise that the yield stresses in the tie steel can be kept in check if the joint opening is limited to an acceptable value. Therefore, steel yield stress is the primary criterion used in this M-E tie bar design, much like in the SDT approach. However, unlike the SDT approach, a secondary linkage to joint opening is made in the M-E based approach. Several other factors separate the M-E tie bar approach from the SDT approach, including the following:

- The M-E approach considers actual environmentally-induced strains as an input to tie bar design; hence, context-sensitive designs can be developed for different climatic regions or pavement structural or geometric configurations.
- The M-E approach better handles tie bar design for situations when multiple lanes and shoulders are tied together. The SDT approach cannot account for multiple lanes and shoulders accurately.
- The M-E approach considered several combinations of pavement cross-section, concrete materials, slab-base friction, tie bar, steel-concrete interface, and longitudinal joint factors and environmentally-induced strains in the finite

element model used to develop the design solutions, which is far beyond the capability of the SDT method.

Making all this possible in the M-E approach is the use of a sophisticated numerical pavement model using ISLAB2005 to analyze the cause-and-effect relationships between environmentally-induced slab movements and pavement and tie bar variables and joint response. In this model, the concrete pavement slab and base are modeled as two independent linear elastic layers—a significant deviation from state-of-the-practice modeling of the pavement for tie bar design purposes. Further, the concrete slab-base interface is characterized using a bilinear friction model. The recommendations of the HIPERPAV program were used for assigning the friction model parameters for various base types. Finally, a simple linear model was used to defining the pull-out behavior of a tie bar. The relationship between pull-out forces and corresponding bar edge slips is derived from the CEB equation between bond stresses and bond slip and the pull-out stiffness for a given set of tie bar dimensions and steel grade was derived from this relationship.

Total equivalent free axial strains due to drying shrinkage (computed 1-year after pavement construction) and uniform temperature drop in concrete from set temperature to the mean monthly temperature of the coldest month at a site were used to define the environmentally-induced slab deformations. Supplemental tie bar design tables for different types of bases were developed for various total equivalent free axial strains.

A sensitivity analysis was conducted to study the effects of design inputs on computed joint opening and tensile stresses in the tie bar steel. The parametric study investigated the significance of design factors such as base types and thicknesses, lane width and number of lanes tied, and tie bar size and spacing, while keeping the assumed total equivalent free axial strain constant. One major finding, which is a direct result of the consideration of the base layer as an independent linear elastic layer, was that the base stiffness played a prominent role in determining tie steel requirements in addition to concrete slab-base interlayer friction. It was found that the resultant tie bar steel stress is lower in concrete pavements constructed of base materials that have low stiffness, such as unbound bases, than when treated bases are used. Consequently, a lesser area of tie bar steel is required for the former (either smaller bars or greater spacing).

The results computed from the proposed M-E design method were compared with those of the SDT-based 1993 AASHTO Guide for two selected locations—Chicago and Las Vegas. The comparison of design solutions for these locations indicated little difference between these two methods in calculating total free strains for concrete slabs placed on unbound bases. However, for CTBs, the proposed M-E tie bar design method required a greater amount of steel for the tie bars (either larger bars or closer spacing) than what is required when using the 1993 AASHTO method for design, for similar design assumptions. However, as the number of tied lanes/shoulders goes

beyond three, the AASHTO 1993 method predicts higher steel requirements when unbound bases are used and approximately the same amount of steel for CTB/cold ATB. Furthermore, the M-E method was found to be more or less insensitive to concrete slab thickness, while the SDT methods predict higher steel contents for thicker pavements. Finally, the M-E method was sensitive to the climatic differences between the two selected locations, whereas the SDT method was not.

The M-E tie bar design procedure was then used to evaluate the effect of multiple tied lanes and shoulders on longitudinal joint design. The results of the ISLAB2005 simulations indicated that the impact of increasing the number of tied lanes on joint condition was insignificant for concrete slabs on unbound bases. However, for concrete slabs on stabilized bases (with higher stiffness and interface friction than the unbound base), the steel stresses increased when the number of tied lanes was changed from two to three. Any further increase in the number of tied lanes did not lead to significant changes in steel stresses for the slabs placed on stabilized bases. Among the base types studied in this project, the maximum tensile stress was found to be lowest for unbound bases and highest for LCBs for the same total equivalent free strain. The increase in maximum tensile stresses was practically insignificant when three or more lanes were tied together.

The M-E tie bar procedure developed under this study is a practical design approach that considers the key performance criterion of interest for which tie bars are placed in the slab—to maintain the integrity of the joint over the life of the pavement while ensuring that there is no excessive longitudinal stress build up when multiple lanes are tied together. The results obtained from the procedure appear to be reasonable from an engineering standpoint. Another conclusion from the information gathered from in-service pavements is that placement of tie bars is as important as good design. Some of the observed failures in the field clearly were due to poor construction practices.

RECOMMENDATIONS FOR FUTURE WORK

As stated earlier, the tie bar design guidance developed under this study produced a series of supplemental look-up tables that designers can use to determine the tie bar spacing and size for a given environmentally-induced loading condition and a given set of pavement variables. It is recommended that this process be computerized for ease of use. It is also recommended that this guidance be validated using a limited number of well-designed field cases.

One of the major limitations of the study, which was recognized at the outset, was the lack of more current experimental data to establish the following parameters in the analytical model used to derive the tie bar design guidance:

- Slab/supporting layer friction characteristics for modern bases in accordance with modern friction theories. The last published data on this topic are from the

mid-1980s. This is a complex topic that requires great planning and care in execution to derive the desired results.

- A systematic investigation of the bond behavior of tie bars and paving concrete. The impact of tie bar pull-out stiffness on the concrete pavement longitudinal joint design developed in this study is significant, especially in the case of pavements on stabilized bases. Guidance from the CEB was adopted in this research, since it was the best available and most practical source of information. It is not possible to easily extend the results of this guidance to shorter embedment lengths (less than standard lengths of approximately 15 in) or bigger bar sizes (e.g., #8 bars) without further experimental verification. This work is expressly recommended to be taken up and requires obtaining pull-out force-slip curves for a combination of concrete strengths, tie bar dimensions, and embedment lengths.

Another shortcoming of this research was the lack of a more comprehensive field investigation of tie bar placement and its influence on joint performance. Construction factors such as misalignment and improper embedment of tie bars into existing pavements were noted to have influenced joint performance. This area needs to be studied further, and practical placement specifications should be developed based on field investigations of a number of in-service pavements.

A comprehensive nationwide survey of multi-lane tied concrete pavements to determine their propensity to exhibit longitudinal distress propagation could not be accomplished in this study. Such a study should entail field visits, records reviews, and limited forensic investigations to derive meaningful results. Such observations can be used to refine the design check developed in this study to minimize the risk of longitudinal cracking. Further, the design check developed herein uses a ratio of tensile stress to indirect tensile strength of concrete as a criterion for assessing the risk of longitudinal cracking in tie bar design. A maximum tensile stress/strength ratio value of 0.75 is recommended. However, the critical ratios could be further evaluated and derived based on the experience gathered from the field surveys. In addition, other mechanisms that cause longitudinal cracking in pavements, e.g., wheel loadings and curling and warping stresses, and their coupling with the tensile stresses computed in the proposed M-E design check need to be fully investigated.

REFERENCES

American Association of State Highway and Transportation Officials (AASHTO), *Mechanistic-Empirical Pavement Design Guide, Interim Edition: A Manual of Practice*, Washington, DC, 2008.

American Association of State Highway and Transportation Officials (AASHTO), *Guide for Design of Pavement Structures*, American Association of State Highway and Transportation Officials, Washington, DC, 1993.

Abe, J., S. Kameta, R. Sato, and Y. Hachya. A New Design Approach for Control of Cracking in Continuously Reinforced Concrete Pavement. *Proceeding, 2nd International Workshop on the Theoretical Design of Concrete Pavements,* Madrid, Spain, 1990, pp. 283-296.

Ahlborn, T., and T. DenHartigh. *A Comparative Bond Study of MMFX Reinforcing Steel in Concrete*. Final Report, Michigan Technological University Center for Structural Durability, Houghton, MI, 2002.

Ardani, A., S. Hussain, and R. LaForce. *Evaluation of Premature PCCP Longitudinal Cracking in Colorado*. Final Report CDOT-DTD-R-2003-1, Colorado Deparment of Transportation, Denver, CO, 2003.

Bendana, L.J., D. McAuliffe, and W.S. Yang. Joint Design Methods Developed for NYS Pavement Design, Special Report, Albany, NY, 1992.

Bergstrom, S.G. Temperature Stresses in Concrete Pavements, Proceeding #14, Swedish Cement and Concrete Research Institute at the Royal Institute of Technology, Stockholm, Sweden, 1950, pp. 1-37.

Bradbury, R.D. Reinforced Concrete Pavements. Wire Reinforcement Institute, Washington, DC, 1938.

CEB-FIP, Model Code for Concrete Structure Comité Euro-International du Béton et Federation Internationale de la Precontrainte, Lausanne, Switzerland, 1990.

Darter, M.I., H. Von Quintus, Y.J. Jiang, E.B. Owusu-Antwi, and B.M. Killingsworth. Catalog of Recommended Pavement Design Features. National Cooperative Highway Research Program, NCHRP Project 1-32, Washington, DC, 1998.

Davids, W.G., Z. Wang, G. Turkiyyah, J.P. Mahoney, and D. Bush. Three-Dimensional Finite Element Analysis of Jointed Plain Concrete Pavement with EverFE2.2. *Transportation Research Record 1853,* TRB, 2003, pp. 92-99.

Eisenman, J., D. Birman, and G. Leykauf. Research Results on the Bond Between Cement Treated Subbases and Concrete Slabs. *Proc., International Seminar on Drainage and Erodability at the Concrete Slab-Subbase_Shoulder Interfaces*, Paris, France, 1983.

Eligenhausen, R., E.P. Popov, and V. Betero. Local Bond-Stress Relationships of Deformed Bar under Generalized Excitations, Technical Report, #UCB/EERC-83/23, Earthquake Engineering Research Center, Berkeley, CA, 1983.

Federal Highway Administration (FHWA). *LTPP Seasonal Monitoring Program: Instrumentation Installation and Data Collection Guidelines*, FHWA Publication Number: FHWA-RD-94-110, Washington, DC, 1994.

Florida Department of Transportation (FDOT). *Rigid Pavement Design Manual,* Florida Department of Transportation, Tallahassee, FL, 2006.

Goldbeck, A.T. Friction Tests of Concrete on Various Subbases. *Public Roads,* Vol. 5, #5, 1924, pp. 19-23.

Gotlif, A., J. Mallela, and L. Khazanovich. Finite Element Study of Partial-depth Cracks in Restrained PCC Slabs. *International Journal of Pavement Engineering*, Vol. 7, #4, 2006, pp. 323-329.

Guide for Mechanistic-Empirical Design of New and Rehabilitated Pavement Structures. Final Report, NCHRP 1-37A, Transportation Research Board, 2004.

Guo, E.H. Mathematical Modeling for Dowel Load Transfer System. PHD Dissertation, Michigan State University, 1992.

Huang Y.H. *Pavement Analysis and Design*. Prentice Hall, Inc., New Jersey, 1993.

Ioannides, A.M., and R.A. Salsilli-Murua. Field Evaluation of Newly Developed Rigid Pavement Design Feature, Phase 1 – Modification No.3, Interim report. Project number DTFH61-85_C-00103. U.S. Department of Transportation, 1988.

Iwama, S. Experimental Studies on the Structural Design of Concrete Pavement. Pavement Laboratory, Public Works Research Institute, Ministry of Construction, Japan, 1964.

Kachlakev, D.I., J.R. Lundy, V. Gillet, A. Le Bonn, Y. Donon, C. Martinad, and G. Guerin. New Procedure for Evaluating Bond Strength of Concrete Reinforcement. *Transportation Research Record 1525,* TRB, National Research Council, Washington, DC, 1996, pp. 124-130.

Kankam, C.K. Relationship of Bond Stress, Steel Stress, and Slip in Reinforced Concrete. *Journal of Structural Engineering,* Vol. 123, No.1, 1997, pp. 79-85.

Kelley, E.F. Applications of the Results of Research to the Structural Design of Concrete Pavements. *Public Roads,* Vol. 20, #5, 1939, pp. 107-126.

Khazanovich L. Structural Analysis of Multi-Layered Concrete Pavement Systems. PhD Dissertation, University of Illinois, 1994.

Khazanovich, L., T. Yu, and C.A. Beckmeyer. Application of ISLAB2000 for Forensic Studies. *Proceedings., Second International Symposium on 3D Finite Element for Pavement Analysis, Design, and Research.* Charleston, WV, 2000.
Lee S.W. "Characteristics of Friction between Concrete Slab and Base," *KSCE Journal of Civil Engineering*, Vol. 4, #4, Seoul, Korea, December 2000, pp. 265-275.

Masad, E., R. Taha, and B. Muhunthan. Finite-Element Analysis of Temperature Effects on Plain Jointed Concrete Pavements. *Journal of Transportation Engineering,* Vol. 122, No.5, 1996, pp. 388-398.

Nishizava, T., M. Koyanagava, and M. Kimura. Study on Mechanical Behavior of Dowel Bar in Transverse Joint of Concrete Pavement. *Proceedings, 7th International Conference on Concrete Pavements,* Orlando, FL, 2001, pp. 571-588.

Olesen, J.F., Concrete-Reinforcement Bond-Slip Behavior. Technical Report , Department of Civil Engineering Technical University of Denmark, Oslo, Denmark, 2002.

Orangun, C.O., J.O. Jirsa, and J.E. Breen. A Reevaluation of Test Data on Development Length and Splices. *ACI Journal*, Vol. 74, #3, 1977, pp. 114-122.

Portland Cement Association (Farny, J. A. and Tarr, S. M.), Concrete Floors on Ground, Publication #EB075, Fourth Edition, Skokie, IL, 2008.

Rassmussen, R.O., and D.K. Rozycki. Characterization and Modeling of Axial Slab-Support Restraint. *Transportation Research Record 1778,* TRB, 2000, pp. 26-32.

Ruiz J.M., P.J. Kim, A.K. Schindler, and R.O. Rasmussen. Validation of HIPERPAV for Prediction of Early-Age Jointed Concrete Pavement Behavior. *Transportation Research Record 1778,* TRB, National Research Council, Washington, DC, 2001, pp. 17-25.

Seong-Min Kim, Moon Won, and B.F. McCullough. Numerical Modeling of Continuously Reinforced Pavement Subjected to Environment Loads. *Transportation Research Record 1629,* TRB, 1998, pp. 76-89.

Seong-Min Kim, Moon Won, and B.F. McCullough. Three-Dimensional Modeling of Continuously Reinforced Pavement. *Transportation Research Record 1730,* Transportation Research Board, 2000, pp. 43-52.

Sparkes, F.N. "Stresses in Concrete Road Slabs." *The Structural Engineer*, London, England, 1939, pp. 98-116.

Stott, J.P. Tests on Materials for Use in Sliding Layers Under Concrete Road Slabs. *Civil Engineering and Public Works Review*, Vol. 56, #663, 1961, pp. 1297-1301.

Tarr, S.M., P.A. Okamoto, M.J. Sheehan, and R.G. Packard. Bond Interaction between Concrete Pavement and Lean Concrete Base. *Transportation Research Record 1668,* TRB, National Research Council, Washington, DC, 1999, pp. 9-17.

Technical Advisory "Concrete Pavement Joints," US Department of Transportation, Washington, DC, 1990.

Teller, L.W., and E.C. Sutherland. The Structural Design of Concrete Pavements, Part 2: Observed Effects of Variations in Temperature and Moisture on the Size, Shape and Stress Resistance of Concrete Pavement Slabs. *Public Roads,* Vol. 16, #9, 1935, pp. 169-197.

Tims, A.G. Evaluation Subgrade Friction-Reducing Mediums for Rigid Pavements. In *Highway Research Record* 60, HRB, National Research Council, Washington, DC, 1964, pp. 23-38.

Van Gauwelaert, F. Partial Friction in Multilayer Theory. *Workshop on Theoretical Design of Concrete Pavement,* Epen, Netherlands, 1986.

Wesevich, J. W., B.F. McCullough, and N.H. Burns. *Stabilization Subbase Study for Concrete Pavement,* Research Report 459-1, Center for Transportation Research, University of Texas at Austin, 1987.

Wimsatt, A.J., and B.F. McCullough. Subbase Friction Effects on Concrete pavements, *Proceedings, 4th International Conference on Concrete Pavement Design and Rehabilitation,* Purdue University, West Lafayette, IN, 1989, pp. 3-21.

Yang, W., W.J.Weiss, and S.P. Shah. Predicted Shrinkage Stress Field in Concrete Slab on Elastic Subgrade. *Journal of Engineering Mechanics,* Vol. 126, No.1, 2000, pp. 35-42.

Yoder, E.J., and M.W. Witczak. *Principles of Pavement Design.* John Wiley & Sons, Inc., New York, 1975.

Zhang, J. and V.C. Li. Influence of Supporting Base Characteristics on Shrinkage-Induced Stresses in Concrete Pavements. *Journal of Transportation Engineering,* Vol. 127, No.6, 2001, pp. 445-462.

APPENDIX A—CLIMATIC DATA FOR 100 LARGEST CITIES IN THE U.S.

Table A-1. Summary of average monthly temperature and relative humidity for 100 largest cities in the United States.

City	Average monthly temperature (°F)[1]				Yearly Relative Humidity, %
	Jan.	April	July	Oct.	
Albany, NY	22.2	46.6	71.1	49.3	69
Albuquerque, NM	35.7	55.6	78.5	57.3	44
Anchorage, AK	15.8	36.3	58.4	34.1	68
Asheville, NC	35.8	54.1	73.0	55.2	74
Atlanta, GA	42.7	61.6	80.0	62.8	69
Atlantic City, NJ	32.1	50.6	75.3	55.1	69
Austin, TX	50.2	68.3	84.2	70.6	71
Baltimore, MD	32.3	53.2	76.5	55.4	66
Baton Rouge, LA	50.1	66.6	81.7	68.1	76
Billings, MT	24.0	46.1	72.0	48.1	55
Birmingham, AL	42.6	61.3	80.2	62.9	72
Bismarck, ND	10.2	43.3	70.4	45.2	71
Boise, ID	30.2	50.6	74.7	52.8	56
Boston, MA	29.3	48.3	73.9	54.1	66
Bridgeport, CT	29.9	48.9	74.0	54.7	67
Buffalo, NY	24.5	45.3	70.8	50.7	72
Burlington, VT	18.0	43.5	70.6	47.7	68
Caribou, ME	9.5	38.1	65.6	42.8	70
Casper, WY	22.3	42.7	70.0	45.7	57
Charleston, SC	47.9	64.2	81.7	66.2	70
Charleston, WV	33.4	54.3	73.9	55.1	70
Charlotte, NC	41.7	60.9	80.3	61.7	68
Cheyenne, WY	25.9	41.6	67.7	45.4	56
Chicago, IL	22.0	47.8	73.3	52.1	71

1. Based on 30-year period 1971–2000.
Source: National Oceanic and Atmospheric Administration (NOAA).

Table A-1. Summary of average monthly temperature and relative humidity for 100 largest cities in the United States, continued.

City	Average monthly temperature (°F)[1]				Yearly Relative Humidity, %
	Jan.	April	July	Oct.	
Cleveland, OH	25.7	47.6	71.9	52.2	71
Columbia, SC	44.6	63.2	82.0	63.7	68
Columbus, OH	28.3	52.0	75.1	54.7	70
Concord, NH	20.1	44.6	70.0	47.8	67
Dallas-Ft. Worth, TX	44.1	65.0	85.0	67.2	70
Denver, CO	29.2	47.6	73.4	51.0	54
Des Moines, IA	20.4	50.6	76.1	52.8	71
Detroit, MI	24.5	48.1	73.5	51.9	71
Dodge City, KS	30.1	53.9	79.8	57.1	66
Duluth, MN	8.4	39.0	65.5	43.5	73
El Paso, TX	45.1	64.6	83.3	64.9	42
Fairbanks, AK	-9.7	31.7	62.4	23.5	63
Fargo, ND	6.8	43.5	70.6	45.3	73
Grand Junction, CO	26.1	50.9	76.8	52.7	49
Grand Rapids, MI	22.4	46.3	71.4	49.9	73
Hartford, CT	25.7	48.9	73.7	51.9	65
Helena, MT	20.2	44.1	67.8	44.8	59
Honolulu, HI	73.0	75.6	80.8	80.2	64
Houston, TX	51.8	68.5	83.6	70.4	77
Indianapolis, IN	26.5	52.0	75.4	54.6	73
Jackson, MS	45.0	63.4	81.4	64.4	76
Jacksonville, FL	53.1	66.6	81.6	69.4	73
Juneau, AK	25.7	40.8	56.8	42.3	75
Kansas City, MO	26.9	54.4	78.5	56.8	72
Knoxville, TN	37.6	57.8	77.7	58.8	73

1. Based on 30-year period 1971–2000.
Source: National Oceanic and Atmospheric Administration (NOAA).

Table A-1. Summary of average monthly temperature and relative humidity for 100 largest cities in the United States, continued.

City	Average monthly temperature (°F)[1]				Yearly Relative Humidity, %
	Jan.	April	July	Oct.	
Las Vegas, NV	47.0	66.0	91.2	68.7	30
Lexington, KY	32.0	54.6	76.1	56.6	71
Little Rock, AR	40.1	61.4	82.4	63.3	71
Long Beach, CA	57.0	63.0	73.8	68.6	67
Los Angeles, CA	57.1	60.8	69.3	66.9	72
Louisville, KY	33.0	56.4	78.4	58.5	70
Madison, WI	17.3	45.9	71.6	49.3	74
Memphis, TN	39.9	62.1	82.5	63.8	70
Miami, FL	68.1	75.7	83.7	78.8	72
Milwaukee, WI	20.7	45.2	72.0	51.4	73
Minneapolis–St. Paul, MN	13.1	46.6	73.2	48.7	71
Mobile, AL	50.1	66.1	81.5	67.7	74
Montgomery, AL	46.6	64.3	81.8	65.4	73
Mt. Washington, NH	5.2	22.9	48.7	30.2	83
Nashville, TN	36.8	58.5	79.1	59.9	72
Newark, NJ	31.3	52.3	77.2	56.4	63
New Orleans, LA	52.6	68.2	82.7	70.0	76
New York, NY	32.1	52.5	76.5	56.6	64
Norfolk, VA	40.1	57.4	79.1	61.1	67
Oklahoma City, OL	36.7	59.7	82.0	62.0	69
Olympia, WA	38.1	47.4	62.8	49.7	78
Omaha, NE	21.7	51.4	76.7	53.2	72
Philadelphia, PA	32.3	53.1	77.6	57.2	66
Phoenix, AZ	54.2	70.2	92.8	74.6	37

1. Based on 30-year period 1971–2000.
Source: National Oceanic and Atmospheric Administration (NOAA).

Table A-1. Summary of average monthly temperature and relative humidity for 100 largest cities in the United States, continued.

City	Average monthly temperature (°F)[1]				Yearly Relative Humidity, %
	Jan.	April	July	Oct.	
Pittsburgh, PA	27.5	49.9	72.6	52.5	68
Portland, ME	21.7	43.7	68.7	47.7	69
Portland, OR	39.9	51.2	68.1	54.3	72
Providence, RI	28.7	48.6	73.3	53.0	65
Raleigh, NC	39.7	59.1	78.8	60.0	70
Reno, NV	33.6	48.6	71.3	52.0	50
Richmond, VA	36.4	57.1	77.9	58.3	68
Roswell, NM	40.0	60.5	80.8	61.4	50
Sacramento, CA	46.3	58.9	75.4	64.4	65
Salt Lake City, UT	29.2	50.0	77.0	52.5	55
San Antonio, TX	50.3	68.6	84.3	70.7	70
San Diego, CA	57.8	62.6	70.9	67.6	70
San Francisco, CA	49.4	56.2	62.8	61.0	73
Savannah, GA	49.2	65.3	82.1	67.1	70
Seattle-Tacoma, WA	40.9	50.2	65.3	52.7	73
Sioux Falls, SD	14.0	45.7	73.0	48.0	73
Spokane, WA	27.3	46.5	68.6	47.2	65
Springfield, IL	25.1	52.8	76.3	55.5	70
St. Louis, MO	29.6	56.6	80.2	58.3	72
Tampa, FL	61.3	71.5	82.5	75.8	74
Toledo, OH	23.9	48.3	73.0	51.8	72
Tucson, AZ	51.7	66.0	86.5	70.5	39
Tulsa, OK	36.4	60.8	83.5	62.6	70
Vero Beach, FL	63.0	71.5	81.7	76.4	70

1. Based on 30-year period 1971–2000.
Source: National Oceanic and Atmospheric Administration (NOAA).

Table A-1. Summary of average monthly temperature and relative humidity for 100 largest cities in the United States, continued.

City	Average monthly temperature (°F)[1]				Yearly Relative Humidity, %
	Jan.	April	July	Oct.	
Washington, DC	34.9	56.1	79.2	58.8	69
Wichita, KS	30.2	55.3	81.0	58.6	69
Wilmington, DE	31.5	52.4	76.6	55.8	66

1. Based on 30-year period 1971–2000.
Source: National Oceanic and Atmospheric Administration (NOAA).

APPENDIX B—SUPPLEMENTARY TIE BAR DESIGN TABLES FOR UNBOUND BASES

Table B-1. Tie bar design for two tied 12-ft lanes on a 6-in unbound base.

Total Equivalent Free Strain, Microstrain	Tie Bar Size Designation	Tie Bar Spacing, in	Tie Bar Length, in	Steel Grade
500	#4	45	24	40
550	#4/#5	45	24	60/40
600	#4/#5	45	24	60/40
650	#4/#5	45	24	60/40
700	#4/#5	45	24	60/40
750	#4/#5	45	24	60/40
800	#4/#5	45	24	60/40

Table B-2. Tie bar design for a 12-ft lane tied to a 14-ft lane on 6-in unbound base.

Total Equivalent Free Strain, Microstrain	Tie Bar Size Designation	Tie Bar Spacing, in	Tie Bar Length, in	Steel Grade
500	#4/#5	45	24	60/40
550	#4/#5	45	24	60/40
600	#4/#5	45	24	60/40
650	#4/#5	45	24	60/40
700	#4/#5	45	24	60/40
750	#4/#5	45	24	60/40
800	#4/#5	45	24	60/40

Table B-3. Tie bar design for two tied 14-ft lanes on a 6-in unbound base.

Total Equivalent Free Strain, Microstrain	Tie Bar Size Designation	Tie Bar Spacing, in	Tie Bar Length, in	Steel Grade
500	#4/#5	45	24	60/40
550	#4/#5	45	24	60/40
600	#4/#5	45	24	60/40
650	#4/#5	45	24	60/40
700	#4/#5	45	24	60/40
750	#4/#5	45	24	60/40
800	#4/#5	45	24	60/40

Table B-4. Tie bar design for three tied 12-ft lanes on a 6-in unbound base.

Total Equivalent Free Strain, Microstrain	Tie Bar Size Designation	Tie Bar Spacing, in	Tie Bar Length, in	Steel Grade
500	#4/#5	45	24	60/40
550	#4/#5	45	24	60/40
600	#4/#5	45	24	60/40
650	#4/#5	45	24	60/40
700	#4/#5	45	24	60/40
750	#4/#5	45	24	60/40
800	#4/#5	45	24	60/40

Table B-5. Tie bar design for four tied 12-ft lanes on a 6-in unbound base.

Total Equivalent Free Strain, Microstrain	Tie Bar Size Designation	Tie Bar Spacing, in	Tie Bar Length, in	Steel Grade
500	#4/#5	45	24	60/40
550	#4/#5	45	24	60/40
600	#4	45	24	60
650	#5	36/45	24	40/60
700	#5	36/45	24	40/60
750	#5	36/45	24	40/60
800	#5	45	24	60

APPENDIX C—SUPPLEMENTARY TIE BAR DESIGN TABLES FOR SOIL CEMENT BASES

Table C-1. Tie bar design for two tied 12-ft lanes on a 6-in soil cement base.

Total Equivalent Free Strain, Microstrain	Tie Bar Size Designation	Tie Bar Spacing, in	Tie Bar Length, in	Steel Grade
500	#5	36	24	60
550	#5	36	24	60
600	#5	36	24	60
650	#5	36	24	60
700	#5	36	24	60
750	#5/#6	30/36	24	60
800	#5/#6	30/36	24	60

Table C-2. Tie bar design for two tied 12-ft lanes on a 5-in soil cement base.

Total Equivalent Free Strain, Microstrain	Tie Bar Size Designation	Tie Bar Spacing, in	Tie Bar Length, in	Steel Grade
500	#5	36	24	60
550	#5	36	24	60
600	#5	36	24	60
650	#5	36	24	60
700	#5	36	24	60
750	#5	36	24	60
800	#5	36	24	60

Table C-3. Tie bar design for two tied 12-ft lanes on a 4-in soil cement base.

Total Equivalent Free Strain, Microstrain	Tie Bar Size Designation	Tie Bar Spacing, in	Tie Bar Length, in	Steel Grade
500	#5	36	24	60
550	#5	36	24	60
600	#5	36	24	60
650	#5	36	24	60
700	#5	36	24	60
750	#5	36	24	60
800	#5	36	24	60

Table C-4. Tie bar design for a 12-ft lane tied to a 14-ft lane on a 6-in soil cement base.

Total Equivalent Free Strain, Microstrain	Tie Bar Size Designation	Tie Bar Spacing, in	Tie Bar Length, in	Steel Grade
500	#5	36	24	60
550	#5	36	24	60
600	#5	36	24	60
650	#5	36	24	60
700	#5	36	24	60
750	#5/#6	30/36	24	60
800	#6	36	24	60

Table C-5. Tie bar design for two tied 14-ft lanes on a 6-in soil cement base.

Total Equivalent Free Strain, Microstrain	Tie Bar Size Designation	Tie Bar Spacing, in	Tie Bar Length, in	Steel Grade
500	#5	36	24	60
550	#5	36	24	60
600	#5	36	24	60
650	#5	36	24	60
700	#5/#6	30/36	24	60
750	#5/#6	30/36	24	60
800	#6	36	24	60

Table C-6. Tie bar design for three tied 12-ft lanes on a 6-in soil cement base.

Total Equivalent Free Strain, Microstrain	Tie Bar Size Designation	Tie Bar Spacing, in	Tie Bar Length, in	Steel Grade
500	#5	36	24	60
550	#5	36	24	60
600	#5	36	24	60
650	#5	36	24	60
700	#5/#6	30/36	24	60
750	#6	36	24	60
800	#6	36	24	60

Table C-7. Tie bar design for four tied 12-ft lanes on a 6-in soil cement base.

Total Equivalent Free Strain, Microstrain	Tie Bar Size Designation	Tie Bar Spacing, in	Tie Bar Length, in	Steel Grade
500	#5	36	24	60
550	#5	36	24	60
600	#5	36	24	60
650	#5	36	24	60
700	#5/#6	30/36	24	60
750	#6	36	24	60
800	#6	36	24	60

APPENDIX D—SUPPLEMENTARY TIE BAR DESIGN TABLES FOR PERMEABLE CEMENT TREATED BASES

Table D-1. Tie bar design for two tied 12-ft lanes on a 6-in PCTB.

Total Equivalent Free Strain, Microstrain	Tie Bar Size Designation	Tie Bar Spacing, in	Tie Bar Length, in	Steel Grade
500	#5	36	24	60
550	#5	36	24	60
600	#5	36	24	60
650	#5	36	24	60
700	#5/#6	30/36	24	60
750	#6	36	24	60
800	#6	36	24	60

Table D-2. Tie bar design for two tied 12-ft lanes on a 5-in PCTB.

Total Equivalent Free Strain, Microstrain	Tie Bar Size Designation	Tie Bar Spacing, in	Tie Bar Length, in	Steel Grade
500	#5	36	24	60
550	#5	36	24	60
600	#5	36	24	60
650	#5	36	24	60
700	#5	36	24	60
750	#5/#6	30/36	24	60
800	#6	36	24	60

Table D-3. Tie bar design for two tied 12-ft lanes on a 4-in PCTB.

Total Equivalent Free Strain, Microstrain	Tie Bar Size Designation	Tie Bar Spacing, in	Tie Bar Length, in	Steel Grade
500	#5	36	24	60
550	#5	36	24	60
600	#5	36	24	60
650	#5	36	24	60
700	#5	36	24	60
750	#5	36	24	60
800	#6	36	24	60

Table D-4. Tie bar design for a 12-ft lane tied to a 14-ft lane on a 6-in PCTB.

Total Equivalent Free Strain, Microstrain	Tie Bar Size Designation	Tie Bar Spacing, in	Tie Bar Length, in	Steel Grade
500	#5	36	24	60
550	#5	36	24	60
600	#5	36	24	60
650	#5/#6	30/36	24	60
700	#6	36	24	60
750	#6	36	24	60
800	#6	36	24	60

Table D-5. Tie bar design for two tied 14-ft lanes on a 6-in PCTB.

Total Equivalent Free Strain, Microstrain	Tie Bar Size Designation	Tie Bar Spacing, in	Tie Bar Length, in	Steel Grade
500	#5	36	24	60
550	#5	36	24	60
600	#5/#6	30/36	24	60
650	#6	36	24	60
700	#6	36	24	60
750	#6	36	24	60
800	#6	36	24	60

Table D-6. Tie bar design for three tied 12-ft lanes on a 6-in PCTB.

Total Equivalent Free Strain, Microstrain	Tie Bar Size Designation	Tie Bar Spacing, in	Tie Bar Length, in	Steel Grade
500	#5	36	24	60
550	#5	36	24	60
600	#5/#6	30/36	24	60
650	#6	36	24	60
700	#6	36	24	60
750	#6	36	24	60
800	#6	36	24	60

Table D-7. Tie bar design for four tied 12-ft lanes on a 6-in PCTB.

Total Equivalent Free Strain, Microstrain	Tie Bar Size Designation	Tie Bar Spacing, in	Tie Bar Length, in	Steel Grade
500	#5	36	24	60
550	#5	36	24	60
600	#5/#6	30/36	24	60
650	#6	36	24	60
700	#6	36	24	60
750	#6	36	24	60
800	#6	36	24	60

APPENDIX E—SUPPLEMENTARY TIE BAR DESIGN TABLES FOR CEMENT TREATED BASES

Table E-1. Tie bar design for two tied 12-ft lanes on a 6-in CTB.

Total Equivalent Free Strain, Microstrain	Tie Bar Size Designation	Tie Bar Spacing, in	Tie Bar Length, in	Steel Grade
500	#5	36	24	60
550	#5	36	24	60
600	#5	36	24	60
650	#6	36	24	60
700	#6	36	24	60
750	#6	36	24	60
800	#6	36	24	60

Table E-2. Tie bar design for two tied 12-ft lanes on a 5-in CTB.

Total Equivalent Free Strain, Microstrain	Tie Bar Size Designation	Tie Bar Spacing, in	Tie Bar Length, in	Steel Grade
500	#5	36	24	60
550	#5	36	24	60
600	#5	36	24	60
650	#5/#6	30/36	24	60
700	#6	36	24	60
750	#6	36	24	60
800	#6	36	24	60

Table E-3. Tie bar design for two tied 12-ft lanes on a 4-in CTB.

Total Equivalent Free Strain, Microstrain	Tie Bar Size Designation	Tie Bar Spacing, in	Tie Bar Length, in	Steel Grade
500	#5	36	24	60
550	#5	36	24	60
600	#5	36	24	60
650	#5/#6	30/36	24	60
700	#6	36	24	60
750	#6	36	24	60
800	#6	36	24	60

Table E-4. Tie bar design for a 12-ft lane tied to a 14-ft lane on a 6-in CTB.

Total Equivalent Free Strain, Microstrain	Tie Bar Size Designation	Tie Bar Spacing, in	Tie Bar Length, in	Steel Grade
500	#5	36	24	60
550	#5/#6	30/36	24	60
600	#6	36	24	60
650	#6	36	24	60
700	#6	36	24	60
750	#6	36	24	60
800	#6	36	24	60

Table E-5. Tie bar design for two tied 14-ft lanes on a 6-in CTB.

Total Equivalent Free Strain, Microstrain	Tie Bar Size Designation	Tie Bar Spacing, in	Tie Bar Length, in	Steel Grade
500	#5	36	24	60
550	#6	36	24	60
600	#6	36	24	60
650	#6	36	24	60
700	#6	36	24	60
750	#6	36	24	60
800	#6	36	24	60

Table E-6. Tie bar design for three tied 12-ft lanes on a 6-in CTB.

Total Equivalent Free Strain, Microstrain	Tie Bar Size Designation	Tie Bar Spacing, in	Tie Bar Length, in	Steel Grade
500	#5	36	24	60
550	#6	36	24	60
600	#6	36	24	60
650	#6	36	24	60
700	#6	36	24	60
750	#6	36	24	60
800	#6	36	24	60

Table E-7. Tie bar design for four tied 12-ft lanes on a 6-in CTB.

Total Equivalent Free Strain, Microstrain	Tie Bar Size Designation	Tie Bar Spacing, in	Tie Bar Length, in	Steel Grade
500	#6	36	24	60
550	#6	36	24	60
600	#6	36	24	60
650	#6	36	24	60
700	#6	36	24	60
750	#6	30	24	60
800	#6	22.5	24	60

APPENDIX F—SUPPLEMENTARY TIE BAR DESIGN TABLES FOR LEAN CONCRETE BASES

Table F-1. Tie bar design for two tied 12-ft lanes on a 6-in LCB.

Total Equivalent Free Strain, Microstrain	Tie Bar Size Designation	Tie Bar Spacing, in	Tie Bar Length, in	Steel Grade
500	#5	36	24	60
550	#5/#6	30/36	24	60
600	#6	36	24	60
650	#6	36	24	60
700	#6	36	24	60
750	#6	36	24	60
800	#6	36	24	60

Table F-2. Tie bar design for two tied 12-ft lanes on a 5-in LCB.

Total Equivalent Free Strain, Microstrain	Tie Bar Size Designation	Tie Bar Spacing, in	Tie Bar Length, in	Steel Grade
500	#5	36	24	60
550	#5/#6	30/36	24	60
600	#5/#6	30/36	24	60
650	#6	36	24	60
700	#6	36	24	60
750	#6	36	24	60
800	#6	36	24	60

Table F-3. Tie bar design for two tied 12-ft lanes on a 4-in LCB.

Total Equivalent Free Strain, Microstrain	Tie Bar Size Designation	Tie Bar Spacing, in	Tie Bar Length, in	Steel Grade
500	#5	36	24	60
550	#5	36	24	60
600	#5/#6	30/36	24	60
650	#6	36	24	60
700	#6	36	24	60
750	#6	36	24	60
800	#6	36	24	60

Table F-4. Tie bar design for a 12-ft lane tied to a 14-ft lane on a 6-in LCB.

Total Equivalent Free Strain, Microstrain	Tie Bar Size Designation	Tie Bar Spacing, in	Tie Bar Length, in	Steel Grade
500	#6	36	24	60
550	#6	36	24	60
600	#6	36	24	60
650	#6	36	24	60
700	#6	36	24	60
750	#6	36	24	60
800	#6	36	24	60

Table F-5. Tie bar design for two tied 14-ft lanes on a 6-in LCB.

Total Equivalent Free Strain, Microstrain	Tie Bar Size Designation	Tie Bar Spacing, in	Tie Bar Length, in	Steel Grade
500	#6	36	24	60
550	#6	36	24	60
600	#6	36	24	60
650	#6	36	24	60
700	#6	36	24	60
750	#6	36	24	60
800	#6	36	24	60

Table F-6. Tie bar design for three tied 12-ft lanes on a 6-in LCB.

Total Equivalent Free Strain, Microstrain	Tie Bar Size Designation	Tie Bar Spacing, in	Tie Bar Length, in	Steel Grade
500	#6	36	24	60
550	#6	36	24	60
600	#6	36	24	60
650	#6	36	24	60
700	#6	30	24	60
750	#6	26	24	60
800	#6	22.5	24	60

Table F-7. Tie bar design for four tied 12-ft lanes on a 6-in LCB.

Total Equivalent Free Strain, Microstrain	Tie Bar Size Designation	Tie Bar Spacing, in	Tie Bar Length, in	Steel Grade
500	#6	36	24	60
550	#6	36	24	60
600	#6	22.5	24	60

APPENDIX G—SUPPLEMENTARY TIE BAR DESIGN TABLES FOR ASPHALT TREATED BASES

Table G-1. Tie bar design for two tied 12-ft lanes on a 6-in ATB.

Total Equivalent Free Strain, Microstrain	Tie Bar Size Designation	Tie Bar Spacing, in	Tie Bar Length, in	Steel Grade
500	#5	36	24	60
550	#5	36	24	60
600	#5	36	24	60
650	#6	36	24	60
700	#6	36	24	60
750	#6	36	24	60
800	#6	36	24	60

Table G-2. Tie bar design for a 12-lane tied to a 14-ft lane on a 6-in ATB.

Total Equivalent Free Strain, Microstrain	Tie Bar Size Designation	Tie Bar Spacing, in	Tie Bar Length, in	Steel Grade
500	#5	36	24	60
550	#5/#6	30/36	24	60
600	#6	36	24	60
650	#6	36	24	60
700	#6	36	24	60
750	#6	36	24	60
800	#6	36	24	60

Table G-3. Tie bar design for two tied 14-ft lanes on a 6-in ATB.

Total Equivalent Free Strain, Microstrain	Tie Bar Size Designation	Tie Bar Spacing, in	Tie Bar Length, in	Steel Grade
500	#5	36	24	60
550	#6	36	24	60
600	#6	36	24	60
650	#6	36	24	60
700	#6	36	24	60
750	#6	36	24	60
800	#6	36	24	60

Table G-4. Tie bar design for three tied 12-ft lanes on a 6-in ATB.

Total Equivalent Free Strain, Microstrain	Tie Bar Size Designation	Tie Bar Spacing, in	Tie Bar Length, in	Steel Grade
500	#5	36	24	60
550	#6	36	24	60
600	#6	36	24	60
650	#6	36	24	60
700	#6	36	24	60
750	#6	36	24	60
800	#6	36	24	60

Table G-5. Tie bar design for four tied 12-ft lanes on a 6-in ATB.

Total Equivalent Free Strain, Microstrain	Tie Bar Size Designation	Tie Bar Spacing, in	Tie Bar Length, in	Steel Grade
500	#6	36	24	60
550	#6	36	24	60
600	#6	36	24	60
650	#6	36	24	60
700	#6	36	24	60
750	#6	30	24	60
800	#6	22.5	24	60